DOE/PC/90910-T1
(DE90001460)
Distribution Category UC-108

ENHANCED COAL LIQUEFACTION BY LOW-SEVERITY CATALYTIC REACTIONS

DOE/PC/90910--T1
DE90 001460

Final Report

by

Alan Davis, F.J. Derbyshire, G.D. Mitchell and H.H. Schobert

Contributors: R. Lin, P.G. Stansberry and E. Zhang

PENNSTATE

(814) 865-6544

Energy & Fuels Research Center

The Pennsylvania State University
University Park, PA 16802

ABSTRACT

This program of research has involved the investigation of the liquefaction of coals by reaction in successive stages of increasing temperature in order to understand the chemical processes occurring in the individual stages. Process variables included the influence of coal rank (lignite, subbituminous, hvCb and hvAb) and the role of catalysts (1.0 wt% Mo or Fe or 1.0% Fe + 0.1% Mo) and vehicle solvents. The exact nature of the relatively subtle reactions occurring in the low- and high-temperature stages have not been clearly identified in this research. Our results suggest that the first stage reactions involve mild hydrogenation. An increase in the pool of hydrogen available within the coal structure could precondition the coal and favorably bias the course of the higher temperature reaction toward hydroliquefaction rather than pyrolysis. We have determined that the temperature-staged reaction sequence can accommodate fairly large changes in reaction conditions before an appreciable effect on product yield becomes apparent.

In most cases the lower rank coals showed higher oil yields under the varying reaction conditions employed in this study. Also, it is clear that the hvCb coal was not reacted under optimum conditions. A greater degree of molecular condensation and crosslinking appears to have occurred during solvent-free hydrogenation of lignite and subbituminous coals than with bituminous coals. One of the roles of the solvents and catalysts is recognized as the promotion of thermoplasticity in the lower rank coals and the reduction of the propensity for retrograde reactions that can lead to the development of anisotropic semicoke.

In comparative coal liquefaction experiments, the Mo and Fe + Mo catalysts were consistently superior to Fe. The high activity of Fe + Mo

catalyst is surprising and suggests synergistic behavior. Molybdenum is believed to be effective for hydrogenation, hydrodesulfurization and hydrocracking, whereas iron may promote the cleavage of oxygen linkages. Experiments using model compounds showed that the Mo catalyst promotes mild hydrogenation and the cleavage of weak (primarily oxygen-containing) linkages.

A series of separate experiments was designed to investigate the function of catalysts during liquefaction. The procedure used to convert ammonium heptamolybdate to the ammonium tetrathiomolybdate catalyst used in this study is believed to result in a mixture of molybdate and thiomolybdate compounds. We have determined by optical and scanning electron microscopy that the sulfided ammonium molybdate forms a surface coating rather than impregnating into the structure of coal. Moreover, not all of the catalyst material is dispersed over coal surfaces by the process of impregnation, but some may exist as discrete particles. The nature of catalyst transformations were studied under various reaction conditions. Detailed evaluation of an aged Mo catalyst demonstrated that it is composed of multiple phases, which are sulfur deficient, and probably represents a mixture of molybdate, thiomolybdate and perhaps oxythiomolybdate. A microscopic comparison of the products of both aged and fresh Mo catalyst precursors makes it clear that there are separate reactions involving the sulfidization of molybdate and the loss of sulfur from the thiomolybdate when carried out in a hydrogen atmosphere. After liquefaction of the freshly prepared catalyst precursor, the resulting material has a higher S/Mo atomic ratio than 2:1.

TABLE OF CONTENTS

TABLE OF CONTENTS (cont.)

TABLE OF CONTENTS (cont.)

SUMMARY

This program of research was intended to investigate in some detail the liquefaction of coals by reaction in successive stages of increasing temperature. The advantages of temperature-staged reaction over single stage conversion have already been demonstrated in earlier work. Of particular interest were the chemical processes occurring in the individual stages, the influence of coal rank and the role of the catalyst. Consequently, tubing-bomb liquefaction experiments were undertaken to gain an understanding of the influences in temperature-staged liquefaction of the presence and absence of alternative catalysts, solvents and gas atmospheres for four different ranks of coal (PSOC-1482, lignite; PSOC-1401, subbituminous; PSOC-1498, hvCb; PSOC-1504, hvAb).

In the attempt to distinguish and elucidate the reactions occurring in the low and high temperature stages, success has been somewhat limited. As was already known, from a consideration of the second stage performance, it is eminently preferable for the first stage to be conducted in the presence of gaseous hydrogen, donor solvent and an active catalyst. However, the benefits ascribed to these parameters, compared to a thermal first stage, are not immediately evident from an examination of the first stage products. The structural changes wrought at low temperature can evidently predispose the coal to more facile conversion in the second stage. Yet the nature of these changes are relatively subtle and have not been clearly identified in this research. Our results suggest that the first stage reactions involve mild hydrogenation which is supported by a shift towards the blue region of the maximum fluorescence intensity for vitrinite, sporinite and cutinite in the hvAb coal. This is the only direct, although inconclusive, evidence of structural changes induced during low-temperature

pretreatment; it could be taken as demonstrating an increase in the pool of hydrogen available within the coal structure which would facilitate radical stabilization and the cleavage of weak crosslinkages in the second stage. In this way, the presumed reactions of the first stage would precondition the coal and favorably bias the course of the higher temperature reaction towards hydroliquefaction rather than pyrolysis. However, sound quantitative evidence is still wanting. It is advocated that, in future research, a more analytical approach be taken.

The numerous temperature-staged experiments conducted in this program have confirmed previous intimations that the temperature-staged reaction sequence can accommodate quite large changes in reaction conditions before an appreciable effect becomes apparent. The situation is ideal from a process standpoint since it allows margins for error and variability. For fundamental research, it can be disadvantageous to have a suppressed response to systematic changes. This should be taken into account in future work.

Three of the coals were examined systematically for the effects of catalysts and solvents during temperature-staged hydrogenation; a lignite and hvC and hvA bituminous coals. In most cases the two lower rank coals afforded higher oil yields. Although the number of coals here is too small to allow firm conclusions, in conjunction with other published findings it is apparent that the potential for oil production increases with decreasing coal rank. A caution must be added in that it seems that there will be a limit to this trend when, with coals which are less mature, oil yield is reduced at the expense of gas production.

The catalysts investigated in this research were Mo (loading 1 wt% maf coal), Fe (loading 1 wt% maf coal) and Fe + Mo (loading 1 wt% + 0.1 wt%

respectively of maf coal). Model compound experiments showed that, under first-stage conditions, the Mo catalyst promotes mild hydrogenation and the cleavage of weak (primarily oxygen-containing) linkages.

In coal liquefaction, the Mo and Fe + Mo catalysts were consistently superior to Fe. The high activity of the Fe + Mo catalyst is particularly interesting and brings into focus the potential for non-additive or synergistic behavior. Synergism has been reported elsewhere for this particular combination of metals. However, in general, the use of multicomponent dissolution catalysts is an unexplored field. The involvement of more than one catalyst component is of interest because it raises the possibility of partially substituting for an expensive component while retaining activity, but most of all because of the exciting prospect of developing a generation of novel and active catalysts for coal liquefaction.

Some thought has been given to the causes of synergism for the particular combination of Fe with Mo. It is considered that the two components must introduce substantially different and complementary functions. Molybdenum is believed to be effective for hydrogenation, hydrodesulfurization and hydrocracking. Iron is much less active in these reactions and in utilizing molecular hydrogen. Evidence derived here and from other work suggests that the main contribution of the iron catalyst is to promote the cleavage of oxygen linkages.

In addition to the detailed product yield and analytical information gathered in support of each liquefaction experiment, a large number of the THF-insoluble residues were evaluated by quantitative optical microscopical techniques. Reflectance, spectral fluorescence and point-count analyses

provide analytical data on the nature and properties of residual materials that can then be related to process variables. Generally, the results of these analyses show that:

- The standard temperature-staged reaction conditions (275°C, 30 min; 425°C, 30 min) were probably not optimum for the hvCb coal (PSOC-1498).

- Reflectance analyses of the vitrinite-derived residue material from temperature-staged liquefaction of the lignite and subbituminous coals have revealed that there may be a greater degree of molecular condensation and crosslinking than with the bituminous coals.

- Reflectance analyses of non-extracted, whole products of solvent-free hydrogenation residues show a bimodal distribution, where the lower reflecting component is highly fluorescent and soluble in THF. This latter component is mostly absent from residues of non-catalytic experiments.

- The tendency of low-rank coal to become plastic during solvent-free temperature-staged hydrogenation in the presence of catalysts suggests that the function of the catalyst is to reduce early crosslinking and condensation that might lead to lower conversions.

- The use of a solvent during liquefaction generally increases conversion, but also changes the characteristic of the residue material. Reflectance values of the vitrinite-derived residue components are lower and there is less tendency to produce anisotropic carbon.

To investigate the function of catalysts during liquefaction, a series of separate experiments was designed and observations made that address the following questions. 1) How do reaction conditions affect catalyst composition during the course of liquefaction? 2) Can we identify the active phases? 3) How effectively is the catalyst impregnated into the structure of coals?, and 4) How is the catalyst associated with coal organic and inorganic matter in liquefaction residues?

From our investigation of catalyst precursor materials and remnants in liquefaction residues, we have learned that the procedure used to convert ammonium heptamolybdate (AHM) to the ammonium tetrathiomolybdate (ATM) catalyst results in a mixture of molybdate and thiomolybdate compounds

which collectively we call "sulfided ammonium molybdate (SAM)". Further, not all of the catalyst material is dispersed over coal surfaces by the process of impregnation, but may form a coating on the slurry vessel during dehydration. Consequently, some variable amount of the catalyst exists as discrete particles during each coal liquefaction test.

We have determined that the sulfided ammonium molybdate catalyst, when applied as a solution and then freeze-dried to remove water, does not significantly impregnate into the structure of a subbituminous or a bituminous coal. However, it can form a fairly uniform surface dispersion which may intrude into pre-existing coal fractures that are exposed to the catalyst solution. Regardless of the apparent imperfect impregnation, SAM has been shown to be an effective catalyst for coal hydrogenation. The remaining question is, how much more effective could the molybdenum catalyst be if deeper penetration of the catalyst into the coal structure could be achieved?

To study the transformation of SAM to MoS_2 during liquefaction, two sets of catalyst residues were prepared from reaction of the catalyst under pretreatment (275°C, 30 min), two-staged (275°C, 30 min and 425°C, 30 min) and high-severity (425°C, 30 min) conditions in hydrogen and nitrogen atmospheres in the absence of solvent and coal. The first set of residues were produced from a catalyst precursor that had been stored under laboratory conditions for an extended period of time, whereas the second set of residues were made from freshly prepared catalyst. Optical evaluation of the aged SAM demonstrated that it is probably a mixture of molybdate, thiomolybdate, and perhaps oxythiomolybdate. Detailed optical and electron microscope analyses of these residues showed that they are composed of multiple phases most of which are sulfur deficient.

From reactions of both aged and fresh SAM catalyst precursor under the conditions of coal liquefaction and in the presence of CS_2, we have shown that there are separate reactions that involve the sulfidization of molybdate and the loss of sulfur from the thiomolybdate when reactions are carried out in a hydrogen atmosphere. Reactions conducted in a nitrogen atmosphere show that there is less removal of sulfur from the thiomolybdate when CS_2 is present and practically no reaction with the molybdate. Under liquefaction conditions, the S/Mo atomic ratio of the thiomolybdate catalyst residue is lower in a hydrogen atmosphere than in nitrogen. Under all reaction conditions, the resulting catalytic material has a higher S/Mo atomic ratio than MoS_2 and is non-crystalline. We suggest that the loss of excess sulfur from the thiomolybdate is responsible for the production of hydrogen and hydrogen sulfide radicals under liquefaction conditions, and that these radicals can promote coal hydrogenation.

Finally, a series of observation using optical and scanning electron microscopy have been made on coal liquefaction residues in an attempt to locate and to characterize the catalyst remnants. Residues produced from liquefaction of a coal using separate iron sulfate and SAM catalyst as well as a mixed iron-molybdenum catalyst were studied. Results show that the iron sulfate is converted to pyrrhotite during temperature-staged and high-temperature liquefaction, and forms reactor solids that are not associated with the organic portion of the residue. Formation of reactor solids is somewhat less pronounced with the molybdenum catalyst. There is also a dispersed form of the molybdenum catalyst that is intimately mixed with organic materials in the residues.

1. INTRODUCTION AND OVERVIEW

The technology to construct and operate commercial-scale plants for converting coals to liquid fuels and chemicals is already in existence, and has been for over half a century.

In the several decades which have elapsed since the first plants were built in Germany, there have been substantial advancements in scientific understanding and process engineering. In direct consequence, coals can now be liquefied under conditions of lower severity and at higher rates of throughput than at any previous time in history.

Despite this progress, coal liquids still cannot be produced cheaply enough to compete with those derived from conventional petroleum resources. According to recent estimates, the cost of liquids from coal is around $35.00/bbl (1) compared to about $20.00/bbl (published prices at the time of writing May 1989) for petroleum crude. It seems unlikely that crude prices can be maintained at these low levels for any extended period. In the same context, changes in national and international circumstances could well precipitate abrupt increases in price. However, the future of coal liquefaction cannot be left to depend upon events which may adversely affect the supply of petroleum. Continuing effort must be directed to improving the economic viability of coal conversion. To this end, Research and Development must proceed along a broad front which simultaneously allows progress in fundamental understanding of the reaction chemistry and the influence of catalysis, engineering and process development and the investigation of exploratory concepts.

Some of the most significant advances over the last few years emanate from the recognition that the processes of coal dissolution and coal liquids upgrading require different reaction regimes, and that preferably

these processes are conducted in separate reactors and with different types of catalyst. As a result, attention has turned from single to two or even multi-staged liquefaction (2-3).

As research has progressed, the two-stage concept has been further refined. Initially, most investigations of two-staged sequencing involved thermal dissolution (aided only by the catalytic effects of coal mineral matter) followed by catalytic upgrading, using supported catalysts. An increasing awareness of the role which catalysis can exert during dissolution has prompted studies of catalytic-catalytic liquefaction using supported or dispersed catalysts in the first stage (4-9).

Effective control of coal dissolution requires the attainment of a balance between the processes of bond cleavage and hydrogenative stabilization of the cleaved fragments. Both processes can be promoted by catalysts. At elevated reaction temperatures, thermally initiated bond cleavage predominates, outstripping the capacity for hydrogenation. The system then no longer operates under a mainly catalytic regime and a considerable proportion of the products is the outcome of condensation reactions. To obviate these undesirable effects, the temperature must be reduced to accommodate the limitations of the catalyst being used. These arguments also apply to coal liquids upgrading although here, it seems, higher reaction temperatures can be tolerated.

In order for the catalyst to exert a significant influence on the conversion of the solid coal feed to a soluble form, the catalyst must be in intimate contact with the coal. This necessitates its introduction in a highly dispersed form. Conventional supported catalysts can only promote the dissolution process through indirect hydrogenation.

This train of logic leads to the conclusion that the first stage must be operated at a lower temperature than the second and, preferably, in the presence of a dispersed catalyst. Studies of temperature staged liquefaction have been supported by DOE at this University on a laboratory scale (8-9) and in 22Kg/d continuous unit at Hydrocarbon Research Inc. (6-7).

Compared to other configurations, temperature staging leads to improved selectivity to distillates and enhanced heteroatom removal. The residual products have low viscosity and there is reduced aging of the second stage catalyst. (For further details, see Derbyshire (10).)

It also appears that the selection of the optimum first stage conditions is coal structure dependent, the temperature decreasing with coal rank (11). This is consistent with the greater tendency of low rank coals to cross-link at low temperatures (12).

The research described in this report took its leads from the findings of earlier studies at this University and at HRI, both of which were cited above. Other research at Penn State relevant to the present program was described by Terrer and Derbyshire (13) and Stansberry and Derbyshire (14).

Having established the general effects of catalytic-catalytic temperature-staged liquefaction, an obvious sequitur is to probe in more detail into their causes and mechanisms. This was the principal objective of this investigation. Topics of specific interest were:

i) the chemical and physical changes associated with the first and second stages, how these influence the overall process,

ii) the dependence of temperature-staged reaction on coal rank, solvent and catalyst, and

iii) the role of catalyst; the importance of its dispersion and composition; insight into catalyst mechanisms.

Liquefaction experiments were performed in tubing bomb reactors in the presence and absence of solvent. Both process-derived and model compound solvents were employed. Coals were selected to represent a range of rank from lignite to hvA bituminous. To define a realistic program, the catalyst choice was mostly confined to sulfided Mo which was added to the coal by impregnation. Some related studies were made with Fe and Fe+Mo catalysts.

Optical and electron microscopy have been used extensively in examining the dispersed form of the catalyst, catalyst-impregnated coals and liquefaction residues in order to study the form and dispersion of the catalyst, to follow the changes in petrographic composition and character under a variety of liquefaction conditions and to elucidate the catalyst mechanisms.

REFERENCES

1. Haggin, J., 1988, C & E News, October 10th, 29-30.

2. Neuworth, M.B. and Moroni, E.C., 1984, Fuel Proc. Technol., 8, 231-239.

3. Curtis, C.W., Tsai, K.-J. and Guin, J.A., 1987, Ind. Eng. Chem., 26, 12-17.

4. Garg, D., Tarrer, A.R., Guin, J.A., Lee, J.M. and Curtis, C.W., 1979, Fuel Proc. Technol., 2, 189-208.

5. Mathur, V.K. and Karri, S.B.R., 1986, Fuel, 65, 790-796.

6. Comolli, A.G., Ganguli, P., Harris E., MacArthur, J.B., McLean, J.B. and Smith, T.O., 1985, DOE-PC-60017-T1, Lawrenceville, NJ, USA, Hydrocarbon Research Inc., 413.

7. McLean, J.B., Comolli, A.G. and Smith, T.O., 1986, American Chemical Society, Division of Fuel Chemistry, Preprints, 31, (4), 268-2/9.

8. Derbyshire, F.J., Davis, A., Epstein, M. and Stansberry, P., 1986, Fuel, 62, 1233-1240.

9. Epstein, M.J. and Derbyshire, F.J., 1987, DOE-PC-70003-F2, University Park, PA, USA, The Pennsylvania State University, 139.

10. Derbyshire, F.J., 1988, IEACR/08, London, UK, IEA Coal Research, 69.

11. Derbyshire, F.J. and Luckie, P.T., 1986, DOE-PC-70003, University Park, PA, USA, The Pennsylvania State University, 23.

12. Derbyshire, F.J. and Stansberry, P.G., 1987, Fuel, 66, 1741-1742.

13. Terrer, M.-T. and Derbyshire, F.J., 1986, DOE-PC-60811-F1, University Park, PA, USA, The Pennsylvania State University, 113.

14. Stansberry, P.G. and Derbyshire, F.J., 1988, DOE-DE-FE22-83PC60811.

2. TEMPERATURE-STAGED LIQUEFACTION

2.1. INTRODUCTION

This section deals with the results of a large number of experiments which were intended to examine the relative effects of coal rank, catalyst type and solvent composition on temperature-staged liquefaction. Three catalysts were used, sulfided Mo at 1% wt dmmf coal, sulfided Fe at 1% wt dmmf coal and an Fe + Mo catalyst, at 1% wt Fe + 0.1% wt Mo.

Liquefaction experiments were conducted in both the absence and presence of solvents. The solvents included both model compounds and process derived coal liquids.

2.2. EXPERIMENTAL

2.2.1. Coal Selection and Preparation

The coals used in this study were obtained from the Penn State Coal Sample Bank and covered a range of rank, from lignite to hvA bituminous. The properties of the coals are summarized in Table 2.1.

The coals were ground without drying to -60 mesh (U.S. sieve size) in a glove box which was purged and maintained under an oxygen-free nitrogen atmosphere to minimize air oxidation. The ground coals were then riffled, and sealed in air-tight containers while still in the glove box.

Coals were impregnated with catalysts of Mo, Fe or a bimetallic Fe/Mo catalyst by impregnation from aqueous solutions of ammonium tetrathiomolybdate (ATM), $(NH_4)_2MoS_4$; iron sulfate, $FeSo_4$; or a mixture of these two salts. The procedure consisted of dissolving the desired quantity of the metal salt(s) in enough distilled water to give an approximate water-to-coal ratio of 1.5:1. The coal was then added to the solution, which was stirred at room temperature for about 30 min before the

Table 2.1. Coal Properties

Penn State Sample Number	PSOC-1482	PSOC-1401	PSOC-1498	PSOC-1504
Seam	Hagel	Lower Wyodak	Wadge	Upper Sunnyside
State	North Dakota	Wyoming	Colorado	Utah
ASTM Rank	lig	subB	hvC	hvA
Mean-Maximum Reflectance of Vitrinite (Romax, %)	0.39	0.42	0.60	0.80
Ultimate Analysis (% daf)				
Carbon	72.32	74.3	77.52	81.96
Hydrogen	2.26	5.2	5.45	5.80
Oxygen	23.46+	19.3+	14.66+	9.66+
Nitrogen	1.02	1.1	1.81	1.75
Organic Sulfur	0.94	0.2	0.56	0.83
Proximate Analysis (a.r. %)				
Moisture	34.71	16.3	9.45	3.38
Volatile Matter	28.07	37.7	38.04	37.49
Fixed Carbon	31.36	41.1	46.08	51.84
Ash	5.86	6.6	6.43	7.29
Petrographic Composition (mineral-free, % vol)				
Vitrinite	88	85	89	87
Liptinite	2	2	2	3
Inertinite	10	13	9	10
Gieseler Fluidity				
Maximum Fluidity (ddpm)	no fluidity	no fluidity	no fluidity	17
Fluid Range				51
Initial Softening T°C				400
Resolidification T°C				451
Chloroform-soluble extract (% dmf)	1.76	NA	1.31	1.06

\+ = By difference
NA = Not available

excess water was removed by vacuum drying. The residual moisture, determined by ASTM D3173, was less than 2% by weight in all cases.

ATM was prepared from ammonium heptamolybdate (AHM), $(NH_4)_6Mo_7O_{24} \cdot 4H_2O$ (Climax Molybdenum) by bubbling H_2S gas through a solution of AHM for 30 min at room temperature while stirring. The conversion to ATM occurs quickly (< 1 min), producing a dark-red solution. The coal was then added to this solution in the manner described above. However, as discussed in Chapter 4, it has been found that complete conversion to the thio-salt is more difficult than this description indicates.

Iron sulfate was obtained from a commercial chemical company (Aldrich) and used as received.

2.2.2. Coal Hydrogenation

Hydrogenation reactions were performed in batch, stainless steel tube reactors (approx. 25 cm^3 capacity) of a design described by Yarzab and others (1) and Szladow and Given (2).

Approximately 2.5 g of coal and 5 g of solvent were charged to the reactor. If hydrogenations were conducted without added solvent, then 5 g of coal were charged to the reactor. If catalyst was present, a stoichiometric amount of CS_2 was added to ensure that enough available sulfur was present to convert the metal to its sulfide form. The assumption was made that ATM would convert entirely to MoS_2, and $FeSo_4$ to FeS_2.

The loaded reactor was purged of air with nitrogen and then purged three times with the desired gas (hydrogen or nitrogen) before finally being pressurized to 7 MPa cold pressure.

The reactor contents were agitated vertically through 2.5 cm at about 200 cycles per minute by an electrically driven cam system while the

reactor was immersed in a pretreated, fluidized sandbath. After reaction for the desired time, the reactor was removed from the sandbath and quenched to room temperature by immersion in cold water. The reaction time was defined as the period between immersion in the sandbath and quenching. Reactions were conducted at 275°C, 425°C or at these temperatures in sequenced stages for times up to 1 h.

In between the steps of the temperature-staged liquefaction experiments, the reactor was quenched to room temperature and the gaseous products vented into a glass gas-trap system for analysis. After the gaseous products were vented, the reactor was repressurized with 7 MPa hydrogen and reaction was continued at the higher temperature. This procedure was adopted to circumvent the possibility of limiting the hydrogen partial pressure. The second-stage gaseous products were also collected and analysed.

2.2.3. Product Work Up

2.2.3.1. Analysis of Gases

The gaseous products were vented from the reactor into a glass trapping vessel of known volume. A syringe was used to remove a sample of gas from the vessel for analysis with a Varian 3700 gas chromatograph equipped with a thermal conductivity detector (TCD). The electrical signal from the TCD was converted into digital form for analysis by a dedicated mini-computer.

The concentrations of gaseous components were calculated from peak areas following calibration using standard gas mixtures. Knowing the volume of the vessel from which the sample was taken, these data were then used to back-calculate the yield of gas to a coal basis.

Hydrogen consumption was calculated knowing the free reactor volume, the initial and final cold reactor pressures and the partial pressures of product gases (CO, CO_2 and C_1-C_4 hydrocarbons).

2.2.3.2. Liquid and Solid Products

Liquefaction experiments were done in duplicate. After venting one of the reactors, the contents were removed and enclosed in 20 mL vials under nitrogen. This sample was used for microscopy and other analyses.

The second reactor was vented into the gas analysis system before the remaining liquefaction products were washed out with tetrahydrofuran (THF) into a dry, tared ceramic extraction thimble. The thimble was transferred to a Soxhlet apparatus and the soluble products extracted with THF into a tared, 250 mL round bottom flask for a period of about twelve hours while under a blanket of nitrogen. After extraction, the THF-soluble products were filtered through a Whatman #42 filter paper before returning the solution back to the round bottom flask.

The residue remaining in the ceramic thimble was dried completely in a vacuum oven at 100°C for twelve hours before weighing.

The contents of the round bottom flask were then partitioned into oils (hexane-soluble) and asphaltenes (hexane-insolubles). The solvent partioning was accomplished by first stripping the excess THF using a rotary evaporator. The asphaltenes were then precipitated by adding about 200 mL of hexane, and the mixture was allowed to stand overnight at room temperature. The flask containing hexane, oils, and asphaltenes was then placed in an ultrasonic bath for about 10 min to dislodge material clinging to the sides of the flask. The asphaltenes were separated from the oils by filtering through a tared Whatman #42 filter paper. The asphaltenes, which

collected on the filter paper, were washed with about 50 mL of cold hexane and dried at 100°C in a vacuum oven for six hours before weighing.

2.2.3.3. Yield Calculations

The conversions and yields of gases and asphaltenes were calculated as percentages of dry, ash- or mineral matter-free coals. Oil yields were calculated by difference because, during the work-up procedure, it was not possible to prevent the loss of light ends from the oil fraction during solvent stripping. This being the case, it was considered more reliable and informative to effectively calculate the oil yield by closing the mass balance.

2.2.4. Coal Swelling in Pyridine

A volumetric swelling procedure first described by Dryden (3) and later used by Liotta and others (4) was applied to the THF-insoluble materials using pyridine as the swelling agent.

Approximately 0.5g of product that passed through a 60 mesh sieve (Tyler mesh) were placed into a glass test tube, sealed with a rubber septum, and the contents settled by centrifugation at about 1700 rpm for 10 min. The height of coal was measured, then 4 mL of pyridine added and the contents shaken.

About 1 mL of pyridine was used to rinse the clinging particles down onto the bed of coal. After 3 days the contents of the test tube were centrifuged and the height of swollen coal measured.

The volumetric swelling ratio (5) is defined as:

$$Q = h_2/h_1$$

where h_1 = height of unswollen coal, and h_2 = height of swollen coal.

2.3. RESULTS AND DISCUSSION

2.3.1. Preliminary Experiments

At the beginning of the research program, a series of single- and two-stage liquefaction experiments were conducted in order to establish the relative influences of catalyst, solvent H-donor capacity and hydrogen gas. This work was initiated prior to the final selection of the project coals. For this reason, a choice was made of a subbituminous coal which had been used in earlier research (6) and for which a reasonable data base had already been established.

Reactions were performed, using tetralin or naphthalene as solvent, in single-stage reactions (representative of the low- and high-severity stages in a temperature-staged reaction) and in a temperature-staged sequence. The experimental data are summarized in Tables 2.2, 2.3 and 2.4.

Upon reaction at 275°C (Table 2.2), the conversion was low and none of the variables appears to have had any appreciable effect upon either conversion or product distribution. As reported previously (7), starting with naphthalene there was essentially no conversion to tetralin under any of the conditions studied.

In the non-catalytic reaction with tetralin, the conversion of tetralin to naphthalene was higher in the absence of hydrogen gas, as might be expected. More interestingly, when catalyst was present, the conversion of tetralin to naphthalene was negligible in either hydrogen or nitrogen atmospheres. In other words, under these conditions, a source of hydrogen external to the coal is not apparently required.

Calculations from the ratio tetralin:naphthalene for the two experiments where catalyst was not present, show that the hydrogen

Table 2.2. Low-Severity Single-Stage Liquefaction (Subbituminous coal PSOC-1401: Reaction at 275°C, 30 min, 7 MPa; solvent-coal ratio = 2.0; sulfided Mo at 1% wt daf coal).

Catalyst	Solvent	Gas	Conversion (% wt)	Yields (% wt)		T/N Ratio in Product
				Asphaltenes	Oil + Gas	
-	Naphthalene	N_2	12.0	3.8	8.2	0.0
-	Naphthalene	H_2	10.2	3.7	6.5	0.0
+	Naphthalene	N_2	11.0	3.5	7.5	0.0
+	Naphthalene	H_2	7.0	3.1	3.9	0.0
-	Tetralin	N_2	11.1	3.5	7.6	76.0
-	Tetralin	H_2	8.7	2.6	6.1	104.9
+	Tetralin	N_2	7.7	3.3	4.4	*
+	Tetralin	H_2	7.9	4.4	3.5	*

*Naphthalene detected in too small a concentration to compute accurately.

consumption was small; about 0.1% daf coal. This quantity of hydrogen could be made available by the coal itself.

Under high-severity conditions, the effects of changes in the reaction variables were more apparent (Table 2.3). In the non-catalytic reactions, tetralin was much more effective in promoting conversion than naphthalene and the influence of hydrogen overpressure was more evident with the non-donor solvent.

From comparisons of catalytic and non-catalytic reactions, the following observations can be made:

i) the system catalyst + naphthalene + hydrogen produced a higher conversion than the combination of tetralin and hydrogen without catalyst. Thus it seems that the catalyst can promote the transfer of gaseous hydrogen to the coal more efficiently than it can be provided by H-donation in a thermal reaction.

ii) in the hydrogen + tetralin system, the addition of catalyst had a substantial promotional effect upon liquefaction and at the same time reduced the quantity of hydrogen provided by the conversion of tetralin to naphthalene. Under the conditions of the catalytic experiment, hydrogen was apparently provided from both the solvent and the gas phase. Comparing the catalytic experiments with naphthalene and tetralin, it would seem that the transfer of gas-phase hydrogen is the more important of these two routes.

iii) the combination of catalyst + tetralin under nitrogen was essentially as effective as tetralin + hydrogen without catalyst, and both systems were somewhat better than tetralin, nitrogen and no catalyst. It is possible that, in the absence of hydrogen gas, the catalyst may be able to promote H-transfer from the tetralin to the coal.

The results of experiments to examine the influence of gas atmosphere and solvent composition upon temperature-staged catalytic liquefaction are shown in Table 2.4. Overall, the magnitude of the effects caused by changes in the reaction variables were much less pronounced in the temperature-staged reactions than were apparent in the single-stage high-severity reations (Table 2.3). However, the performance attained in the two-stage system was greatly superior to that of the single-stage

Table 2.3. High-Severity Single-Stage Liquefaction (Subbituminous coal PSOC-1401: Reaction at 425°C, 30 min, 7 MPa; solvent-coal ratio = 2.0; sulfided Mo at 1% wt daf coal).

Catalyst	Solvent	Gas	Conversion (% wt)	Yields (% wt)		T/N Ratio in Product
				Asphaltenes	Oil + Gas	
-	Naphthalene	N_2	37.2	3.4	33.8	0.0
-	Naphthalene	H_2	55.4	7.8	47.6	0.0
+	Naphthalene	N_2	34.5	3.0	31.5	0.0
+	Naphthalene	H_2	88.7	38.1	50.6	0.02
-	Tetralin	N_2	76.4	29.6	46.8	5.1
-	Tetralin	H_2	78.5	29.0	49.5	5.5
+	Tetralin	N_2	79.0	29.2	49.8	3.3
+	Tetralin	H_2	91.8	30.0	61.8	14.7

Table 2.4. Temperature-Staged Catalytic Liquefaction
(Subbituminous coal PSOC-1401; solvent-coal ratio = 2.0; sulfided Mo at 1% wt daf coal).

Solvent	Gas		Conversion (% wt)	Yields (% wt)		T/N Ratio in Product
	First	Second		Asphaltenes	Oil + Gas	
Naphthalene	N_2	H_2	90.3	35.5	54.9	0.02
Naphthalene	H_2	H_2	91.1	33.0	58.1	0.02
Tetralin	N_2	H_2	92.0	31.0	61.0	19.3
Tetralin	H_2	H_2	91.0	28.2	62.8	33.6

First stage: 275°C, 30 min, 7 MPa
Second stage: 425°C, 30 min, 7 MPa

reactions. The two-stage catalytic configuration appears to be less sensitive to changes in operating parameters than a single-stage reaction, which is a great asset in terms of process design and development.

There is seen to be some advantage in using a hydrogen atmosphere in the first stage and in using tetralin rather than naphthalene. These findings are hardly unexpected. However, it is not clear why the presence of hydrogen in the first stage is so important. It is to be noted that, when using tetralin, hydrogen over-pressure in the first stage reduced the net conversion of tetralin to naphthalene (Table 2.4). With either solvent, the use of hydrogen in the first stage produced some reduction in the asphaltene yields and increases in the oil and gas yields. Yet, the results of the first-stage experiments alone (Table 2.2) showed that the catalyst, solvent and gas atmosphere had negligible influences upon the conversion or product distribution and that the conversion of tetralin to naphthalene was small or negligible in either nitrogen or hydrogen.

As noted by Terrer and Derbyshire (6), there seem to be important reactions which occur at low temperatures. These reactions evidently influence the events which occur in the second, high-temperature stage, including the demand for donor hydrogen. Since the low-temperature product yields do not afford any insight, the answers must be sought in the composition of the low-temperature liquid and gaseous products, or perhaps more importantly, in the low-temperature insoluble coal products. It is anticipated that subtle structural changes in the as-yet unliquefied coal occur during the low-severity reactions and predetermine the subsequent course of liquefaction.

Low temperatures are favorable for hydrogenation and, presumably, the main function of the catalyst under these conditions is to promote

hydrogenation reactions. Depending on the nature of the coal and the reaction temperature, there may be some accompanying cleavage and stabilization of weak bonds, although judging from the liquid yields, this is evidently limited. It may be that only some of the bonds linking particular structures to the main 'network' are severed, or fragments are liberated which are too large either to diffuse out of the coal or to dissolve in the solvent.

Low-temperature catalytic hydrogenation may facilitate partial 'depolymerization' of the coal structure, while minimizing the extent of condensation reactions. This involves the breaking and stabilization of weak bonds, creating a 'pool' of hydrogen within the coal structure and weakening stronger bonds through the hydrogenation of aromatics. These processes would further promote 'depolymerization' at higher temperatures. By minimizing condensation reactions, gas make is reduced and the efficiency of hydrogen utilization is increased. Quantitative analytical evidence is needed to substantiate and modify these propositions.

The hydrogen introduced to the coal at low temperatures (and its addition need not significantly alter the elemental composition) may be extremely mobile. Consequently, it could be instantly available to stabilize thermally generated radicals during higher temperature reaction.

It is anticipated that the rate of this type of hydrogenative transfer would greatly surpass that of conventional solvent H-donor transfer, simply because, in the former, hydrogen is already available within the coal. The role of hydrogen sources internal to the coal in the development of coal fluidity and in 'autostabilization' during liquefaction has been discussed by Neavel (8) and is central to this research.

Further support for these hypotheses has been provided by the results of pyrolysis experiments using prehydrogenated coals. This work, conducted by colleagues and collaborators in other laboratories (Dr. H. Meuzelaar, Biomaterials Profiling Center, Salt Lake City; Professor R. Cypres, Free University of Brussels; Dr. C. Snape, formerly of British Coal, U.K., now of the University of Strathclyde) has shown that low-temperature catalytic hydrogenation can substantially increase the yield and ease of liberation of liquids upon pyrolysis, without major increase in gas make, Table 2.4a.

On the subject of the routes for H-transfer in these various systems, it appears that hydrogen is supplied to the coal by the most readily available pathways (9). The mechanisms are direct hydrogenation, H-transfer from existing H-donors, H-transfer from donors generated in situ and hydrogen rearrangement within the coal. The extent to which direct hydrogenation and solvent H-transfer are competitive will depend upon the activity of the catalyst and the composition of the solvent. As shown by the preceding data, the preferred situation seems to be that in which all possible hydrogen sources are present.

2.3.2. Solvent-free Hydrogenation

The results of liquefaction experiments are summarized in Table 2.5, 2.6 and 2.7. In all cases, as expected, the addition of catalyst gave higher conversions and, in most cases, higher oil yields than the thermal experiments.

With increasing coal rank, there were generally reductions in the oil yields, in the oil to asphaltene ratio and in the yield of CO_x.

The greater proportion of the CO_x yields was due to carbon dioxide and it is the abundance of this compound which was rank-dependent; the yield of

Table 2.4a. Effect of Prehydrogenation on Pyrolysis Yields

Product	Yield (% wt daf)	
	Parent Coal	Hydrogenated Coal
$CO + CO_2$	2.1	0.5
CH_4	1.7	2.5
Total C_1-C_4	4.9	4.3
Char	60.3	42.0
Total liquids	34.8	53.0

Bituminous coal (UK)
Hydrognation: 400°C, 60 min, 7 MPa H_2, 1% wt sulfided Mo.
Pyrolysis: fluidized bed in N_2, 600°C, atmospheric pressure.

Data from Bolton and others, (10).

Table 2.5. Two-Staged Liquefaction of PSOC-1482 (lignite) in Absence of Solvent

Catalyst	Conversion (% wt)	Yields (% wt)				
		Asphaltenes	Oils	CO_x	C_1-C_4	O/A
None	38.1	11.2	15.4	10.11	1.42	1.38
Mo	70.8	28.5	29.6	10.29	2.35	1.04
Fe	51.9	19.1	17.8	12.56	2.38	0.93
Fe + Mo	66.5	25.4	26.6	12.13	2.34	1.05

First stage: 275°C, 30 min, 7 MPa H_2 (initial pressure)
Second stage: 425°C, 30 min, 7 MPa H_2 (initial pressure)

Mo, 1% wt; Fe, 1% wt; Fe + Mo, 1% wt + 0.1% wt of dmmf coal

Table 2.6. Two-Staged Liquefaction of PSOC-1498 (hvCb) in Absence of Solvent

Catalyst	Conversion (% wt)	Yields (% wt)				
		Asphaltenes	Oils	CO_x	C_1-C_4	O/A
None	21.3	10.6	7.2	3.18	0.59	0.68
Mo	56.1	38.1	12.6	4.43	0.96	0.33
Fe	41.6	25.3	10.6	4.82	0.83	0.42
Fe + Mo	54.3	34.8	12.9	4.78	1.79	0.37

First stage: 275°C, 30 min, 7 MPa H_2 (initial pressure)
Second stage: 425°C, 30 min, 7 MPa H_2 (initial pressure)

Mo, 1% wt; Fe, 1% wt; Fe + Mo, 1% wt + 0.1% wt of dmmf coal

CO was always in the range 0.1 to 0.6% wt dmmf coal for the experiments in Tables 2.5-2.19 and appeared to be insensitive to coal rank.

Typically, 20-25% of the total CO_x yield was produced during the first, low-temperature stage. In comparison, the light hydrocarbons were produced entirely during the second stage and were not present in detectable quantities in the gaseous first-stage products.

The highest oil yields and selectivities to oils were obtained with the lignite (PSOC-1482): the oil to asphaltene ratio was about 1.0 or higher while, for the other two coals, it ranged from about 0.3 to 0.8.

Of the catalysts, Mo consistently afforded higher conversions and oil yields than Fe. Where comparisons can be drawn, the combination Fe + Mo was similar to Mo.

These observations must be qualified, as there are a number of possible explanations for differences in catalyst activity. Apparent distinctions may simply reflect differences in the relative degrees of dispersion of the catalysts or the correspondence of the prevailing catalyst phase to the most active one. Catalyst activity will be strongly influenced by the composition and mode of addition of the catalyst precursor. As will be shown in subsequent sections, the presence of solvent alters the catalyst activities and their order of ranking.

The activity of Fe + Mo is interesting because the Mo is present at only one tenth of the concentration used for Mo alone. Examples of apparent 'synergy' for this and other catalyst combinations have been reported in the literature (see Derbyshire, 9, p. 20-21). These experiments have not, however, established the dependence of liquefaction behavior on the concentration of the Mo catalyst and it could well be active at concentrations below 1% wt. Hawk and Hiteshue (11) reported

Table 2.7. Two-Staged Liquefaction of PSOC-1504 (hvAb) in Absence of Solvent

Catalyst	Conversion (% wt)	Yields (% wt)				
		Asphaltenes	Oils	CO_x	C_1-C_4	O/A
None	29.3	15.1	11.5	1.57	1.12	0.76
Mo	62.4	39.2	19.2	2.12	1.90	0.49
Fe	38.9	25.6	8.6	3.16	1.51	0.34
Fe + Mo	57.3	30.8	21.9	2.56	2.01	0.71

First stage: 275°C, 30 min, 7 MPa H_2 (initial pressure)
Second stage: 425°C, 30 min, 7 MPa H_2 (initial pressure)

Mo, 1% wt; Fe, 1% wt; Fe + Mo, 1% wt + 0.1% wt of dmmf coal

Table 2.8. Two-Staged Liquefaction of PSOC-1482 (lignite) in Pyrene

Catalyst	Conversion (% wt)	Yields (% wt)				
		Asphaltenes	Oils	CO_x	C_1-C_4	O/A
None	54.0	29.2	13.7	10.28	0.83	0.47
Mo	68.5	62.2	- 4.2	9.63	0.84	--
Fe	64.6	37.0	15.9	10.77	0.93	0.43
Fe + Mo	78.7	48.5	17.0	11.83	1.37	0.35

First stage: 275°C, 30 min, 7 MPa H_2 (initial pressure)
Second stage: 425°C, 30 min, 7 MPa H_2 (initial pressure)

Mo, 1% wt; Fe, 1% wt; Fe + Mo, 1% wt + 0.1% wt of dmmf coal
Solvent to Coal ratio (daf) = 2.0

that, in the solvent-free hydrogenation of a Wyoming coal, molybdenum added as a naphthenate was equally as effective at concentrations of 0.1 and 1.0 wt%.

On the other hand, depending upon the system, higher concentrations may be yet more effective. Anderson and Bockrath (12) studied the conversion of an hvAb Kentucky coal in a distillate process solvent using dispersed Fe and Mo catalysts. Both metals were added in the form of 2-ethyl-hexanoic acid complexes and were sulfided in situ by elemental sulfur. With increasing Mo concentration, conversion tended to a limiting value, although this was also dependent upon the S/Mo ratio. When no sulfur was added, Mo sulfiding was dependent upon the sulfur already present in the system and the coal conversion reached a maximum at an Mo concentration of about 1.0 wt% coal; further increases in Mo concentration had no effect. The addition of elemental sulfur at Mo concentrations above about 0.3% wt coal caused further increases in conversion until the S/Mo atomic ratio reached 2.0, above which there was no improvement. In the presence of excess sulfur, conversion had still not apparently reached a maximum at 3.0% wt Mo.

2.3.3. Liquefaction in Pyrene

Pyrene was selected as a model example of a non-donor solvent which can function as a shuttler of hydrogen. The results of liquefaction experiments in pyrene are shown in Tables 2.8, 2.9 and 2.10.

For all of the systems studied, the conversions were higher than those obtained in the solvent-free experiments. The presence of solvent is known to effect an increase in catalyst activity. One interpretation is that the solvent is instrumental in dispersing the catalyst (see Weller, 13).

Table 2.9. Two-Staged Liquefaction of PSOC-1498 (hvCb) in Pyrene

Catalyst	Conversion (% wt)	Yields (% wt)				
		Asphaltenes	Oils	CO_x	C_1-C_4	O/A
None	47.4	61.3	-24.0	9.2	0.90	--
Mo	90.6	61.6	20.7	5.4	2.87	0.34
Fe	66.8	61.8	-2.3	5.9	1.46	--
Fe + Mo	88.7	55.2	21.3	7.8	1.38	0.39

First stage: 275°C, 30 min, 7 MPa H_2 (initial pressure)
Second stage: 425°C, 30 min, 7 MPa H_2 (initial pressure)

Mo, 1% wt; Fe, 1% wt; Fe + Mo, 1% wt + 0.1% wt of dmmf coal
Solvent to coal ratio (daf) = 2.0

Table 2.10. Two-Staged Liquefaction of PSOC-1504 (hvAb) in Pyrene

Catalyst	Conversion (% wt)	Yields (% wt)				
		Asphaltenes	Oils	CO_x	C_1-C_4	O/A
None	76.3	34.4	37.4	3.8	0.57	1.09
Mo	81.8	66.9	12.0	1.56	1.39	0.18
Fe	67.2	54.1	8.5	2.35	1.26	0.16
Fe + Mo	86.5	62.8	18.3	3.25	2.19	0.29

First stage: 275°C, 30 min, 7 MPa H_2 (initial pressure)
Second stage: 425°C, 30 min, 7 MPa H_2 (initial pressure)

Mo, 1% wt; Fe, 1% wt; Fe + Mo, 1% wt + 0.1% wt of dmmf coal
Solvent to coal ratio (daf) = 2.0

While this may be a contributory factor, the chemistry of catalyst-solvent-coal-H_2 interactions must exert an important influence.

As well as any associated chemical effects (e.g. hydrogen shuttling), the solvent medium will serve to reduce mass and heat transfer limitations. The influence of mass transfer limitations should not be underestimated. In related work, comparisons were made of catalytic two-stage liquefaction in a microreactor and in a stirred autoclave (14). Conversions and liquid yields were higher in the stirred autoclave and changes in reaction variables had significantly less influence on the yields. It may be concluded that the enhanced coal liquefaction in the autoclave was attributable to greatly improved heat and mass transfer.

By solubilizing and dispersing the coal-derived fragments, the solvent will also tend to inhibit the progress of second-order condensations.

The improved conversions in pyrene were mostly due to increases in the asphaltene yields. The oil yields were appreciably reduced in many cases and the oil to asphaltene ratios were correspondingly lower than in the solvent-free experiments.

The apparent decreases in oil yields upon the introduction of the solvent is rather surprising. A previous comparison of temperature-staged liquefaction in the absence of solvent and using naphthalene as a vehicle showed that the solvent increased the net conversion and enhanced the selectivity to oils (14-15). For a bituminous coal (PSOC-1266), the associated changes in oil and asphaltene yields due to the addition of solvent were from 23.0 to 38.8% wt and from 58.0 to 36.8% wt, respectively. It could be that, in some instances, the difficult partition into oils and asphaltenes was not effectively achieved or was altered by the solvent itself. The Mo-catalyzed conversion of PSOC-1482 (Table 2.8) and the

thermal and Fe-catalyzed conversions of PSOC-1498 (Table 2.9), indicate such a possibility. The very high asphaltene yield produces, by the method of calculation, a negative oil yield. Normally, a negative value would be interpreted to mean that solvent-coal adducts and solvent condensation products have contributed to the asphaltene yield. This is a reasonable assumption for solvents which have a propensity for participating in regressive reactions (14). For pyrene, this does not seem likely and, under these circumstances, the results must be regarded with some suspicion.

With respect to conversion and oil yield, the Fe + Mo catalyst was the most active. The relative activities of the Mo and Fe catalysts varied with the coal and the criteria selected for assessment.

Differences are apparent in the behavior of the coals. In the presence of the Mo catalyst, conversions and oil yields were highest for the middle rank coal, PSOC-1498, then the hvAb coal (PSOC-1504) and then the lignite (PSOC-1482); for the Fe catalyst the highest oil yield was produced with the lignite. Overall, the system (Fe + Mo) - (PSOC-1498) gave the highest conversion, oil yield and oil/asphaltene (O/A) ratio. The Fe + Mo system was demonstrably superior to Mo alone and is evidently worthy of continuing investigation.

With increasing rank, the CO_x yield (predominantly CO_2) tended to decrease (as noted in section 2.3.2), while the C_1-C_4 yields did not exhibit any systematic rank trends. However, the C_1-C_4 yield correlates approximately with increasing conversion for the three coals taken together.

2.3.4. Liquefaction in Tetralin

Many of the remarks concerning the two-stage experiments with pyrene also apply to those with tetralin, Tables 2.11, 2.12 and 2.13. The principal difference was that the presence of an active H-donor served to further increase conversion, oil yields and O/A ratios; the magnitude of the response was most evident with the two lower rank coals. The distinctions between the reaction variables, especially the type of catalyst and coal, became less distinct.

In this solvent system, none of the catalysts was unequivocally outstanding. The order of catalyst activities was:

	Conversion	Oil Yield
PSOC-1482	Mo > Fe > Fe + Mo	Mo > Fe > Fe + Mo
PSOC-1498	Mo > Fe + Mo > Fe	Mo > Fe + Mo > Fe
PSOC-1504	Fe + Mo > Mo > Fe	Fe + Mo > Mo > Fe

The Fe catalyst was never the most active and the top honors were shared by Mo and Fe + Mo. It may be worth noting that the iron catalyst was more in contention when used with the lower rank coals. Conversely, the Fe + Mo catalyst was the most active with the hvAb coal.

Compared to pyrene, the differences in product distribution caused by changes in coal and catalyst were not as acute. Given an appropriate catalyst, the three coals appear capable of attaining similar levels of conversion and oil yields. Nevertheless, the general trend was for the oil to asphaltene ratio to decrease with increasing rank.

Under conditions where there is a plenitude of sources of available hydrogen, it may not be possible to readily identify the most active catalyst system, or most appropriate feed coal. Thus, for effective screening, other parameters (compositional) should be monitored or other

Table 2.11. Two-Staged Liquefaction of PSOC-1482 (lignite) in Tetralin

Catalyst	Conversion (% wt)	Yields (% wt)				
		Asphaltenes	Oils	CO_x	C_1-C_4	O/A
None	76.0	41.3	24.8	8.68	1.24	0.60
Mo	89.2	44.4	35.0	8.17	1.67	0.79
Fe	82.3	43.4	26.9	10.41	1.57	0.62
Fe + Mo	80.7	45.4	22.9	10.78	1.59	0.50

First stage: 275°C, 30 min, 7 MPa H_2 (initial pressure)
Second stage: 425°C, 30 min, 7 MPa H_2 (initial pressure)

Mo, 1% wt; Fe, 1% wt; Fe + Mo, 1% wt + 0.1% wt of dmmf coal
Solvent to coal ratio (daf) = 2.0

Table 2.12. Two-Staged Liquefaction of PSOC-1498 (hvCb) in Tetralin

Catalyst	Conversion (% wt)	Yields (% wt)				
		Asphaltenes	Oils	CO_x	C_1-C_4	O/A
None	73.9	52.1	14.1	6.71	0.97	0.27
Mo	92.1	59.2	27.2	3.90	1.75	0.46
Fe	88.5	58.4	21.5	6.69	1.87	0.37
Fe + Mo	90.1	56.3	26.0	5.93	1.83	0.46

First stage: 275°C, 30 min, 7 MPa H_2 (initial pressure)
Second stage: 425°C, 30 min, 7 MPa H_2 (initial pressure)

Mo, 1% wt; Fe, 1% wt; Fe + Mo, 1% wt + 0.1% wt of dmmf coal
Solvent to coal ratio (daf) = 2.0

Table 2.13. Two-Staged Liquefaction of PSOC-1504 (hvAb) in Tetralin

Catalyst	Conversion (% wt)	Yields (% wt)				
		Asphaltenes	Oils	CO_x	C_1-C_4	O/A
None	78.8	62.0	13.7	1.45	1.65	0.22
Mo	89.6	68.1	18.1	1.61	1.84	0.27
Fe	81.0	66.4	7.2	6.16	1.29	0.11
Fe + Mo	92.7	60.6	27.5	2.70	1.92	0.45

First stage: 275°C, 30 min, 7 MPa H_2 (initial pressure)
Second stage: 425°C, 30 min, 7 MPa H_2 (initial pressure)

Mo, 1% wt; Fe, 1% wt; Fe + Mo, 1% wt + 0.1% wt of dmmf coal
Solvent to coal ratio (daf) = 2.0

Table 2.14. Two-Staged Liquefaction of PSOC-1482 (lignite) in 850+°F Process Solvent

Catalyst	Conversion (% wt)	Yields (% wt)				
		Asphaltenes	Oils	CO_x	C_1-C_4	O/A
None	73.6	36.7	26.2	9.14	1.55	0.71
Mo	81.3	45.8	15.1	12.59	7.83	0.33
Fe	84.1	44.8	25.7	11.27	2.37	0.57
Fe + Mo	79.8	49.7	17.4	11.0	1.73	0.35

First stage: 275°C, 30 min, 7 MPa H_2 (initial pressure)
Second stage: 425°C, 30 min, 7 MPa H_2 (initial pressure)

Mo, 1% wt; Fe, 1% wt; Fe + Mo, 1% wt + 0.1% wt of dmmf coal
Solvent to coal ratio (daf) = 2.0

reaction conditions should be selected (e.g. non-donor solvent, evaluation in a continuous process and/or investigating the impact of two-stage liquefaction on the ease of further processing).

2.3.5. Liquefaction in 850+°F Process Solvent

The results obtained with this high-boiling process solvent fraction (Lummus ITSL process) are shown in Tables 2.14, 2.15 and 2.16. Essentially, the results were similar to those obtained with tetralin and rather better than those obtained in pyrene. The catalyst activity rankings were:

	Conversion	Oil Yield
PSOC-1482	Fe > Mo > Fe + Mo	Fe > Fe + Mo > Mo
PSOC-1498	Fe + Mo > Mo > Fe	Fe + Mo > Mo > Fe
PSOC-1504	Mo > Fe + Mo > Fe	Fe + Mo > Mo = Fe

As noted in section 2.3.4, the iron catalyst was more effective with lower rank coals: with this solvent, as with pyrene, the lignite was clearly the most responsive to Fe insofar as oil production was concerned. The Mo and Fe + Mo catalysts were superior for the higher rank coals.

The highest oil yield was obtained with the hvCb coal, although, overall, the performance of this coal and the lignite were comparable. The hvAb coal had lowest propensity for oil production.

Earlier work had shown that this particular process solvent fraction was an effective liquefaction medium (14). It contains a high concentration of condensed aromatics (c. 30% from ^{1}H n.m.r. analysis) which would be expected, like pyrene, to promote H-shuttling and to enhance the solubilization of coal-derived liquids. The presence of H-donors may account for the improved yield structure over that obtained with pyrene.

Table 2.15. Two-Staged Liquefaction of PSOC-1498 (hvCb) in 850+°F Process Solvent

Catalyst	Conversion (% wt)	Yields (% wt)				
		Asphaltenes	Oils	CO_x	C_1-C_4	O/A
None	73.0	55.0	8.7	8.01	1.32	0.16
Mo	90.2	66.1	17.6	4.32	2.15	0.27
Fe	86.4	65.2	12.6	6.37	2.20	0.19
Fe + Mo	93.1	54.1	34.3	3.04	1.63	0.63

First stage: 275°C, 30 min, 7 MPa H_2 (initial pressure)
Second stage: 425°C, 30 min, 7 MPa H_2 (initial pressure)

Mo, 1% wt; Fe, 1% wt; Fe + Mo, 1% wt + 0.1% wt of dmmf coal
Solvent to coal ratio (daf) = 2.0

Table 2.16. Two-Staged Liquefaction of PSOC-1504 (hvAb) in 850+°F Process Solvent

Catalyst	Conversion (% wt)	Yields (% wt)				
		Asphaltenes	Oils	CO_x	C_1-C_4	O/A
None	72.2	55.8	13.2	1.63	1.56	0.24
Mo	89.7	73.8	11.5	1.97	2.40	0.16
Fe	84.8	67.2	11.5	3.91	2.17	0.17
Fe + Mo	88.2	66.9	15.4	3.38	2.50	0.23

First stage: 275°C, 30 min, 7 MPa H_2 (initial pressure)
Second stage: 425°C, 30 min, 7 MPa H_2 (initial pressure)

Mo, 1% wt; Fe, 1% wt; Fe + Mo, 1% wt + 0.1% wt of dmmf coal
Solvent to coal ratio (daf) = 2.0

2.3.6. Liquefaction in Distillate Process Solvent

The experimental results of liquefaction experiments using a distillate process solvent fraction (a 220-500°C boiling H-Coal fractionator bottoms sample from Consolidation Coal Company) are shown in Tables 2.17, 2.18 and 2.19. The data are quite different from those produced with the other solvents and show rather more scatter.

With the lignite (PSOC-1482), the yield structure tended to be rather better than obtained with pyrene; for the hvAb coal (PSOC-1504) it was more comparable (the result with the Fe + Mo catalyst, Table 2.15, must be considered questionable).

However, with the hvCb coal (PSOC-1498, Table 2.18) there was consistent evidence of incompatibility between the solvent and coal, as inferred from the negative oil yields. It was explained in section 2.3.3 that the negative values arise from the method of calculation and mean that, due to solvent incorporation, the asphaltene yield is higher than can be realized by conversion of coal.

When negative oil yields were obtained in earlier temperature-staged research using a distillate process solvent, it was found that condensation occurred during catalytic hydrogenation of the solvent in the absence of coal, resulting in the appearance of hexane-insoluble products (14). If it were simply that the solvent is prone to regressive reactions, it would be expected that similar results would be obtained with the two other coals. That this was not the case, raises the possibilities either that some systematic error was present in these experiments or that the cause was some peculiar combination of properties of the coal and solvent.

Neither suggestion is easy to accept. If the second is genuinely a possibility, it is important to determine the chemistry of the coal-solvent

Table 2.17. Two-Staged Liquefaction of PSOC-1482 (lignite) in Distillate Process Solvent

Catalyst	Conversion (% wt)	Yields (% wt)				
		Asphaltenes	Oils	CO_x	C_1-C_4	O/A
None	62.8	37.0	14.8	9.24	1.74	0.40
Mo	87.8	47.0	31.0	7.73	2.05	0.66
Fe	78.0	50.6	15.8	9.64	1.98	0.31
Fe + Mo	73.5	49.7	12.0	10.02	1.74	0.24

First stage: 275°C, 30 min, 7 MPa H_2 (initial pressure)
Second stage: 425°C, 30 min, 7 MPa H_2 (initial pressure)

Mo, 1% wt; Fe, 1% wt; Fe + Mo, 1% wt + 0.1% wt of dmmf coal
Solvent to coal ratio (daf) = 2.0

Table 2.18. Two-Staged Liquefaction of PSOC-1498 (hvCb) in Distillate Process Solvent

Catalyst	Conversion (% wt)	Yields (% wt)				
		Asphaltenes	Oils	CO_x	C_1-C_4	O/A
None	55.0	71.9	-18.3	0.57	0.75	--
Mo	77.8	77.8	- 3.0	2.21	0.76	--
Fe	68.0	76.0	-13.0	4.09	0.87	--
Fe + Mo	91.8	94.7	- 9.3	4.60	1.84	--

First stage: 275°C, 30 min, 7 MPa H_2 (initial pressure)
Second stage: 425°C, 30 min, 7 MPa H_2 (initial pressure)

Mo, 1% wt; Fe, 1% wt; Fe + Mo, 1% wt + 0.1% wt of dmmf coal
Solvent to coal ratio (daf) = 2.0

Table 2.19. Two-Staged Liquefaction of PSOC-1504 (hvAb) in Distillate Process Solvent

Catalyst	Conversion (% wt)	Yields (% wt)				
		Asphaltenes	Oils	CO_x	C_1-C_4	O/A
None	71.6	62.4	6.2	1.58	1.46	0.10
Mo	89.1	76.2	8.7	1.84	2.37	0.11
Fe	65.7	54.8	6.9	2.40	1.57	0.13
Fe + Mo	81.5	51.1	26.4	2.21	1.79	0.52

First stage: 275°C, 30 min, 7 MPa H_2 (initial pressure)
Second stage: 425°C, 30 min, 7 MPa H_2 (initial pressure)

Mo, 1% wt; Fe, 1% wt; Fe + Mo, 1% wt + 0.1% wt of dmmf coal
Solvent to coal ratio (daf) = 2.0

interactions which can render such effects. The subject cannot be pursued further in this program.

Before leaving this topic, it is germane to mention that the composition of designer solvents is often considered without due reference to coal structure. Tacitly, it is assumed that the ideal solvent, with appropriate H-donor, H-shuttling and other properties will be suitable for all coals. Thus it has long been recognized that certain solvent characteristics are preferable to others (16).

Given the extent of the structural changes over the range of coal rank which is of interest to direct liquefaction (which is reflected by significant differences in the composition of the liquefaction products) it is not unreasonable to suppose that the composition of the most effective solvent will require adjustment to suit the characteristics of individual coals.

2.3.7. Hydrogen Consumption

The net consumption of gaseous hydrogen is shown in Table 2.20 for all of the experiments described in sections 2.3.2 to 2.3.6. No correlation appears to exist between the figures in the Table and coal conversion, oil yields or solvent type.

In the solvent-free experiments, the ratio of the yield of light hydrocarbon gases to conversion was, in most instances, higher than in solvent liquefaction, although the actual conversions were much lower. The disproportionate production of hydrogen-rich gases can account for much of the increased hydrogen uptake.

Depending upon its composition, the solvent can reduce the consumption of molecular hydrogen by providing a source of labile hydrogen and aiding in the redistribution of hydrogen in the slurry phase, thereby reducing

Table 2.20. Net Consumption of Gaseous Hydrogen in Temperature-Staged Experiments (% wt dmmf coal)

		Solvent				
	Catalyst	None	Pyrene	Tetralin	850+°F Solvent	Distillate Solvent
PSOC-1482 (lignite)	None	0.61	0.56	0.53	0.57	0.83
	Mo	1.97	2.15	2.44	2.31	2.95
	Fe	1.41	1.22	2.30	1.76	1.79
	Fe + Mo	1.89	2.07	1.94	1.94	2.24
PSOC-1498 (hvCb)	None	0.50	0.75	0.41	0.50	0.12
	Mo	1.12	2.11	1.90	2.76	1.72
	Fe	0.71	1.15	1.02	1.15	1.30
	Fe + Mo	1.22	2.48	1.82	1.54	2.35
PSOC-1504 (hvAb)	None	0.18	0.36	0.24	0.22	0.22
	Mo	1.43	1.85	1.80	2.48	2.19
	Fe	0.50	0.89	0.86	0.52	0.63
	Fe + Mo	0.94	1.58	1.56	1.51	1.50

inefficiencies which can increase hydrogen demand. It is therefore rather surprisingly that there appears to be no relationship between solvent type and hydrogen consumption.

The hydrogen consumption does, however, correlate with coal rank and catalyst composition. With some exceptions, when the solvent and catalyst type are held constant, the amount of hydrogen consumed is seen to decrease with increasing coal rank. The trend is predictable and follows the decrease in coal oxygen content with increasing rank (Table 2.1, section 2.2.1).

A comparison of the catalysts shows that the net hydrogen consumption follows the order of catalyst activity with respect to conversion and product distribution. The Fe catalyst consistently gave the lowest values; the data for the Fe + Mo and Mo catalysts were quite similar, neither being clearly superior to the other.

2.3.8. Solvent Swelling of Liquefaction Residues

The THF-insoluble products from the various temperature-staged liquefaction experiments were characterized by measuring the extent of their swelling in pyridine. The experimental method (see section 2.2.4) allows the quantitative measurement of a swelling ratio, Q (see Liotta and others, 2; Green and others, 5). The value of the swelling ratio is determined by the quotient h_2/h_1, where h_1 is the original height of a column of coal (or residue) in a glass tube after centrifuging, and h_2 is the centrifuged height after soaking for 3 days in pyridine. The Q values are summarized in Table 2.21 and presented graphically as a function of residue yield in Figures 2.1-2.3.

The cause of swelling in coals and residues is considered to be due to the reorientation of macromolecular chains located between non-covalent

Table 2.21. Swelling Ratio (Q) in Pyridine of Liquefaction Residues (THF-insolubles, temperature-staged reaction)

		Solvent		
	Catalyst	None	Tetralin	Process Distillate
PSOC-1482 (lignite)	None	2.1	2.1	1.8
	Mo	1.8	1.7	1.4
	Fe	2.1	1.5	1.7
	Fe/Mo	2.7	1.8	1.6
PSOC-1498 (hvCb)	None	1.7	1.8	1.4
	Mo	1.3	1.5	1.2
	Fe	1.6	1.7	1.7
	Fe/Mo	1.6	1.3	1.1
PSOC-1504 (hvAb)	None	1.9	1.5	1.6
	Mo	1.6	1.5	1.5
	Fe	1.7	1.7	1.5
	Fe/Mo	1.6	1.6	1.3

crosslinks, such as hydrogen bonds, when these particular linkages are weakened by solvent interactions. The extent of swelling is a measure of the density of covalent crosslinks and will be a function of the coal structure and its thermal history. Suuberg and others (17) have shown that mild thermal treatment of a low-rank coal reduces the swelling ratio. It is supposed that there is an increase in cross-link density resulting from the thermally-initiated condensation of, primarily, oxygen-containing groups.

The swelling ratio of liquefaction residues decreases with conversion due to the increased concentration of more highly cross-linked components. These may include the less reactive constituents of vitrinite and inertinite macerals and also vitrinite components which have the potential to be liquefied but have been rendered more refractory by condensation reactions, perhaps representing localized hydrogen deficiencies (18).

Consistent with the foregoing, it can be seen from Figures 2.1-2.3 that the swelling ratio decreases with increasing conversion, despite the wide scatter of the results. Overall, the highest swelling ratios were obtained with the residues from lignite liquefaction. The overlap of the data for the other two coals is such that no further distinction can be made with any degree of confidence. For coals (as opposed to residues), the propensity for swelling increases with decreasing coal rank (19).

The implication that there is a lower cross-link density in low-rank coals is consistent with their high reactivity in combustion, gasification and liquefaction, provided that the reaction conditions counter the ready tendency of these coals to cross-link. The higher proportion of weak crosslinks of low-rank coals, coupled with the smaller size (as is believed) of their structural units contributes to the production of coal

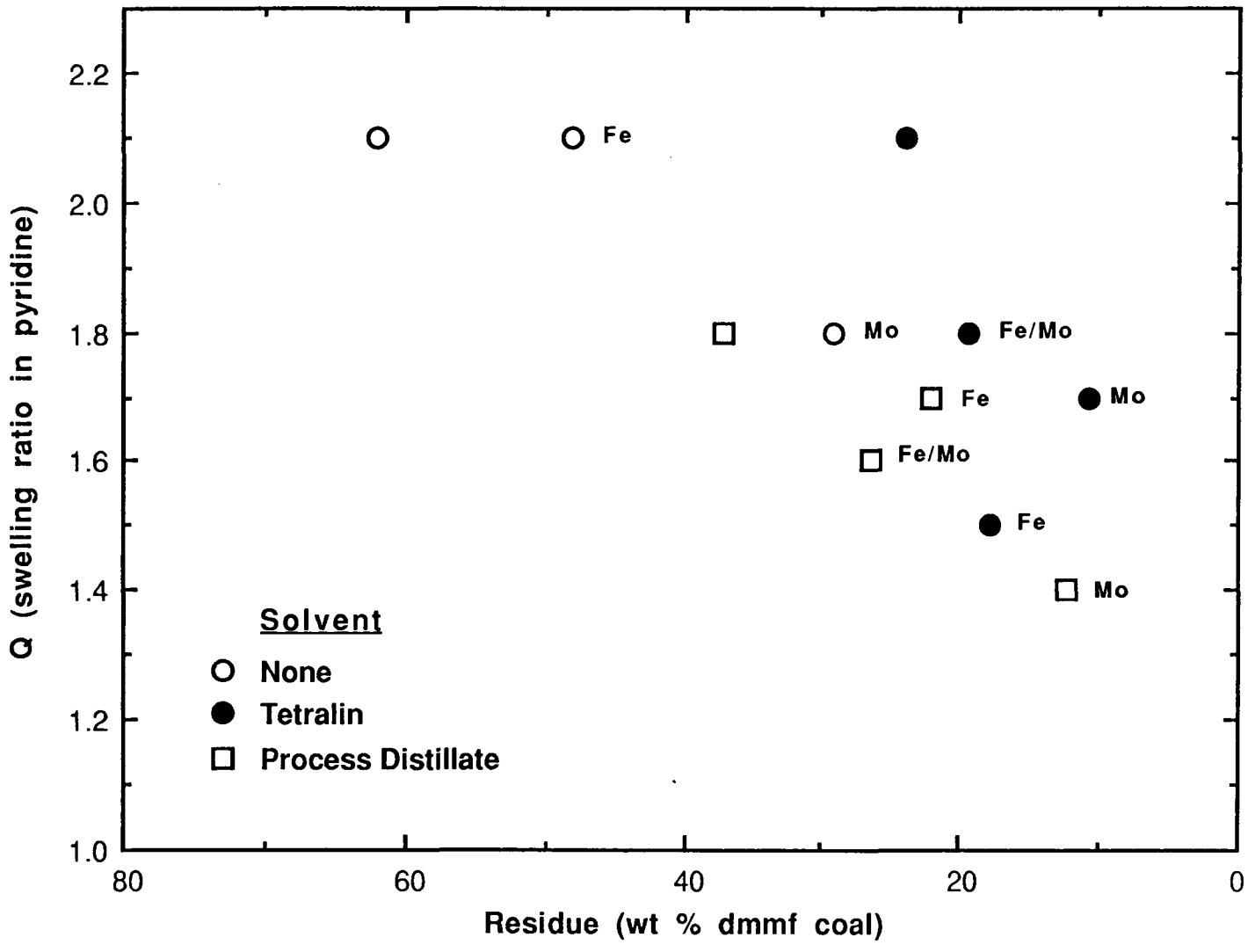

Figure 2.1 Swelling Ratios of THF-insoluble Residues (temperature-staged liquefaction of lignite, PSOC-1482)

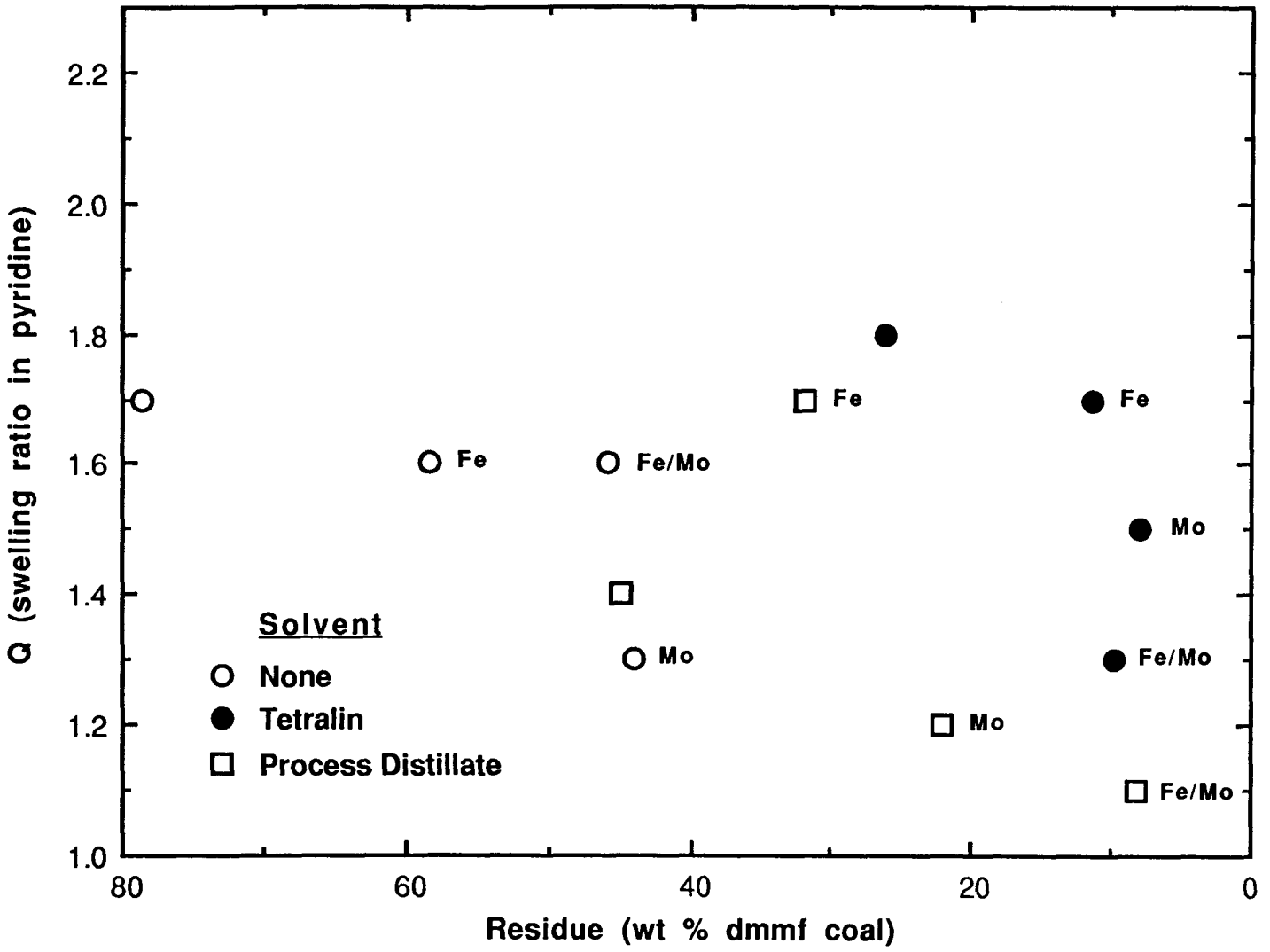

Figure 2.2 Swelling Ratios of THF-insoluble Residues (temperature-staged liquefaction of hvCb coal, PSOC-1498)

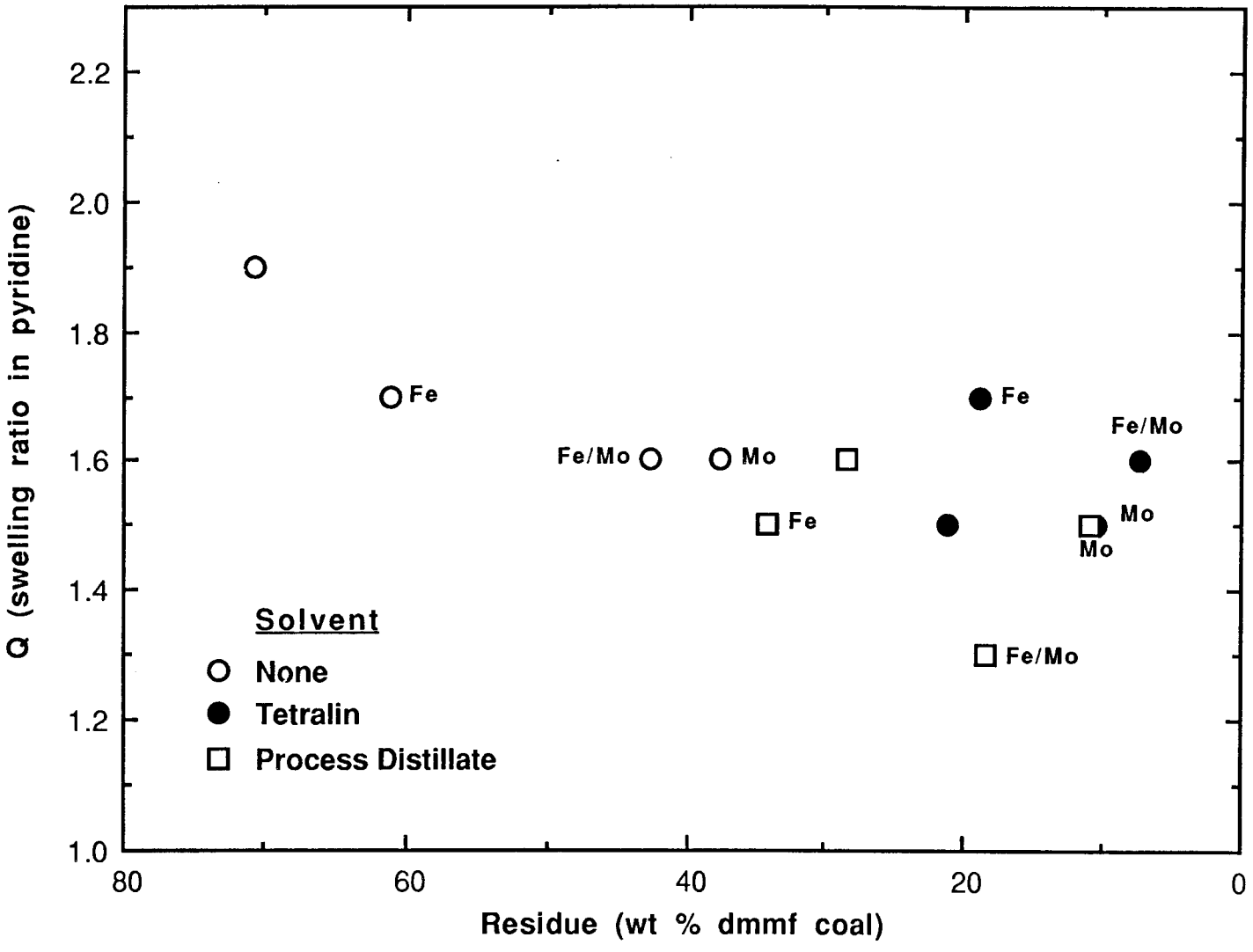

Figure 2.3 Swelling Ratios of THF-insoluble Residues (temperature-staged liquefaction of hvAb coal, PSOC-1504)

liquids which are more volatile and of lower molecular weight than the corresponding liquids from bituminous coals (see Derbyshire and Stansberry, 20). Further weight is added to the statements by the results described in sections 2.3.2-2.3.6; in particular, the lignite and hvCb coal gave significantly higher oil yields than the hvAb coal.

From the figures, it is apparent that for each of the coals the swelling ratios are higher relative to the degree of conversion after liquefaction in tetralin than in the process distillate or in the solvent-free experiments. An obvious inference is that, with the donor solvent, there is a lower probability that cross-linking in the non-solubilized coal material will increase due to regressive reactions. This is really the same logic which is used to explain the greater ability of H-donor solvents to liquefy coals.

For a given coal-solvent system, there is some suggestion that the residues from Fe-catalysed reactions have a higher swelling ratio relative to conversion than those from thermal reactions or catalyzed by Mo and Fe + Mo. This effect is least evident with the highest rank coal and in the presence of tetralin. Further discussion of the possible significance of these observations will be given in section 2.3.10.

2.3.9. Reactions of Model Compounds

In an attempt to identify some of the functions of the sulfided Mo catalyst, a series of thermal and catalytic hydrogenation experiments were performed with selected model compounds under the conditions used for liquefaction.

The experiments reproduced the conditions used in the first stage (275°C), second stage (425°C) and combined temperature-staged sequence.

2.3.9.1. Experimental Procedure

The tubing bomb reactor was charged with 5 g of the pure compound (> 98% purity), purged twice with nitrogen and then three times with hydrogen before pressurizing to a cold hydrogen pressure of 7 MPa. Reaction conditions were 275°C, 30 min; 425°C, 30 min; both reactions in series.

For catalytic experiments, those compounds which are solid at room temperature were mixed with ammonium tetrathiomolybdate using a mortar and pestle. The liquid compounds were admixed with the catalyst by vigorous shaking. In all cases, the loading was 1% wt of molybdenum.

Following reaction, gas samples were analyzed by chromatography for CO, CO_2 and C_1-C_4 hydrocarbons. The nongaseous products were dissolved in CH_2Cl_2 and examined on a 30m SPB-5 bonded-phase capillary column. Product identification was not attempted. Instead, the time of elution of components from the column was used to indicate their approximate boiling point by reference to a calibration curve.

Product yields were estimated from integrated peak areas. The assumption was made that the flame ionization detector responds primarily to the number of carbon atoms per molecule. Significant departures are expected for oxygen-containing compounds. Moreover, the calculation does not take into account those products which are insoluble in methylene chloride or which do not elute from the column.

To minimize possible 'memory' effects, due to residual catalytic activity, and to prevent contamination from other model compounds, the reactors were deactivated before each experiment. The deactivation step involved a blank run, in which the chosen model compound was thermally reacted in a particular tubing bomb. The reactor was then washed

thoroughly with THF and dried for 1 h at 100°C. Following this procedure, the subject experiment was performed with the same model compound in the same reactor.

The model compounds used in these experiments are shown in Table 2.22.

2.3.9.2. First-Stage (275°C) Reaction

The changes produced in thermal and catalytic reactions under first-stage conditions are summarized in Table 2.23.

In the case of p-hydroxybenzaldehyde, no peaks could be detected because the product, formed either thermally or catalytically, was insoluble in CH_2Cl_2. This substance was the only one that produced detectable quantities of light gases. In all other cases, gas production was negligible. In thermal hydrogenation, p-hydroxybenzaldehyde liberated considerable amounts of CO_2. Catalytic hydrogenation produced still greater amounts of CO_2 and, in addition, appreciable quantities of CO. No other gases were detected.

Further examination of the Table 2.24 reveals some clues about the functions of the catalyst in low-temperature hydrogenation. The reaction of pyrene suggests that the catalyst is quite effective in hydrogenating condensed aromatics. Low temperatures create a favorable thermodynamic driving force for such reactions and, as suggested in section 2.3.1, they may well be the single most important cause of the gains attributable to temperature-staged reaction.

The catalyst also appears to be selective in the type of linkages which are broken. There was no appreciable cleavage of aryl-aryl, alkyl-aryl or alkyl-aryl-ether bridges but changes were observed with aryl-ketones and aryl and phenyl-ethers. It would have been informative to have made a comparison of Fe and Fe/Mo catalysts as the inferred

Table 2.22 Structures and Some Physical Properties of Model Compounds

		Melting Point °C	Boiling Point °C
* 3,5-dimethyl-phenol	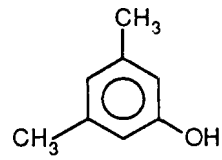	68	219
Diphenyl ketone	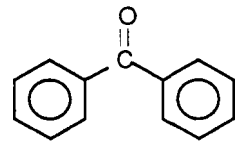	48	306
* P-hydroxybenzaldehyde	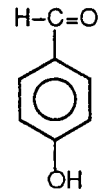	117	-
* Tetrahydro-1-naphthol	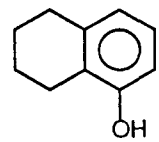	70	265
Bibenzyl	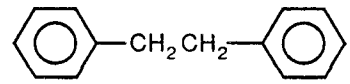	52	285
Biphenyl	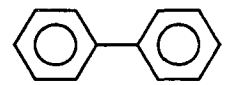	71	256
Pyrene	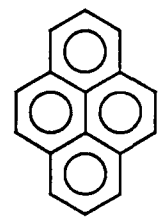	156	393
* Benzyl ether	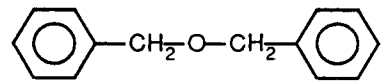	36	298
Phenyl ether	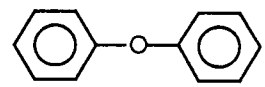	27	258
* Phenyl-ethyl-ether	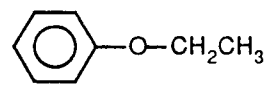	-29	170
* Decahydronaphthalene	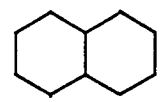	-43	195

* Studied only under first-stage (275°C) conditions

Table 2.23. Number of Products Generated by Model Compound Reactions (275°C, 30 min, 7 MPa H_2)

Compound	Thermal		Catalytic	
	Number of Products	Level of Change	Number of Products	Level of Change
3, 5 dimethylphenol		0		0
diphenyl ketone		0	-2, +1	L
p-hydroxybenzaldehyde		I		I
tetrahydro-1-naphthol	+1	S		0
bibenzyl	-1	S		0
biphenyl		0		0
pyrene		0	-4	L
benzyl ether	-8, +3	L	-8, +3	L
phenyl ether		0	-1	S
phenyl-ethyl-ether	+1	S		0
decahydronaphthalene		0		0

Code: Negative = lower boiling; Positive = higher boiling
0 = negligible change
S = small effect
L = large
I = indeterminate

Table 2.24. Number of Products Generated by Model Compound Reactions (425°C, 30 min; 275°C, 30 min + 425°C, 30 min; 7 MPa H_2)

	Second Stage		Temperature-staged
Compound	Thermal	Catalytic	Catalytic
diphenyl ketone	-3, +2	-8, +7	-5, +4
bibenzyl	-3, +2	-4, +1	-5, +3
biphenyl	-1, +1	n.c.	+1, -2
pyrene	-5	-5	-8
phenyl ether	n.c.	-2, +1	-8

Code: Negative = lower boiling; Positive = higher boiling
n.c. = no change

interaction of Fe with oxygen functionalities (section 2.3.10) might have been ratified. Unfortunately, time did not allow for the inclusion of additional studies and these considerations must be reserved for future work.

The Mo catalyst may also have a stabilizing effect on the fragmentation of some structures: tetrahydro-1-naphthol, bibenzyl and phenyl-ethyl-ether reacted under thermal but not under catalytic conditions.

2.3.9.3. Second Stage and Temperature-Staged Reactions

The results of the reactions of five model compounds under second-stage and temperature-staged conditions are given in Table 2.24. Consistent with the higher reaction temperatures used in these experiments, greater numbers of reaction products were formed than at 275°C. The effects of the various reaction conditions on product yields and their established boiling points are shown in Figures 2.4-2.8. The horizontal lines on the figures show the boiling points of the parent compounds.

The high stability of biphenyl is indicated by the small number and low yields of products which were generated only under the more severe reaction conditions (Figure 2.4). There were no detectable gaseous products. The highest yields were obtained under thermal conditions.

The catalyst had more direct influence on bibenzyl conversion (Figure 2.5). The highest product yields were obtained in the presence of catalyst and under temperature-staged conditions. The anticipated reactions of bibenzyl are hydrocracking to produce toluene and ethyl benzene, which is consistent with the estimated boiling points around 110°C and 136°C. Methane and ethane were detected in small quantities.

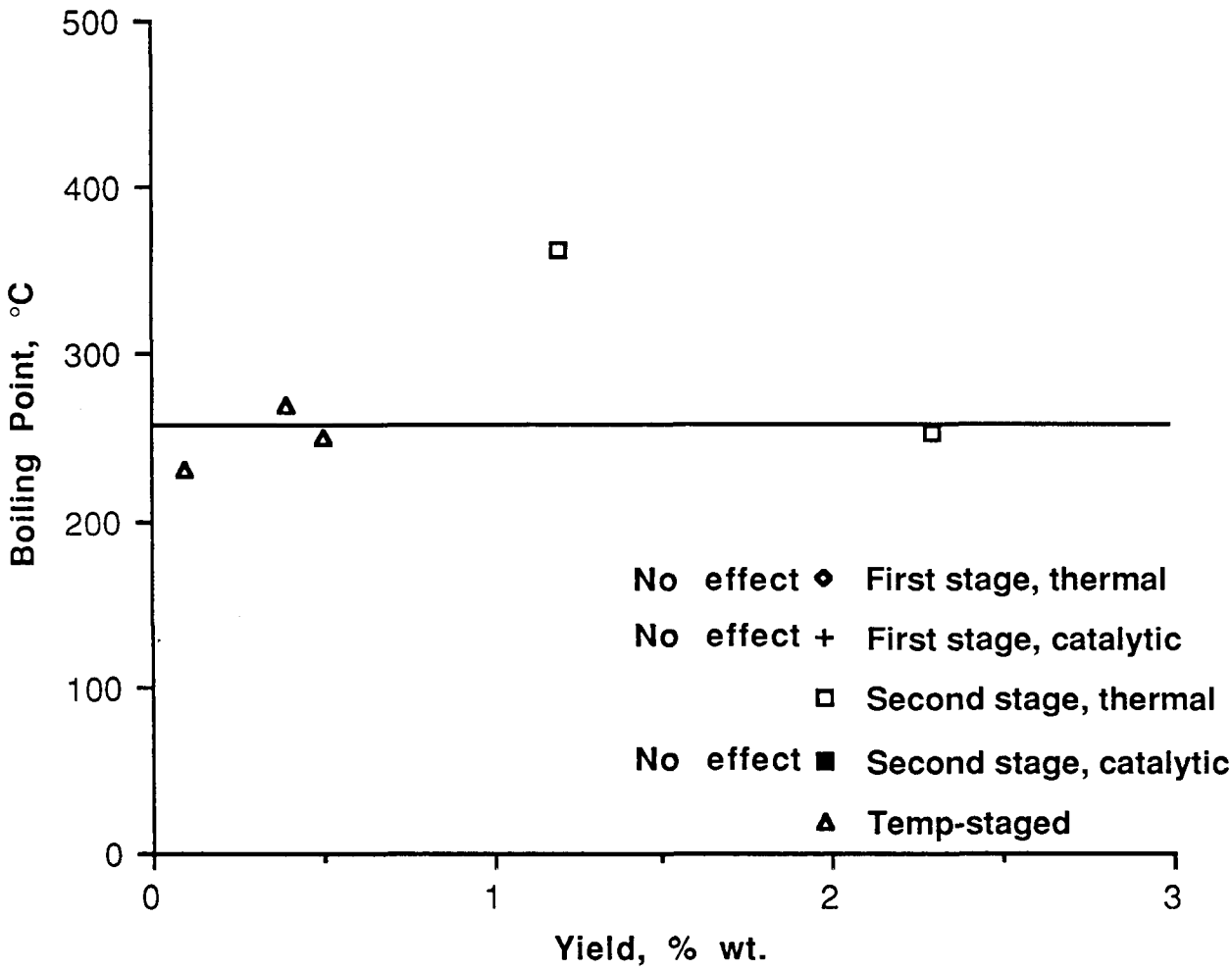

Figure 2.4 Boiling-Point Distribution of Products Derived from Biphenyl

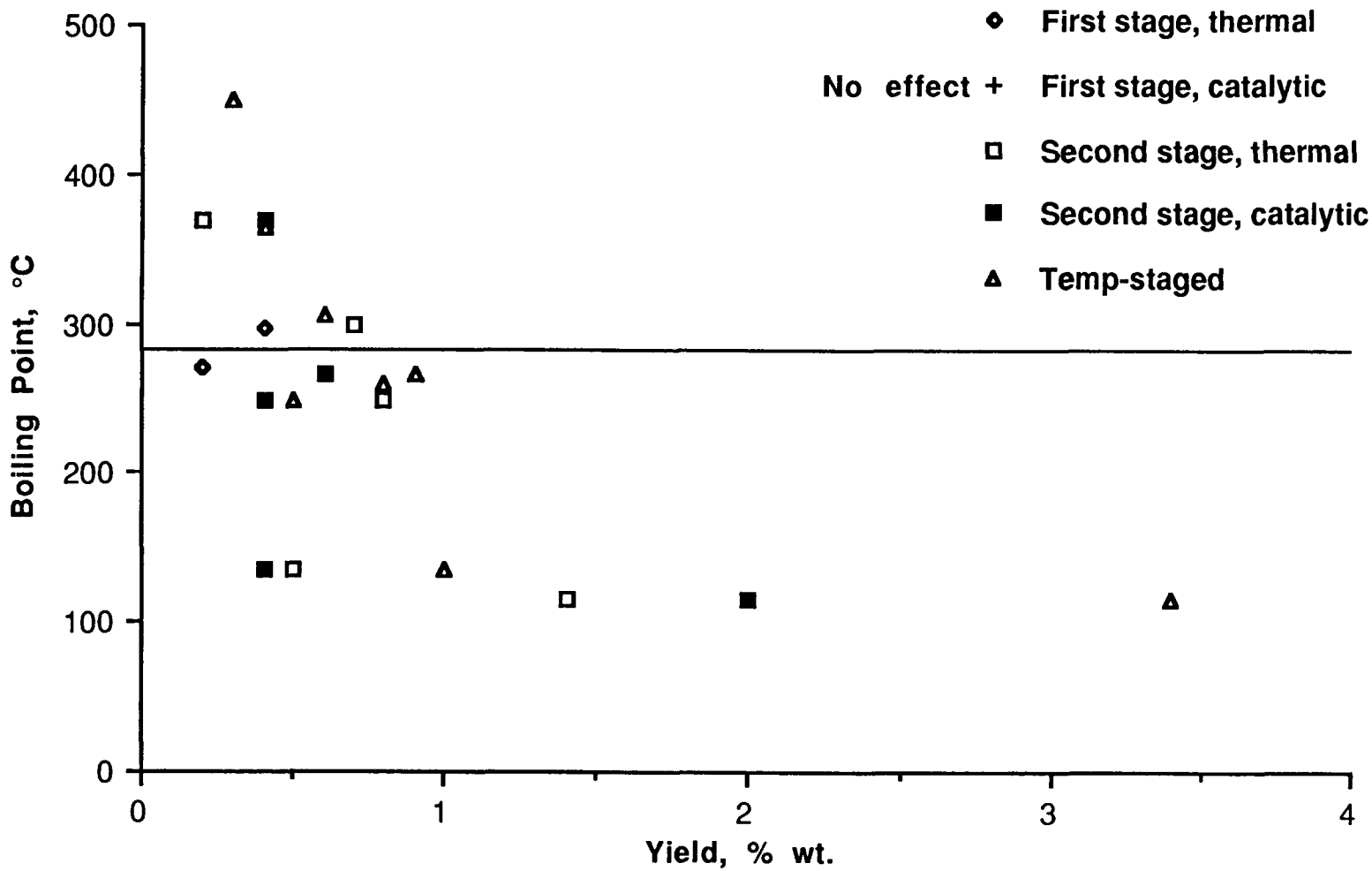

Figure 2.5 Boiling-Point Distribution of Products Derived from Bibenzyl

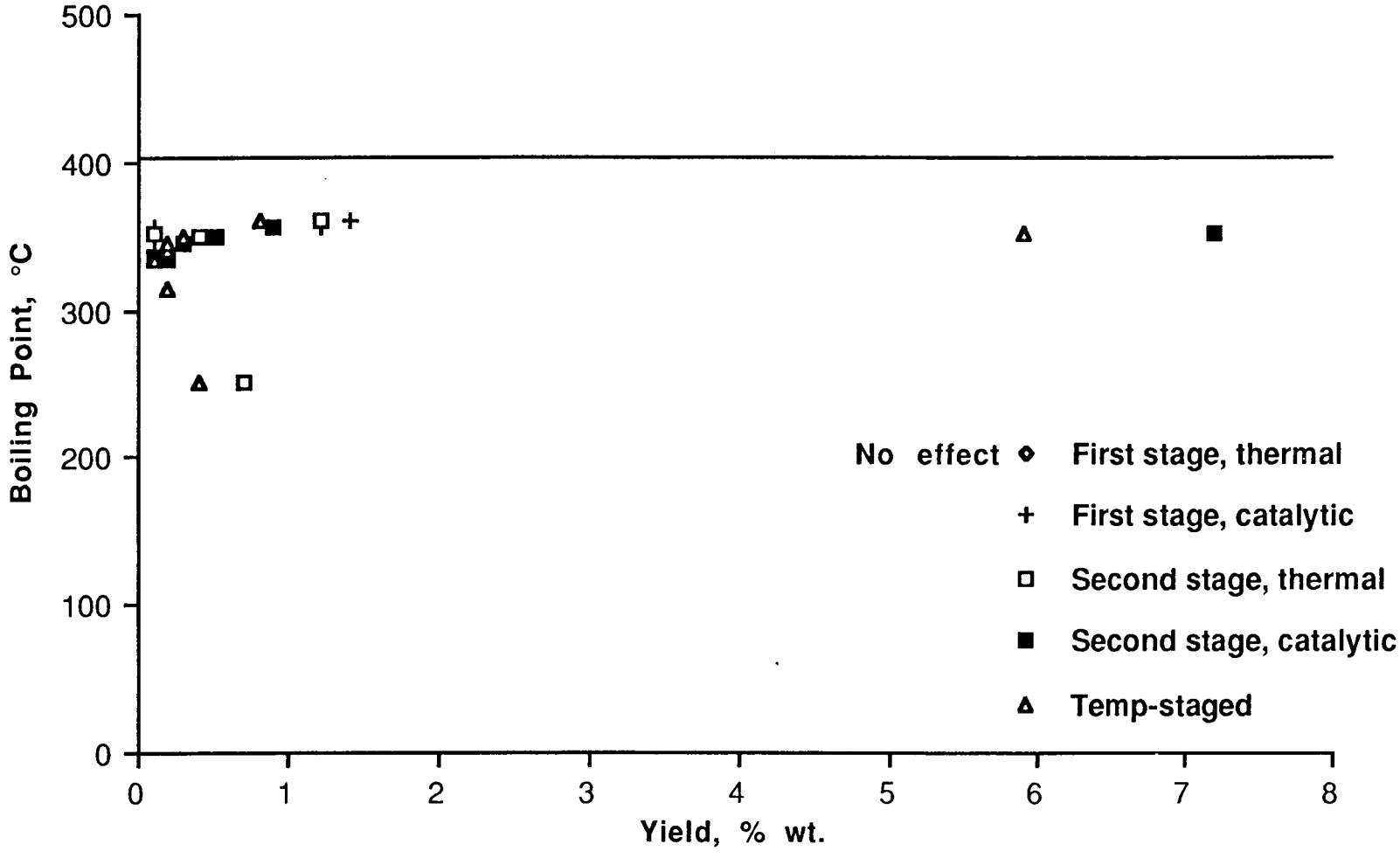

Figure 2.6 Boiling-Point Distribution of Products Derived from Pyrene

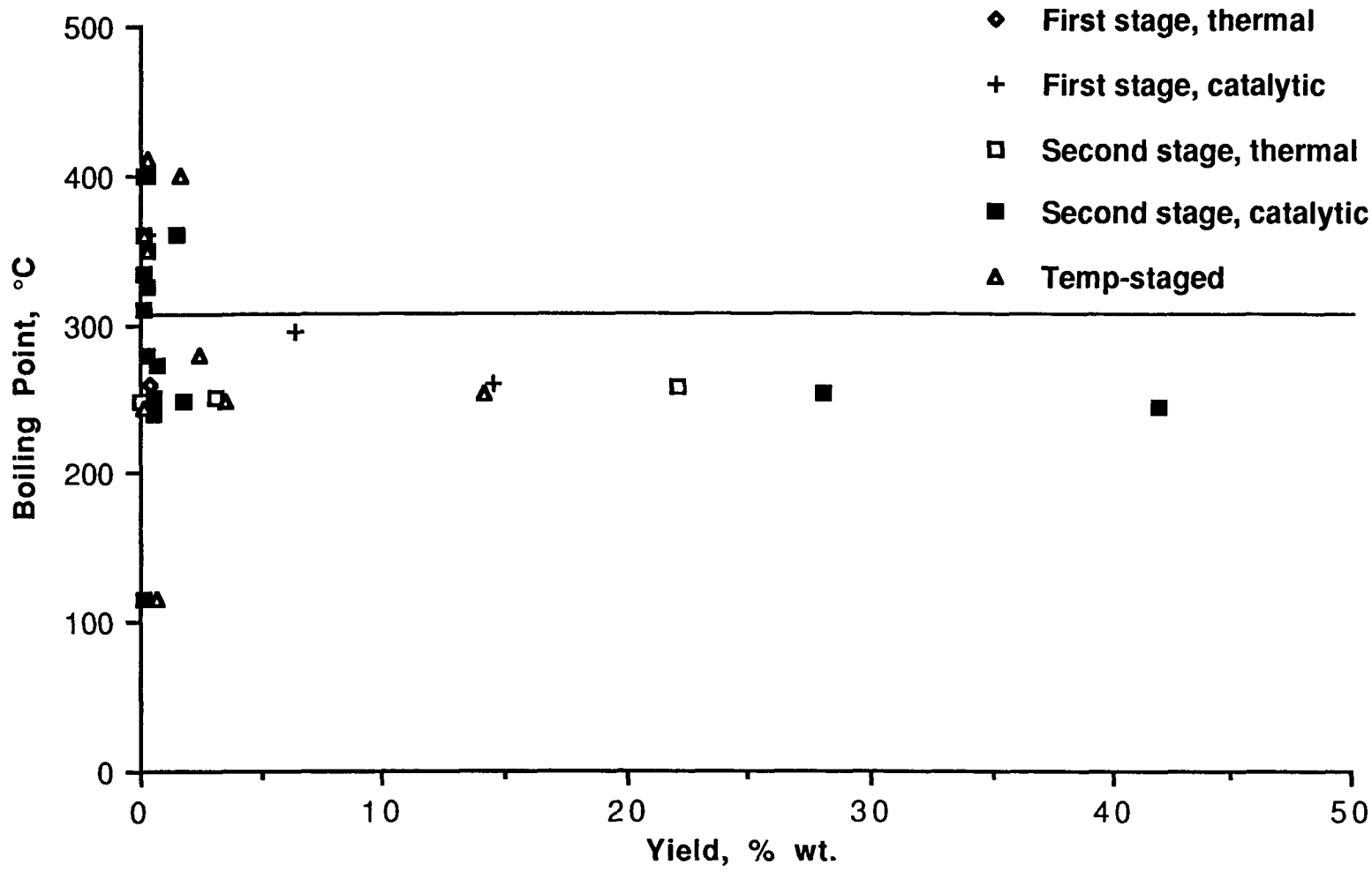

Figure 2.7 Boiling-Point Distribution of Products Derived from Diphenyl-Ketone

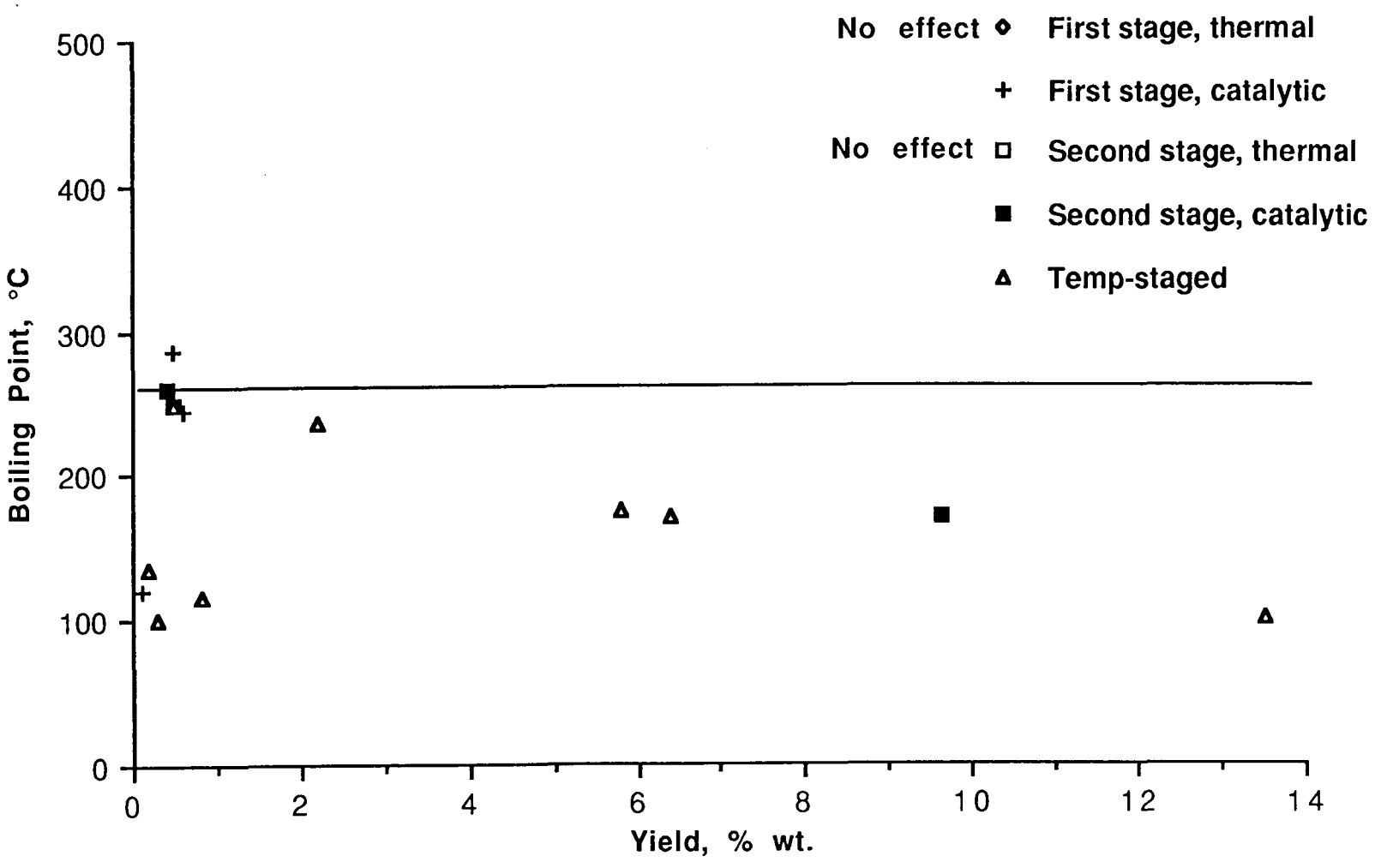

Figure 2.8 Boiling-Point Distribution of Products Derived from Phenyl-ether

Most of the products from pyrene had boiling points in the range 310-350°C (Figure 2.6). It is reasonable to assume that these were all hydro-derivatives. The highest yields were only obtained after catalytic hydrogenation at 425°C. The generation of small quantities of a compound boiling at about 250°C is suggestive of ring opening reactions.

The boiling point of the principal product from the reactions of diphenyl ketone corresponds approximately to that of diphenylmethane (Figure 2.7). Less was produced in temperature-staged reaction than in single-stage, high-temperature thermal or catalytic reactions. In catalytic, high-temperature reactions, very small amounts of a low-boiling compound were formed. This could well be toluene, which is a product of cracking diphenylmethane. The co-product is benzene, which was not detected.

For phenyl ether, temperature-staged reaction and the presence of catalyst gave rise to highest yields (Figure 2.8). From the boiling point estimates, the principal products could well be benzene and phenol.

While the results of this limited survey are far from conclusive, they have indicated that the main functions of the Mo catalyst are to promote hydrogenation and cracking reactions. This essentially endorses previous suppositions.

At low temperature (275°C), the extent of hydrogenation is only moderate, even though it is thermodynamically favored, and the limitations must be kinetic. Weak oxygen-containing linkages are attacked but stronger bonds are not affected. Hydrogenation and the cleavage and stabilization of weak links are believed to be the main low-temperature processes which facilitate control of subsequent reactions at higher temperature and lead

to the overall conversion and selectivity gains of temperature-staged liquefaction.

At higher temperature (425°C), hydrogenation proceeds more rapidly, strong connecting bonds are cleaved and conditions begin to favor ring-opening reactions.

2.3.10. Discussion

A large number of experiments have contributed to the data which have been presented in this Chapter. In some cases, there have been unexpected results which may indicate scatter or problems with the experimental method, or be indicative of new and relevant facets of liquefaction chemistry. Until such time as further studies are made, and in some detail, these findings must remain open to interpretation. There are, in addition, a number of evident trends and observations which are supported by considerable weight of evidence and these will be outlined in this section.

In temperature-staged liquefaction, the work here and elsewhere (6-18) has shown that, while the presence of catalyst in the first, low-temperature hydrogenation stage is essential to realizing the overall gains from liquefying in stages of increasing temperature, there is little obvious difference between thermal and catalytic reaction at low temperature. That is, the total conversion and product distributions are similar. The effect of the catalyst must be quite subtle and the nature of the changes wrought in the presence of catalyst must be sought by other investigative methods.

As shown by the model compound studies (Section 2.3.9), the sulfided Mo catalyst can effect mild hydrogenation and the cleavage of weak (primarily oxygen-containing) linkages under first-stage conditions.

Consistent with these findings, low-temperature solvent-free catalytic hydrogenation has been shown to increase the extent of swelling in pyridine thereby providing evidence of the severing of a limited number of crosslinks (6). It is anticipated that there would also be a measurable increase in volatile yield, as determined by proximate analysis. Indeed, pyrolysis techniques might be usefully employed to study the chemistry of low-temperature coal hydrogenation (see Bolton and others, 10).

Temperature-staged liquefaction conditions mute the effects caused by altering various reaction parameters. The magnitudes of changes in product yields are much less than are found in single-stage, high-temperature reactions. Previous studies (14) showed that catalytic temperature-staged liquefaction could accommodate quite significant changes (reductions) in solvent quality before the consequences became significant. Generally, the work reported here has revealed surprisingly small effects due to quite large shifts in solvent type. Differences in liquid product distribution attributable to coal rank were also less than expected. From a process standpoint, this can only be considered advantageous; the relative insensitivity to changes in process conditions will allow easier control and steadier operation. For fundamental research, it means that it is more difficult to study the impact of different variables on the liquefaction process. In a sense, the situation is rather like attempting to rank catalysts for a reaction which is close to equilibrium. Either different analytical measurements must be sought or different conditions employed for this research.

The foregoing comments notwithstanding, an examination of the present data shows quite conclusively that it is preferable to have a donor

solvent, catalyst and hydrogen overpressure in both low- and high-temperature stages.

With respect to coal rank, the lower rank coals exhibit greater potential for oil production. While the present data base includes only four coals, the general validity of this conclusions is strongly supported by the result of other studies (see Derbyshire and Stansberry, 20; Snape and others, 21).

Fundamentally, caution must be exercised in making sweeping statements about the relative activities of the three catalysts investigated here, since so many factors can influence their behavior. From a pragmatic standpoint, it can be reasonably argued that if one catalyst could be superior provided that conditions were finely tuned to optimize its activity, then it is not a realistic proposition. The best practical choice is that catalyst, or catalyst precursor, which is sufficiently robust to perform adequately under non-ideal circumstances. Both of these positions have their logic. In the current research, the Mo and Fe + Mo catalysts proved to be superior to the iron catalyst under all of the conditions which were studied. The superiority of Mo and Fe catalysts has been concluded from numerous other studies (9,11-13). Synergism for Fe + Mo catalysts has also been recorded (30) as well as for other metal combinations (see Derbyshire, 9).

As discussed earlier, the high activity of the two-component catalyst is of particular note since the molybdenum was present at one tenth of its concentration in the Mo catalyst. Synergistic (non-additive) affects of using catalysts in combination are of interest for at least two reasons; the exciting potential which this offers for the development of new and enhanced activity dissolution catalysts and/or the ability to reduce

catalyst cost by the partial substitution of a less expensive catalyst component whilst retaining the same level of activity.

The existence of synergism in catalysis can be understood to imply that the presence of the second component somehow alters or 'promotes' the chemical state of the first, in which case one component is seen in a supporting role. Alternatively, it can be viewed that the two components exert individual and complementary effects, each providing a function or functions which the other does not. The authors incline to the second possibility for the reasons which are expanded below.

The principal functions of sulfided molybdenum catalysts are generally believed to be that of hydrogenation, hydrodesulfurization and hydrocracking (13). The specific functions of Fe catalysts are not well defined. However, since they undoubtedly catalyze coal dissolution, they must possess generally similar attributes to Mo. They are, however, less effective and, as shown in section 2.3.7, are less able to utilize gaseous hydrogen. Relatedly, Fe appears to be less active than Mo for hydrocracking reactions. Gary and Givens (22) showed that at similar levels of converion (ca 85%) with Fe (1 wt%) and Mo (0.02 wt%) catalysts, the yield of oils was higher and the yields of asphaltenes and preasphaltenes were lower for Mo than Fe.

Montano (23) has reported that iron sulfide surfaces are involved in the cleavage of oxygen bonds in coals and coal-derived products. Similarly, Tekely and others (24) found that pyrite promoted the cracking of ether bridges, even in the absence of gaseous hydrogen. The interactions of Fe catalysts with oxygen groups is further indicated in the present work. The difference in activity between the iron catalysts and the other two catalysts distinctly decreased with decreasing coal rank,

that is with increasing coal oxygen content (see Table 2.1). The pyridine swelling ratios tended to be higher, at similar conversion levels, for the residues from Fe-catalyzed reactions, suggesting an ability to break and stabilize crosslinks (selective towards oxygen-containing linkages?).

A tentative interpretation of the foregoing is that, Fe and Mo can act in concert, iron selectively attacking oxygen-containing linkages and molydenum providing strong hydrogenation activity.

Reaction with coal oxygen will tend to remove sulfur from the catalyst. The importance of H_2S partial pressure during catalytic liquefaction is consistent with a need to maintain the catalyst in a sulfided form and to control its composition. The reversability of catalyst oxidation and sulfidation may be intrinsic to the reaction mechanism.

It has been suggested that hydrogenation catalysts may promote the initial reactions leading to coal dissolution by an indirect route. Through a hydrogen spillover mechanism, hydrogen atoms are generated at catalyst sites and migrate to the ipso positions of linkages to aromatic systems where they actively induce bond cleavage. Equally, HS radicals produced by the catalyst dissociation of H_2S could perform a similar function (see Derbyshire, 9). These mechanisms which are based upon the work of McMillen and others (25-27), Vernon (28) and Hei and others (29), can account for the ability of the catalyst to promote dissolution when, even at high dispersion, the catalyst particles must be remote in atomic dimensions from most of the bonds which are broken.

Hydrogen spill-over has been invoked to account for the catalytic hydrogenation of organic solids (30). The H-atoms thus produced will increase the pool of hydrogen available within the coal and will be

available for aromatic hydrogenation as well as bond cleavage reactions. The latter will depend upon the nature of the bond and the reaction temperature.

The proposition implies that hydrogenation catalysts will all be effective in the same temperature range, since bond scission will depend ultimately upon a thermal reaction involving H atoms. Charcosset and others (31) have reported some experimental results which lend support to this hypothesis. These workers followed the changes in reactor pressure and temperature during bituminous coal conversion in the presence of various catalysts. For sulfided Sn, Fe and Mo catalysts there was a break in the pressure curve at about 370°C, indicative of the onset of measurable hydrogen consumption.

The threshold temperature for conversion is, however, coal dependent, as it will be determined by the strength and density of the structural crosslinks and, as expected, it decreases with decreasing coal rank (21 and 32). Taken together with the smaller size of structural units in low-rank coals, this begins to explain the increase in the potential for oil production with decreasing rank.

The spillover mechanism will be less significant if the catalyst is poorly dispersed and/or is not especially active for dissociating molecular hydrogen. Both factors could explain the markedly lower activity of the Fe catalyst in solvent-free liquefaction, compared to Mo and Fe + Mo, than when solvent was present. The addition of solvent provides a medium which can augment dispersion and assist in the transport of hydrogen atoms to sites within the coal.

REFERENCES

1. Yarzab, R.F., Given, P.H., Spackman, W. and Davis, A., 1980, Fuel, 59, 81.

2. Szladow, A.J. and Given, P.H., 1981, Ind. Eng. Chem. Proc. Res. Dev, 20, 27.

3. Dryden, I.G.C., 1951, Fuel, 30, 145.

4. Liotta, R., Brons, G. and Isaacs, J., 1983, Fuel, 62, 781.

5. Green, T., Kovac, J., Brenner, D. and Larsen, J.W., 1982, In: Coal Structure, Academic Press, New York, NY, USA, 199-282.

6. Terrer, M.-T. and Derbyshire, F.J., 1986, DOE-PC-60811-F1, University Park, PA, USA, The Pennsylvania State University, 113.

7. Derbyshire, F.J., Davis, A., Epstein, M. and Stansberry, P., 1986, Fuel, 62, 1233-1240.

8. Neavel, R.C., 1982, In: Coal Science Volume 1, New York, NY, USA, Academic Press Inc., 1-19.

9. Derbyshire, F.J., 1988, IEACR/08, London, UK, IEA Coal Research, 69.

10. Bolton, C., Riemer, C., Snape, C.E., Derbyshire, F.J. and Terrer, M.-T., 1988, Fuel, 67, 1477-1481.

11. Hawk, C.O. and Hiteshue, R.W., 1965, Bulletin 622, Washington, DC, USA, U.S. Dept. of the Interior, Bureau of Mines, 42.

12. Anderson, R.R. and Bockrath, B.C., 1984, Fuel, 63, 329-333.

13. Weller, S.W., 1982, In: Fourth International Conference on the Chemistry and Uses of Molybdenum, Golden, Colorado, USA, Climax Molybdenum Company of Michigan, 179-186.

14. Epstein, M.J. and Derbyshire, F.J., 1987, DOE-PC-70003-F2, University Park, PA, USA, The Pennsylvania State University, 139.

15. Stansberry, P.G. and Derbyshire, F.J., 1988, DOE-DE-FE22-83PC60811.

16. Bockrath, B.C., 1983, In: Coal Science Volume 2, New York, NY, USA, Academic Press Inc., 65-124.

17. Suuberg, E.M., Lee, D. and Larsen, J.W., 1985, Fuel, 64, 1668-1671.

18. Derbyshire, F.J., Terrer, M.-T., Davis, A. and Lin, R., 1988, Fuel, 67, 1029-1035.

19. Peppas, N.A., Lucht, L.M., Hill-Lievense, M.E. and Hooker, D.T., 1983, Final Technical Report to U.S. DOE, DE-FG22-80PC30222.

20. Derbyshire, F.J. and Stansberry, P.G., 1987, Fuel, 66, 1741-1742.

21. Snape, C.E., Derbyshire, F.J., Stephens, H.P., Kottenstette, R.J. and Smith, N.W., 1989, Paper to be presented at the American Chemical Society Meeting, Miami, FL, USA, September 1989.

22. Garg, D. and Givens, E.N., 1983, American Chemical Society, Division of Fuel Chemistry, Preprints, 28, (5), 200-209.

23. Montano, P.A., 1986, American Chemical Society, Division of Fuel Chemistry, Preprints, 31, (2), 226.

24. Tekely, P., Bacaud, R., Charcosset, H., Delpuech, J.-J., Kister, J., Nicole, D. and Oberson, M., 1988, Fuel, 67, 932-937.

25. McMillen, D.F., Malhotra, R., Chang, S.-J. and Nigenda, S.E., 1985a, In: Proceedings - 1985 Internat. Conf. Coal Science, Sydney, NSW, Australia, Pergamon Press, 91-94.

26. McMillen, D.F., Malhotra, R., Chang, S.-J. and Nigenda, S.E., 1985b, American Chemical Society, Division of Fuel Chemistry, Preprints, 30, (4), 297-307.

27. McMillen, D.F., Malhotra, R., Hum, G.P. and Chang, S.-J., 1987, Jour. Energy and Fuels, 1, 193-198.

28. Vernon, L.W., 1980, Fuel, 59, 102-106.

29. Hei, R.D., Sweeny, P.G. and Stenberg, V.I., 1986, Fuel, 65, 577-585.

30. Lamartine, R. and Perrin, R., 1983, In: Spillover of Adsorbed Species, Amsterdam, Netherlands, Elsevier, 251-259.

31. Charcosset, H., Bacaud, R., Besson, M., Jeunet, A., Nickel, B. and Oberson, M., 1986, Fuel Proc. Technol., 12, 189-201.

32. Derbyshire, F.J., Davis, A. and Lin, R., in press, Experimental Observations Concerning the Two-Component Concept of Coal Structure, American Chemical Society, Division of Fuel Chemistry.

3. THE OPTICAL MICROSCOPY OF LIQUEFACTION RESIDUES

Microscopic analysis is an effective diagnostic technique for evaluating problems and inefficiencies in bench-scale and pilot-plant coal hydrogenation operations (1-3). For example, operations at too high or too low a temperature or with too high a throughput rate may be reflected in the absolute and relative amounts of the different residue types. Excessive proportions of unreacted vitrinite, vitroplast (a plastic pitch-like isotropic phase derived mainly from vitrinite) or semi-coke (including that formed via the mesophase mechanism) could indicate that conditions were not optimal for a given coal. On the other hand, large amounts of fusinite, semifusinite or granular residue might be indicative of far more efficient operation.

Optical examination of residues provides some insight into the different responses of coals of varying rank to liquefaction conditions (4). The vitrinite (huminite) of lignites and subbituminous coals is only occasionally rendered plastic during hydrogenation. Dissolution usually leaves skeletal remnants of the original petrographic structure. Plastic behavior is more increasingly evident in the residues of high volatile C through A bituminous coals. This is apparent mainly through the formation of vitroplast, a solvent-insoluble remnant of once-plastic vitrinite or even liquid products derived from coal. Vitroplast derives its name from vitrinite because this is the main reactive component of coal during liquefaction. Vitroplast is a very important component of residues because it has been shown to form at relatively low temperatures and, therefore, can act as an intermediate material in the formation of other, more highly condensed residue materials, notably isotropic and anisotropic semicoke.

The development of plasticity in coals is caused, in part, by the thermal rupturing of bonds and the mobilization of the polynuclear aromatic structure (or network phase) of coal. In coal liquefaction, the objectives are to cleave large aromatic molecules into smaller units and to stabilize the molecules and free radicals by the addition of hydrogen, thereby forming products of lower molecular weight. The success or failure of these objectives are measured by the solubility of the products and by the distribution and characteristics of components of the insoluble residue. For example, the reflectance and isotropy properties of vitroplast can suggest different responses to reaction conditions. A low-reflecting vitroplast indicates that perhaps depolymerization reactions are incomplete and that the residue materials might be reactive under more favorable reaction conditions. A high-reflecting vitroplast demonstrates that the vitrinite portion of coal depolymerized and was partially hydrogenated, but for some reason then recondensed into a high molecular weight material that is now insoluble. Vitroplast that has become both high-reflecting and anisotropic is referred to as anisotropic semicoke and its presence suggests that there was sufficient molecular mobility and planarity to form an ordered or stacked carbon structure. Because of an improved alignment of the aromatic structure, the anisotropic residue should be extremely resistant to any further hydrogenation.

We have speculated that the development of plasticity could aid dissolution through improved hydrogen mass transport, although it could also have some potential negative effects. If the plastic mass is not effectively dispersed by the vehicle solvent and/or by agitation, the loss of porosity as coal melts and the tendency for the development of spherical vitroplast as an immiscible phase during liquefaction could eliminate

access of hydrogen, catalyst and solvent to radicals as they form. When this situation arises, repolymerization of coal-derived materials can occur, leading to the development of a solvent-insoluble residue.

One of the primary objectives of this project has been to examine the potentials and limitations of coal liquefaction. For this purpose, certain variables of reaction conditions, mainly temperature staging, catalysis, solvent, atmosphere, coal rank and petrographic composition, have been investigated. It is expected that process conditions effecting conversion to liquids can be optimized on the basis of such investigations. The role of residue and whole-product microscopy in this project has been to provide information on the relative reactivity of macerals, the degree of hydrogenation of the soluble product and extent of regressive condensation of the insolubles in the residues. In this way it is hoped to improve our understanding of liquefaction mechanisms and the selection of optimum reaction conditions. In Section 3.3 we discuss the results of petrographic, reflectance and fluorescence analyses of liquefaction residue materials and describe how their characteristics have been influenced by the reaction conditions employed.

3.1. EXPERIMENTAL

The techniques used in this facet of our investigation include various forms of quantitative microscopy. Point-count analysis was used to determine the volume percentage distribution of the different residue components; mean maximum reflectance of (predominantly) the vitrinite-derived residue materials was determined as a means of characterizing competing hydrogenation and carbonization reactions; and fluorescence spectrophotometry was used to identify gross trends in the chemistry of vitrinite-derived residue materials.

Optical microscopy was performed on samples that were first mixed with a cold-setting epoxy resin (Epolite 5313A and B resin and hardener manufactured by the Hexcel Corporation). Because of sample size (usually less than one gram) most of the residues were combined with the resin in glass vials and centrifuged to remove trapped air and to form a sample graded by mass and density. After the epoxy resin hardened, the glass vial was removed and each sample cut in half, longitudinally. The cut surfaces were re-embedded in epoxy resin and polished using a series of grit papers and polishing slurries.

Reflectance determinations were performed using a modified Leitz MPV-II Orthoplan Pol microscope with a 50X oil-immersion objective (625X total magnification), an EMI 9558 photomultiplier and computer-assisted data acquisition and processing software. A Zeiss Universal microscope with total magnification of 625X was used for point-counting the residues using the terminology described in Section 3.2.

Quantitative point-count analyses were performed on a variety of residue materials to obtain a volumetric distribution of the different residue components. Results of these analyses are summarized in Appendix A and are presented on a whole-coal, dmmf basis to enable comparisons to be made among reaction conditions, solvents, catalysts and coals. The data are presented as a "weight-volume" percentage and are calculated by multiplying the dmmf weight percentage of residue remaining after reaction (residue yield) by the fractional contribution of each residue component determined by point-count (volume percent). This method of presentation allows a direct comparison to be made of the characteristics of residues produced from different coals and reaction conditions by factoring in the degree of conversion attained during liquefaction. Appendix A is organized

first by coal and then by the different reaction conditions employed, and includes the weight percentage residue yield.

Fluorescence microscopy was performed using a photometer system constructed at the Energy and Fuels Research Center of The Pennsylvania State University. In this system light from a ultra-high-pressure mercury lamp passes through a heat filter and then through a 390-490 nm band-pass excitation filter. The excitation light is then reflected by a 510 nm short-pass dichromatic beam splitter (dichroic mirror) and condensed onto the sample through a 50 X NPL FLUOTAR objective. After absorption of excitation light, electrons within the residue materials that are in the ground state are promoted to orbitals of higher energy. As the excited electrons return to the ground state, part of the absorbed energy is released as fluorescence emission, which is of longer wavelength than that of the absorbed light. This fluorescent light, mostly in the visible range, passes back through the dichromatic beam splitter, and a 515 nm long-pass barrier filter blocks off any reflected excitation light. The fluorescence emission is directed to a double grating monochromator where the light is split into its component wavelengths. The optical signals of fluorescence are transformed into electronic signals and then amplified by a photomultiplier. The amplified electronic signals are finally recorded, corrected and processed by a computer. In the current investigation, the intensity observed at the wavelength of maximum intensity (I_{max}) and the intensities at 650 nm and 500 nm were compared for vitrinite-derived residue materials.

3.2. TERMINOLOGY OF LIQUEFACTION RESIDUE MICROSCOPY

The terminology used to quantitatively describe the tubing-bomb coal liquefaction residues produced in this study was borrowed, in part, from a

classification of hydrogenation residues that has been adopted by the International Committee for Coal Petrology (5). Some additions and modifications have been made to this classification in an attempt to either simplify the system or provide quantitative information on specific entities observed during the course of qualitative evaluations.

Partially Reacted Coal Macerals: Includes three distinct residue entities retaining sufficient maceral structure that their maceral origin can be identified. In this context we distinguish partially reacted remnants of vitrinite (huminite), liptinite and inertinite. The extent of reaction may include a slight increase in reflectance, loss of fluorescence properties, swelling and/or partial dissolution. However, the essential feature of residue materials identified in this category is that structural characteristics of the original maceral be retained at least in part.

The presence of partially reacted coal macerals in liquefaction residues can represent process inefficiency, particularly when normally reactive macerals appear in the insoluble residue. However, when vitrinite (huminite) particles are recognized in a residue it suggests that reaction conditions were less than optimum (Plate Ia). Residues from coals lower in rank than bituminous are often composed mainly of these particle types when reaction conditions result in low conversions. The reflectance of this partially reacted vitrinite/huminite usually is significantly higher than that of the parent coal.

Identifiable partially reacted liptinite macerals are recognized as a separate category. Because of their hydrogen-rich and relatively aliphatic character they have been thought of as being the most susceptible of the macerals to hydrogenation conditions. Consequently, their presence in a

Blank Page

PLATE I

Figure Descriptions

Figure a -- Partially reacted vitrinite (huminite) with included liptinite and inertinite found in this temperature-staged, non-catalytic hydrogenation residue from reaction of PSOC-1482 (lig.) with the distillate process solvent (P74-19-R2).

Figure b -- Granular residue serves as the matrix of this particle with included inertinite and semi-coke as found in the single-stage, high-temperature hydrogenation residue following reaction of PSOC-1498 (hvCb) with an Fe + Mo catalyst and a 1:1 solvent mix of 850+°F recycle and naphthalene (P73-G3-R2).

Figure c -- Skeletal remains of remnant coal particle as found in this temperature-staged residue from the reaction of PSOC-1401 (Subbit.) with a Mo catalyst in tetralin (run #40).

Figure d -- A large agglomerate of high-reflecting vitroplast as seen in the same sample as Figure c.

Figure e -- Low-reflecting vitroplast (L) as a coating on anisotropic semicoke from a whole-product residue following temperature-staged, catalytic (Mo), dry hydrogenation of PSOC-1504 (hvAb, P-2-3).

Figure f -- Anisotropic semicoke under crossed nicols from a temperature-staged, catalytic (Mo), dry hydrogenation residue from reaction of PSOC-1482 (lig., EX-3-6).

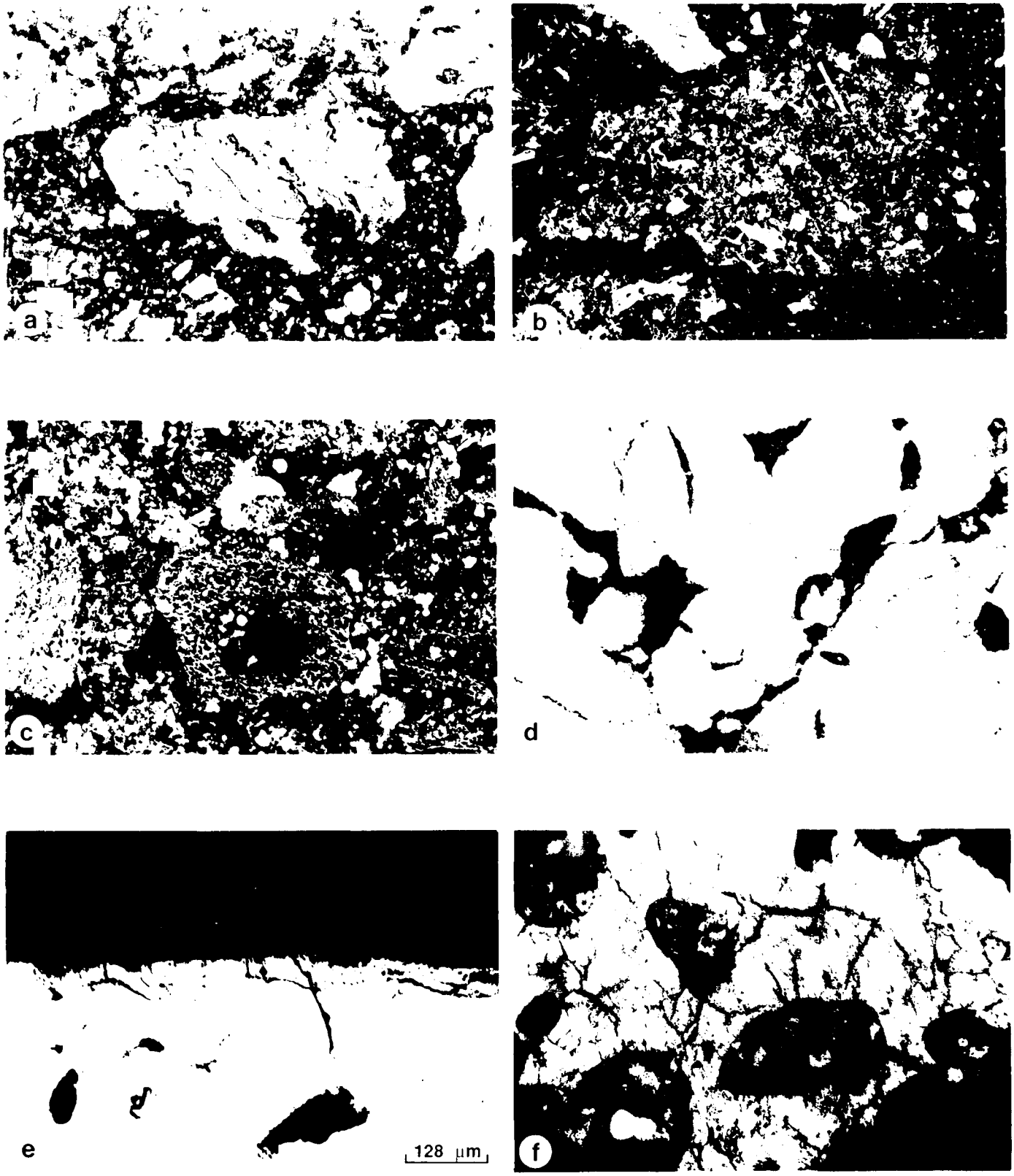

PLATE I

liquefaction residue implies that reaction time or residence time and temperature may have been insufficient.

It has been demonstrated that some semifusinite and most fusinite are not altered during coal liquefaction. These entities are identified together as inertinite in this report.

Granular Residue: As seen in Plate Ib this consists of very fine organic debris (about 1 μm), resulting from the dissolution of coal; large numbers of individual grains may be observed agglomerated into relatively large, irregular-shaped masses. Generally, large proportions of granular residue observed in a liquefaction residue are likely to indicate that reaction conditions have been more effective in converting coal to liquids.

Skeletons: Like granular residue, skeletons also consist of very fine particles, but in these instances, their outline can be related to that of a pre-existing coal or residue particle. The particles generally are competent with an open, lacy structure like that seen in Plate Ic.

Vitroplast: Refers to a plastic or once-plastic, isotropic, pitch-like material derived usually from vitrinite during liquefaction. The material can occur as spheres, but in this study it is mostly found as massive areas in the residues, as seen in Plate Id and e. Also, our use of the terminology deviates from the ICCP definition of vitroplast, by distinguishing low- and high- reflecting populations of which the former has a a similar reflectance to that of the original coal. The low reflectance of this vitroplast suggests that, under somewhat improved reaction conditions, the material could be converted to liquid products. Vitroplast of higher reflectance implies that a greater degree of molecular condensation or carbonization has occurred and that reaction conditions might have been inordinately severe. The high-reflectance vitroplast can

develop a granular anisotropic texture; and in so doing becomes recognizable as anisotropic semicoke. In this report the two population of vitroplast are distinguished when reflectance data are discussed, but have been grouped under a single heading in Appendix A.

Anisotropic semicoke: This term embraces both primary and secondary semicoke described in the ICCP proposed classification (5). It refers to a high-reflecting carbonaceous material with an anisotropic texture. It may have formed directly from unhydrogenated coal particles, from vitroplast or through the development of mesophase. Anisotropic mosaics consisting of units of less than one micron have been observed in the remnants of semifusinite, vitrinite and high-reflecting vitroplast (Plate 1e and f). However, if the isochromatic areas of an anisotropic carbon are relatively large or of spherical shape they are recognized as having formed via the mesophase mechanism similar to the formation of nematic liquid crystals. Generally, solid anisotropic carbons are produced from a thermoplastic, isotropic pitch when their molecules, while still in a mobile or liquid state, develop a one-dimensional stacking order that gives the liquid an orientational order. The degree of molecular mobility required to form large isochromatic areas suggests that this type of carbon is formed from the liquid phase. The source of the mesophase (anisotropic semicoke) in liquefaction residues could be coal or solvent; its presence is significant because of its tendency to agglomerate and deposit on any inert substrate. Mesophase has been identified in most liquefaction pilot-plant deposits and forms following a highly undesirable retrogressive reaction (2,3).

3.3. RESULTS AND DISCUSSION

3.3.1. Introduction

Appendix B contains the results on the more than 70 residue samples that were evaluated by quantitative microscopy during the course of this project. The analyses included reflectance, fluorescence and petrographic point-counting. In addition, approximately 20 samples were evaluated qualitatively. Samples were selected so as to provide information on the effects of temperature-staging compared to single-stage liquefaction, and the absence and presence of different atmospheres, catalysts and solvents for four coals of different rank (PSOC-1482, lignite; PSOC-1401, subbituminous; PSOC-1498, hvCb; PSOC-1504, hvAb). Because dry liquefaction typically results in lower conversion and eliminates the possibility of contributions to the residue material from vehicle solvent, the sections that follow are organized so that dry hydrogenation tests are discussed separately from those runs in which a solvent was employed.

3.3.2. Dry Hydrogenation Residues

3.3.2.1. Effects of Temperature Staging

Preceding a coal liquefaction reaction with a low-temperature pretreatment stage has been shown to have a profound effect on conversion and product selectivity, particularly where catalysts are employed in the reaction (6). Consequently, some detailed microscopy was performed on residues that represent pretreatment conditions alone. Three of the coals which had been reacted at 275°C (PSOC-1482, 1401 and 1504) under different atmospheres were evaluated to determine whether there had been any discernable changes in the structure of the reacted coal.

Under pretreatment conditions (275°C, 30 min, 7 MPa hydrogen) the lignite and subbituminous coals showed almost no microscopic evidence of

change in the coal structure other than some separation of coal particles along bedding planes. This type of alteration probably results from loss of moisture in response to heating. Desiccation was not observed for the hvC or A bituminous coals, but some particle edges were found to be irregular and tattered, a result perhaps of physical abrasion during the reaction. It is important to note that the vitrinite/huminite macerals show no rims of low reflectance that would signify that hydrogenation has proceeded via a shell progressive mechanism. Also, there is no evidence for maceral devolatilization or the onset of fluidity that would help to explain the improved conversion and product selectivity that occurs when a low-temperature hydrogenation is employed prior to the reaction under full liquefaction conditions.

Fluorescence microscopy also was used in an attempt to detect any potential chemical changes that might have occurred during pretreatment stage reactions for various macerals of hvAb and subbituminous coals. Qualitative inspection of residues using blue-light irradiation showed no perceptible alteration. However, quantitative measurements of maximum intensity (I_{max}) and of the red/green quotient (Q), as summarized in Table 3.1, showed that there may be minor structural rearrangements. The fluorescence intensity of vitrinite, sporinite and cutinite in the bituminous coal (PSOC-1504) decreased following reaction under pretreatment conditions in hydrogen and the spectra shifted into the blue region; the latter is a phenomenon associated with partial hydrogenation. In contrast, a red shift was observed for sporinite in the case of the subbituminous coal (PSOC-1401) after pretreatment when naphthalene was used as a solvent (Table 3.1); the red shift was found to be larger when the molybdenum catalyst was present.

Table 3.1. Fluorescence Measurements on THF-insoluble Residues

		Raw	275°C, H_2	275°C, N_2	Second Stage and Two-Stage
PSOC-1504 [dry, non-catalytic liquefaction]					
Vitrinite	I_{max}	0.74	0.52	0.15	No visible fluorescence
	Q	1.99	1.53	1.62	
Sporinite	I_{max}	1.70	1.30	1.20	Absent
	Q	1.72	1.25	1.37	
Cutinite	I_{max}	0.94	0.59.	0.62	Absent
	Q	2.80	2.66	2.67	
PSOC-1401 [Naphthalene as solvent, 2:1 ratio]					
Sporinite*					
Catalytic	I_{max}	0.18	0.09	0.09	
	Q	0.62	1.07	1.17	
Non-catalytic	I_{max}	0.18	0.11	0.15	
	Q	0.62	0.94	1.11	

*Sporinite not present in residues of second-stage reaction
I = Intensity
$Q = I_{650nm}/I_{500nm}$

Maximum reflectance values were measured for a selection of residues from pretreated coals and are presented in Figure 3.1. Compared to the reflectance of the feed coal, little change was observed following pretreatment. Only in the case of the subbituminous coal was there a significant increase. These general relationships are consistent whether a hydrogen or a nitrogen atmosphere was employed during the reaction (Table 3.2).

Major changes in the appearance and optical properties of residues were observed following the high-temperature (425°C, 30 min, 7 MPa gas pressure) and temperature-staged (275°C, 30 min; 425°C, 30 min; 7 MPa gas pressure) reactions. For the most part the liptinite macerals were converted and no longer present in the residues. Huminite/vitrinite remnants and vitroplast were the predominant components found in residues of the lignite (PSOC-1482) and subbituminous (PSOC-1401) coals, whereas vitroplast was the dominant component found in residues from the hvCb (PSOC-1498) and hvAb (PSOC-1504) coals. The maximum reflectance of these residue components were greatly increased over those of the original coal.

Figure 3.1 compares the trends in reflectance for the different reaction conditions and coals used during this project. For lower coal ranks, temperature-staged residues have a higher reflectance than the single-stage high-temperature liquefaction residues. Reflectance is lower for temperature-staged compared to high-temperature reactions for the hvC and A bituminous coals. If higher reflectance is indicative of a greater degree of molecular condensation, then these data suggest that the lower rank coals have a greater tendency to develop crosslinks and condense under temperature-staged, dry, non-catalytic liquefaction than the conventional high-temperature liquefaction. The reversal of this tendency, and

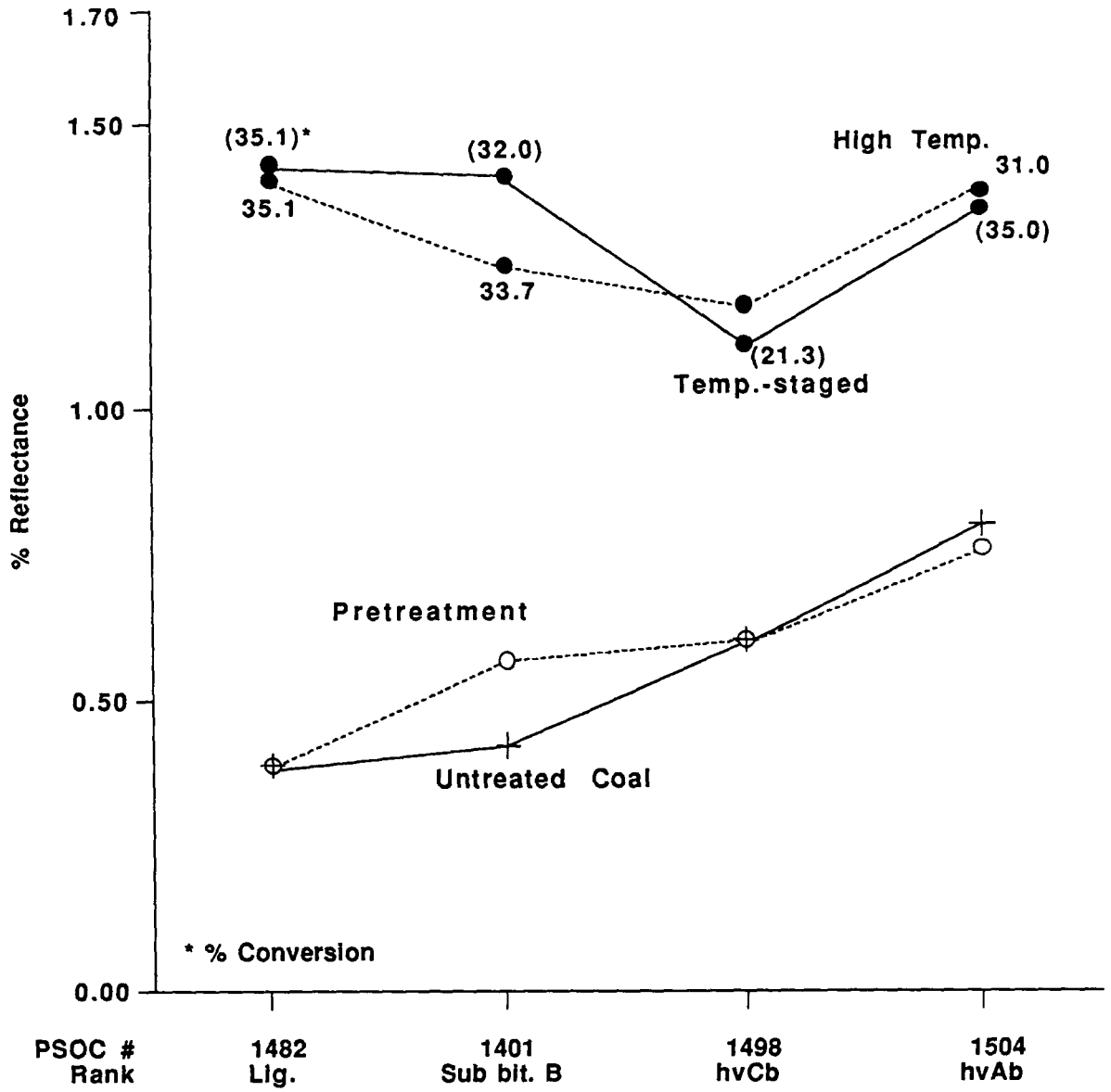

Figure 3.1 Mean Reflectance of Vitroplast & Vitrinite Remnants as a Function of Reaction Conditions for Dry, Non-catalytic Hydrogenation Residues

Table 3.2. Maximum Reflectance Measurements on Vitrinite-Derived THF-Insoluble Residue Material From Dry, Non-catalytic Liquefaction

	Raw	275°C, H_2	275°C, N_2	425°C, H_2	425°C, N_2	275°C, H_2 + 425°C, H_2	275°C, N_2 + 425°C, N_2
PSOC-1482	0.39	0.39	0.38	1.40	1.42	1.43	1.42
PSOC-1401	0.42	0.57	0.56	1.25	1.41	1.41	1.40
PSOC-1504	0.80	0.76	0.73	1.38	1.36	1.35	1.37

therefore a lower degree of molecular condensation under temperature-staged conditions, is seen in the residues from the higher rank coals. Finally, the reflectance values measured for both the temperature-staged and high-temperature residues of PSOC-1498 are somewhat low compared to the other coals (Figure 3.1). We suspect that the maximum temperature (425°C) used for liquefaction of this hvCb coal may be too low to be optimal. Conversion yield for this coal (PSOC-1498) also supports this conclusion and averages 21% compared to 34% conversion for the other coals.

3.3.2.2. Effects of Catalyst

The Molybdenum Sulfide Catalyst:

General reflectance relationship

The general relationship in the reflectance of vitrinite-derived residues between non-catalytic and catalytic (1% Mo) temperature-staged hydrogenation experiments is provided in Figure 3.2. This figure shows that the residual materials from the catalytic runs generally have higher reflectances than those from non-catalytic runs. The notable exception to this is PSOC-1401 which will be discussed separately later in this section. The higher volumetric conversion of each coal in the presence of the molybdenum catalyst means that there is much less of the original coal material remaining; therefore, the residues will be of higher molecular weight and more highly condensed than in runs which achieve significantly lower levels of conversion.

The significance of the foregoing is that a reflectance measurement made on residual material, considered in isolation from all pertinent information, may not be a good indication of the conversion of coal to a soluble product. In particular, low molecular weight products generated as a result of efficient hydrogenation are presumed to have had a relatively

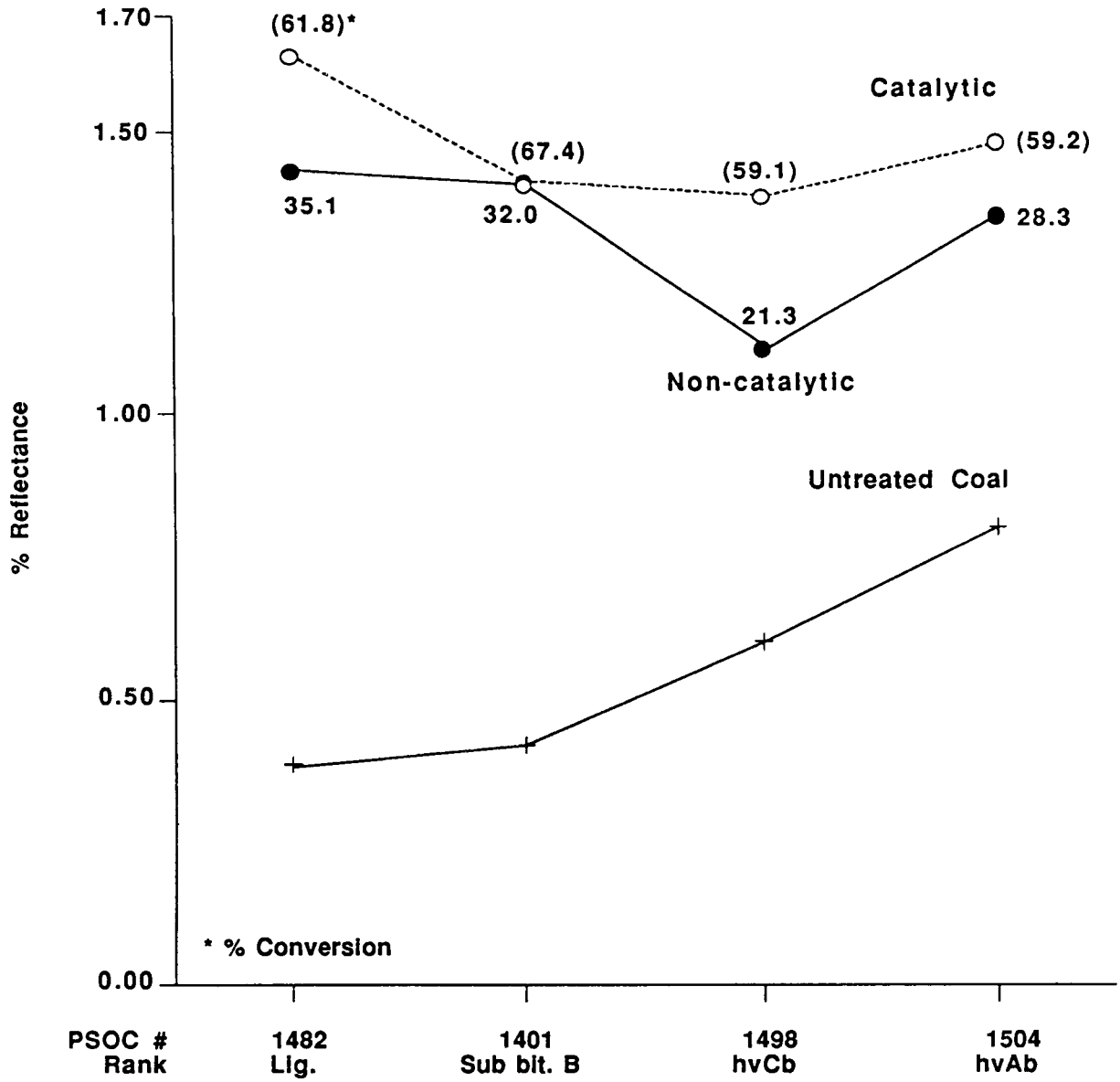

Figure 3.2 Mean Reflectance of Vitroplast & Vitrinite Remnants in Temp.-staged, Dry, Catalytic (Mo) and Non-catalytic Hydrogenation Residues

low reflectance; however, these materials have dissolved in the solvent (THF) used to separate the soluble products from the insoluble residues. Consequently, a series of experiments was undertaken specifically to study the reflectance distribution of the whole products (without extraction), as well as the insoluble residues of catalytic and non-catalytic temperature-staged hydrogenation. The results, as described below, are extremely revealing.

Whole-product residue analyses

Whole-product analysis, i.e. the analysis of residues before solvent extraction, is only possible with residues produced from dry hydrogenation. When a vehicle solvent is used, the whole-product residues have the consistency of a sticky tar and can not be formed into a pellet or polished for optical microscopy. Reflectograms of the whole products and residues for three coals (PSOC-1504, 1498 and 1482) are shown in Figures 3.3, 3.4 and 3.5, respectively.

The very obvious effect of the molybdenum catalyst during temperature-staged, dry liquefaction of the hvAb coal (PSOC-1504) is apparent when the reflectogram of the whole product after catalytic reaction is compared to that of the non-catalytic run (Figures 3.3a and c). The former (3a) has a bimodal distribution composed of low-reflecting (Ro max = 0.02-1.00%) and high-reflecting (Ro max = 1.05-1.60%) populations, whereas the latter (3c) consists predominantly of only one population (Ro max = 1.15-1.45%). The low-reflecting material formed during catalytic liquefaction is strongly fluorescent under blue-light illumination, and is mostly soluble in THF and so is no longer present in the extracted residue (Figure 3.3b). The higher-reflecting material, on the other hand, is non-fluorescent and insoluble in THF. The whole product (3c) and extracted

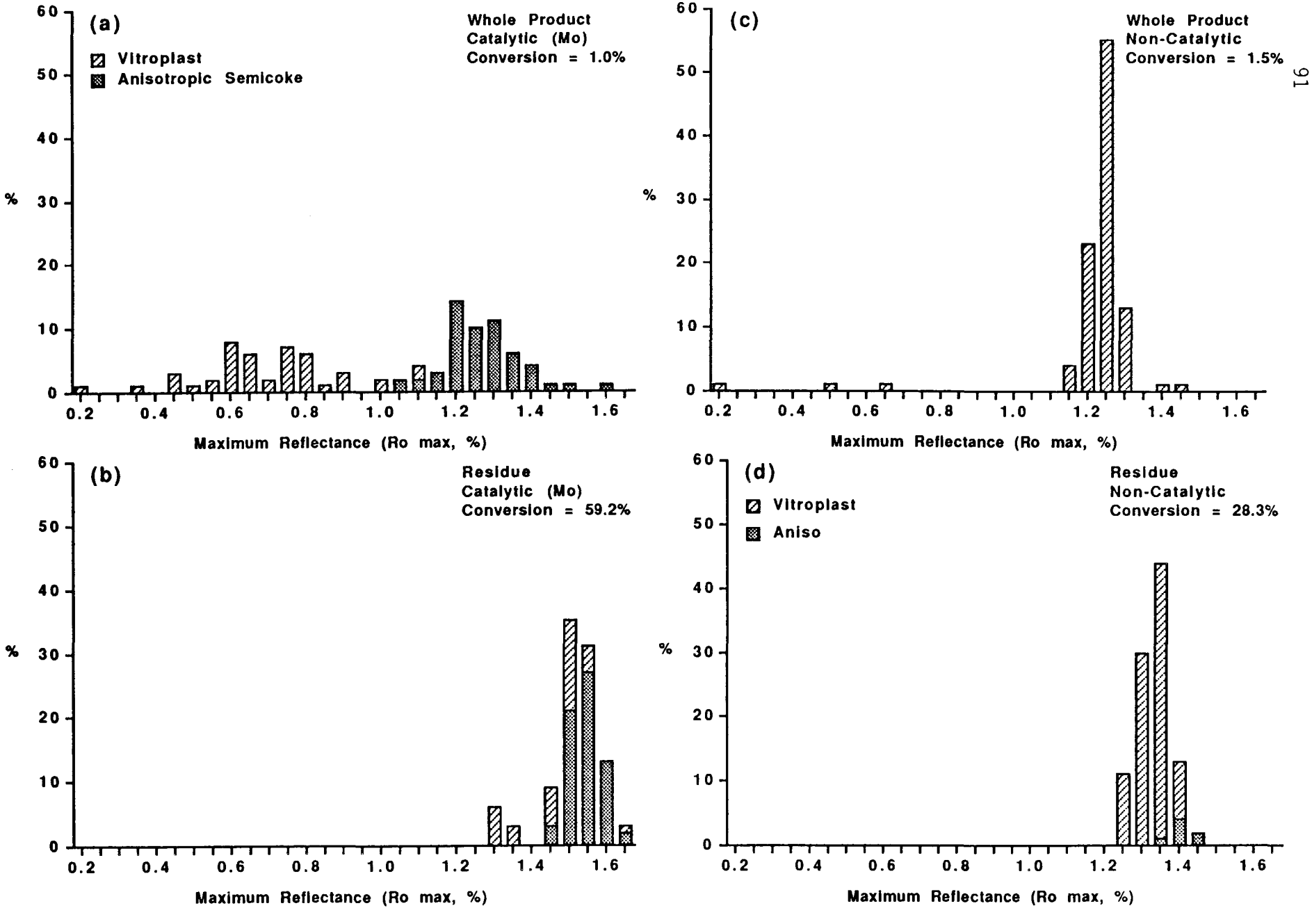

Figure 3.3 Reflectograms of Temperature-Staged Whole-product and THF-Insoluble Residues for the hvAb Coal (PSOC-1504)

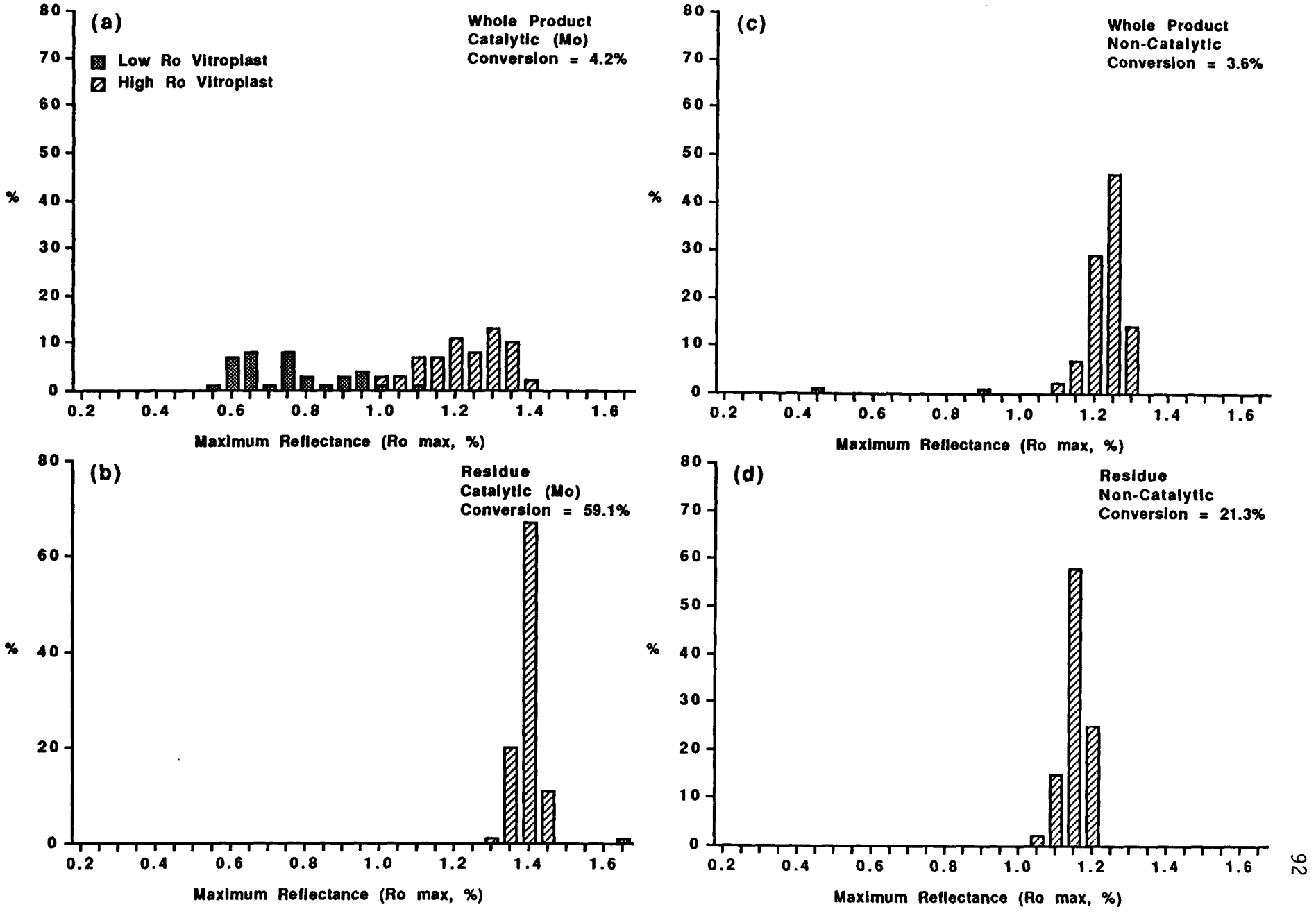

Figure 3.4 Reflectograms of Temperature-Staged Whole-product and THF-Insoluble Residues for the hvCB Coal (PSOC-1498)

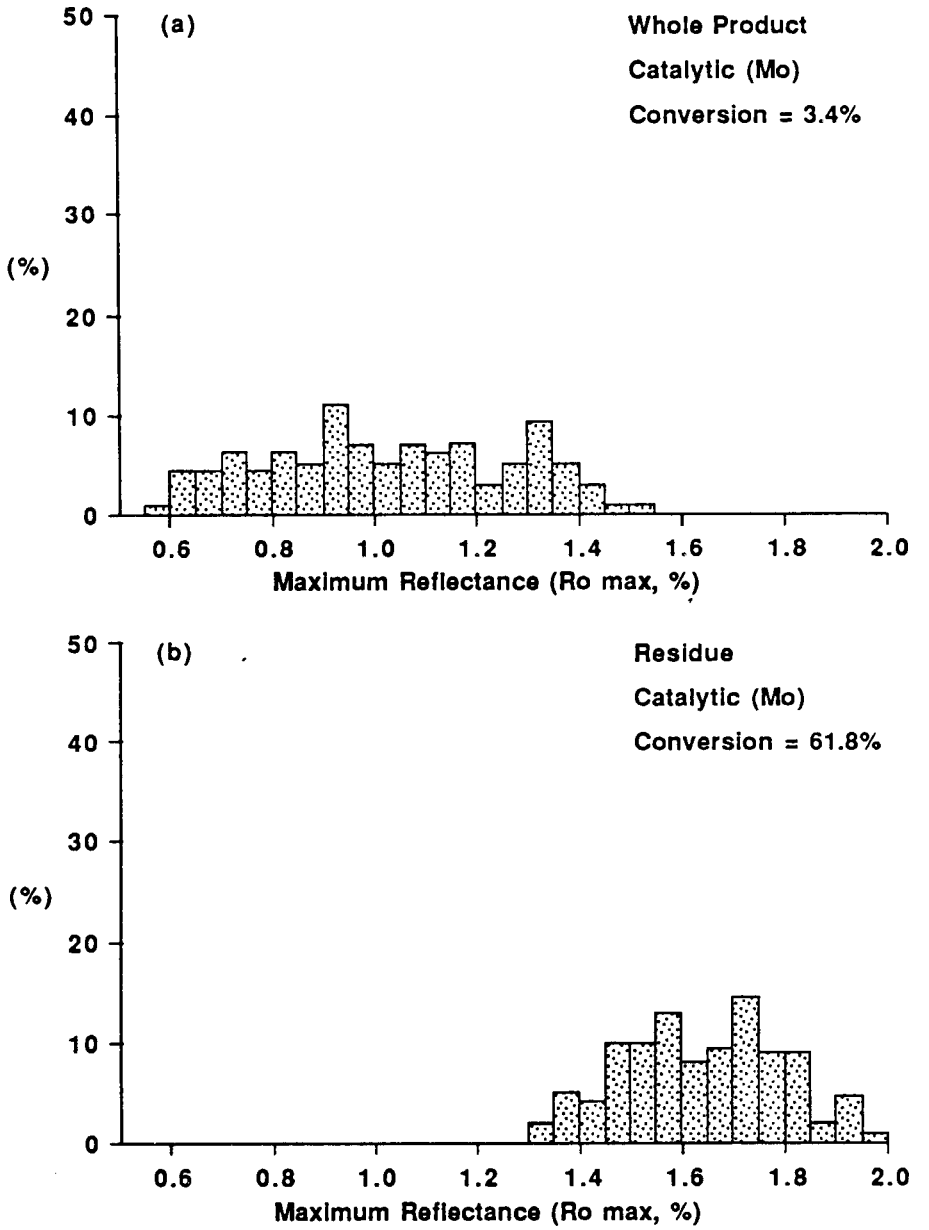

Figure 3.5 Reflectograms of Temperature-Staged Whole Product and THF Insoluble Residues for the Lignite (PSOC-1482)

residues (3d) of the non-catalytic runs have similar reflectance distributions because of the limited production of soluble products.

The goal of achieving optimum conversion is the same as optimizing the generation of low-reflecting materials while minimizing the formation of high-reflecting materials. A comparison of the catalytic and non-catalytic reflectograms (Figures 3.3a and c) suggests that the involvement of molybdenum catalyst greatly promotes the formation of a more saturated, less condensed component that is low reflecting, highly fluorescent and THF-soluble. The fact that this soluble material is solid at room temperature implies that it is still of relatively high molecular weight, and probably would report to the asphaltene fraction following extraction in THF. In the absence of the molybdenum catalyst, production of these asphaltenic molecules is clearly reduced because much less of the low-reflecting material appears in the whole-product residue and the total conversion is lower (Figure 3.3c and d). It is concluded that in the absence of the catalyst, a smaller proportion of the free radicals formed by thermal rupture are stabilized by hydrogen and possibly that there has been less radical formation.

During the course of the reflectance analysis a distinction was not only made among the high- and low-reflecting vitroplast materials, but also of the anisotropic semicoke that formed from the vitroplast in residues of the hvAb (PSOC-1504) coal. Anisotropic semicoke was found in higher concentration following use of the molybdenum catalyst, whereas only a minor amount was seen in the THF-extracted residue when the catalyst was not present. Initially, this observation would appear to be inconsistent with the fact that the catalyst contributed to a two-fold improvement in conversion compared to the thermal run. Yet, the presence of anisotropic

semicoke usually is indicative of retrogressive coking reactions. The explanation probably lies in the absence of a vehicle solvent during the runs. One role of the solvents must be to separate and disperse free radicals as they form from the coal, so that there is less tendency to interact with one another and more likelihood of reaction with hydrogen radicals. The results of point-count analyses on the residues of the hvAb coal (Appendix A) shows that, when a distillate process solvent was used with the molybdenum catalyst, negligible anisotropic semicoke was produced. During dry hydrogenation the molybdenum catalyst could promote the formation and/or lateral growth of planar aromatic molecules that are able to stack and align sufficiently to produce an anisotropic carbon. When hydrogen radicals are available to prevent their growth, it is likely that these aromatic molecules contribute to a higher asphaltene content. When catalyst and solvent are absent, these planar molecules are formed to a much lesser extent; their progenitors contributing to a greater amount of insoluble residue that is optically isotropic.

The whole-product reflectogram of the catalytic liquefaction of the hvCb coal (PSOC-1498) also has the same bimodal distribution (Figure 3.4a) as that of the hvAb coal just described. With no catalyst, very little of the low-reflecting population was produced (Figure 3.4c) and total conversion was lower, once again suggesting that the function of the catalyst is that of stabilizing free radicals formed in the thermally disrupted coal. Comparison of the THF-extracted residue (Figure 3.4b) with the whole-product again shows that most of the low-reflecting material is soluble after dry hydrogenation. A major difference between the behavior of this hvCb coal and that of the hvAb coal, is that no anisotropic material appears in the high-reflecting population; possibly the aromatic

fragments that form during catalytic liquefaction of the hvCb coal are less planar than those which are produced from the hvAb coal.

The whole-product reflectogram of the catalytic liquefaction of the lignite (PSOC-1482) has a very broad distribution (Figure 3.5). In comparison to the equivalent reflectograms (catalytic) of the two bituminous coals (Figures 3.3 and 3.4) that of the lignite has a residue population (Figure 3.5b) which has shifted to a higher reflectance range following THF-extraction. This same phenomenon is observable to a lesser degree in the reflectograms of residues from the bituminous coals and may be due to a relative enrichment in high-reflecting materials including semifusinite. Once again, it is apparent that the low-reflecting population of the whole-product residues is removed during solvent extraction.

Effect of hydrogen and nitrogen atmospheres

Comparison of reflectance data collected from liquefaction runs performed under different atmospheres for three of the coals (Table 3.2) shows that there is almost no significant difference in reflectance of residual materials when reactions are performed under hydrogen or nitrogen during dry, non-catalytic liquefaction. This is somewhat surprising given the fact that the best conversion is observed for the temperature-staged reaction of the bituminous coal in a hydrogen environment. These observations suggest that the reflectance increase of vitrinite-derived residual material from runs made in the absence of a solvent may be directly related to the maximum temperature used in the reaction.

Reflectance analyses also have been performed on THF-insoluble residues of dry catalytic and non-catalytic, single- and two-staged liquefaction of the subbituminous coal (PSOC-1401) reacted under N_2 and H_2

Table 3.3. Maximum Reflectance of Vitrinite-Derived Residue Material from Liquefaction of PSOC-1401

Sample Identification	Dry, catalytic (1% Mo)				Dry, non-catalytic			
	Run#	Reflectance, %	Vitrinite Type	Conversion, %	Run#	Reflectance, %	Vitrinite Type	Conversion, %
Raw	--	0.42	(unreacted)	--	--	0.42	(unreacted)	--
275°C, N_2	82	0.62	(unreacted)	4.5	62	0.56	(unreacted)	7.7
275°C, H_2	83	0.60	(unreacted)	4.1	50	0.57	(unreacted)	9.0
425°C, N_2	84	1.25	(unreacted)	25.9	66	1.41	(unreacted)	32.0
425°C, H_2	85	1.58	(reacted)	60.3	54	1.25	(unreacted)	33.7
275°C, N_2 + 425°C, H_2	88	1.46	(reacted)	58.7	78	1.62	(reacted)	41.0
275°C, H_2 + 425°C, N_2	89	1.24	(unreacted)	25.7	74	1.43	(unreacted)	32.0
275°C, N_2 + 425°C, N_2	86	1.19	(unreacted)	24.8	70	1.40	(unreacted)	32.2
275°C, H_2 + 425°C, H_2	87	1.40	(reacted)	67.4	58	1.41	(reacted)	40.4

atmospheres and a combination of the two gases. Like the residues of other pretreated coals, those prepared in this series of experiments resembled the parent coal in their optical appearance; liptinite macerals remained intact and huminite (vitrinite) macerals maintained their original morphology. Table 3.3 shows that, for both catalytic and non-catalytic runs, maximum vitrinite reflectance values of the residues of pretreatment are low whether generated in a nitrogen or a hydrogen atmosphere. The reflectance of vitrinite in the presence of the Mo catalyst is only slightly higher of that subjected to thermal pretreatment.

The influence of atmosphere and catalyst becomes more evident as a result of high-temperature and temperature-staged reactions (425°C). The residues no longer contain liptinite macerals, indicating that these have been converted to liquid or gaseous products. The vitrinite was also subject to significant changes as shown by a large increase in maximum reflectance and by the qualitative descriptions provided in Table 3.3. In this table, "reacted" vitrinite (or vitroplast) refers to those vitrinite particles which underwent thermoplastic deformation and might have developed a granular anisotropy: "unreacted" vitrinite refers to those not showing evidence of thermoplasticity, for the most part retaining their original morphology.

In the presence of the molybdenum catalyst and hydrogen atmosphere, most of the vitrinite particles became plastic in the tubing bomb reactor and were partially subject to recondensation with the development of a granular anisotropy. In comparison, the other three high-temperature residues processed in a nitrogen atmosphere are composed mainly of "unreacted" vitrinite particles. This demonstrates that the presence of a catalyst and hydrogen gas play an important role in promoting vitrinite

reactivity during liquefaction of the subbituminous coal. Although the "unreacted" vitrinite particles may possess a lower reflectance than the "reacted" particles, the latter were again associated with a higher volumetric conversion.

During the temperature-staged reactions (275°C + 425°C), the effect of the first stage is negligible when a nitrogen atmosphere was used during the second stage. However, the effect is evident when a hydrogen gas atmosphere was used in the second stage. It is found, for residues of reactions at 425°C, N_2; 275°C, N_2 + 425°C, N_2; and 275°C, H_2 + 425°C, N_2, that the reflectance values are very similar in the catalytic runs and again in the non-catalytic runs (Table 3.3). This suggests that first-stage reactions did not play an important role in liquefaction if an inert atmosphere is used in the second stage. This is further supported by the conversion data for these three reactions (Table 3.3).

The impact of first-stage reaction becomes important when a hydrogen atmosphere is employed. In all residues after two-stage reactions with a hydrogen atmosphere, no granular anisotropic carbons were formed from the subbituminous coal (PSOC-1401), whereas this material is present in the residue of the corresponding single, high-temperature stage reaction. Also, the reflectance of the "reacted" vitrinite only is lowest when a hydrogen atmosphere was used in both stages, representing the condition which gave rise to the highest conversion. This implies that first-stage reaction may have created products or molecular structures which are not as likely to undergo the recondensation reactions that would otherwise take place during the second stage.

As in the case of single second-stage reaction, the influence of atmosphere is manifested during the temperature-staged reactions. The

residues obtained from reactions in the nitrogen atmosphere are primarily composed of "unreacted" vitrinite, whereas those reacted in an hydrogen atmosphere (second stage) are predominantly "reacted" vitrinite particles. This again suggests that the presence of hydrogen promotes the thermoplastic development of vitrinite during liquefaction, in turn enhancing conversion.

During the temperature-staged reactions, the presence of the catalyst was able to minimize the retrogressive recondensation reactions in the subbituminous coal. The reflectance values of the residues from the non-catalytic runs are consistently higher than those of the catalytic ones in the temperature-staged reactions (Table 3.3).

Briefly, the influence of different parameters on dry liquefaction are interrelated. The effects of atmosphere and catalysis are manifested during the second stage, whereas they have relatively little importance during the first stage. The presence of a hydrogen gas and catalyst promotes the thermoplastic development of vitrinite in the tubing bomb reactor, in turn favoring liquid conversion as a consequence of enhanced hydrogen transfer and catalyst dispersion.

Comparison of Catalysts:

Appendix A includes the results of quantitative point-count analyses performed as part of a comparison of the influence of different catalysts. From these results we have extracted those data which will allow comparison of the proportions of vitrinite-derived residue components from temperature-staged, dry hydrogenation runs in which no catalyst, 1.0% iron or 1.0% molybdenum were employed. Figure 3.6 shows that use of the molybdenum catalyst resulted in the lowest production of vitroplast (ranging from 9% to 39%) for all coal ranks, whereas the use of no catalyst

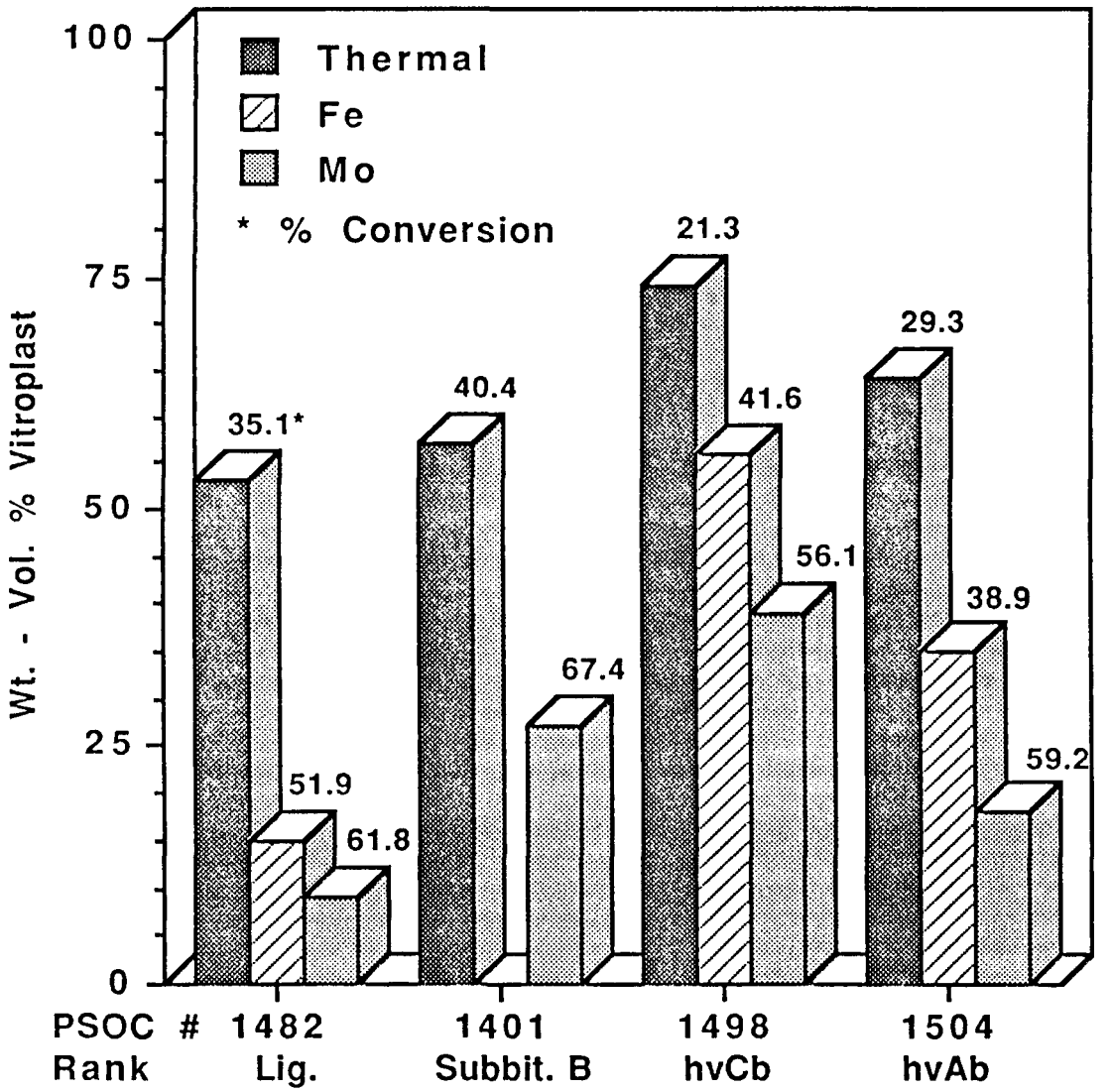

Figure 3.6 Wt. % Vitroplast Measured in Temperature-Staged, Dry Hydrogenation Residues as a Function of Coal Rank and Catalyst

led to the greatest concentration (ranging from 53% to 74%). This comparison also shows that the hvCb coal (PSOC-1498) residues contain a greater proportion of vitroplast, regardless of the catalyst used, than the residues from any other coal. This is further evidence (see Section 3.3.2.1) that the reaction conditions used for this coal were not optimal for conversion.

If the total amount of vitrinite-derived material (vitroplast and anisotropic semicoke) is considered, the hvCb coal again has provided the greatest amount under dry hydrogenation conditions. The production of vitrinite-derived residue components actually increases in the order Subbit. (PSOC-1401) < Lig. (PSOC-1482) < hvAb (PSOC-1504) < hvCb (PSOC-1498). Almost no remnant coal particles were seen in residues from the lignite and subbituminous coals under catalytic, temperature-staged liquefaction conditions. Prior work has shown that low-rank coals rarely become fluid and form vitroplast under conventional single-stage high-temperature liquefaction (4). Apparently, the combination of temperature-staging and the presence of catalysts profoundly influences the development of thermoplasticity during hydrogenation of low-rank coals, and must contribute to the relatively high conversion observed when catalyst materials are present.

3.3.3. Microscopy of Residues from Hydrogenation with Vehicle Solvents

A series of residues generated during reactions with a low-temperature distillate process solvent was selected from the matrix of temperature-staged reactions employing different solvents discussed in Chapter 2. In addition, residues from reactions with other solvents were evaluated during the course of this research including: a 850+°F recycle solvent, a 1:1 mixture of 850+°F recycle and naphthalene, naphthalene

alone, and tetralin. Petrographic and reflectance analyses were performed, the results of which are summarized in Tables 3.4 and 3.5 and in Figures 3.7 and 3.8, as well as Appendix A.

Figure 3.7 compares the concentration of vitroplast in temperature-staged residues generated when three of the coals (PSOC-1482, 1498 and 1504) were hydrogenated with the distillate process solvent. In general, here, as in the case in the dry hydrogenation, the presence of molybdenum catalyst resulted in a relatively low generation of vitroplast compared to runs using iron or no catalyst. Comparison of Figures 3.7 and 3.6 reveals how much more effective liquefaction is when conducted in the presence of a vehicle solvent. Even the generation of anisotropic semicoke in significant concentrations was confined to the hvAb residues in which the Fe and no catalyst were employed (Appendix A). Apparently, the molbydenum catalyst used in conjunction with the distillate process solvent limits the production and/or growth and alignment of planar aromatic molecules that could give rise to anisotropic carbon.

The mean reflectance of the vitroplast generated during temperature-staged liquefaction using different catalysts, dry and with solvents is plotted against total conversion for the hvCb coal (PSOC-1498) in Figure 3.8. The reflectance of vitroplast from the dry hydrogenation residues increases linearly with conversion in the order: No catalyst < Fe < Fe + Mo < Mo. As was discussed in Section 3.3.2.2, this relationship suggests that as volumetric conversion increases the residual vitroplast material becomes more highly condensed and/or less saturated.

When solvents are used during hydrogenation there is substantially more conversion to solvent-soluble products and we would expect the remaining residue material (vitroplast) to attain a higher reflectance.

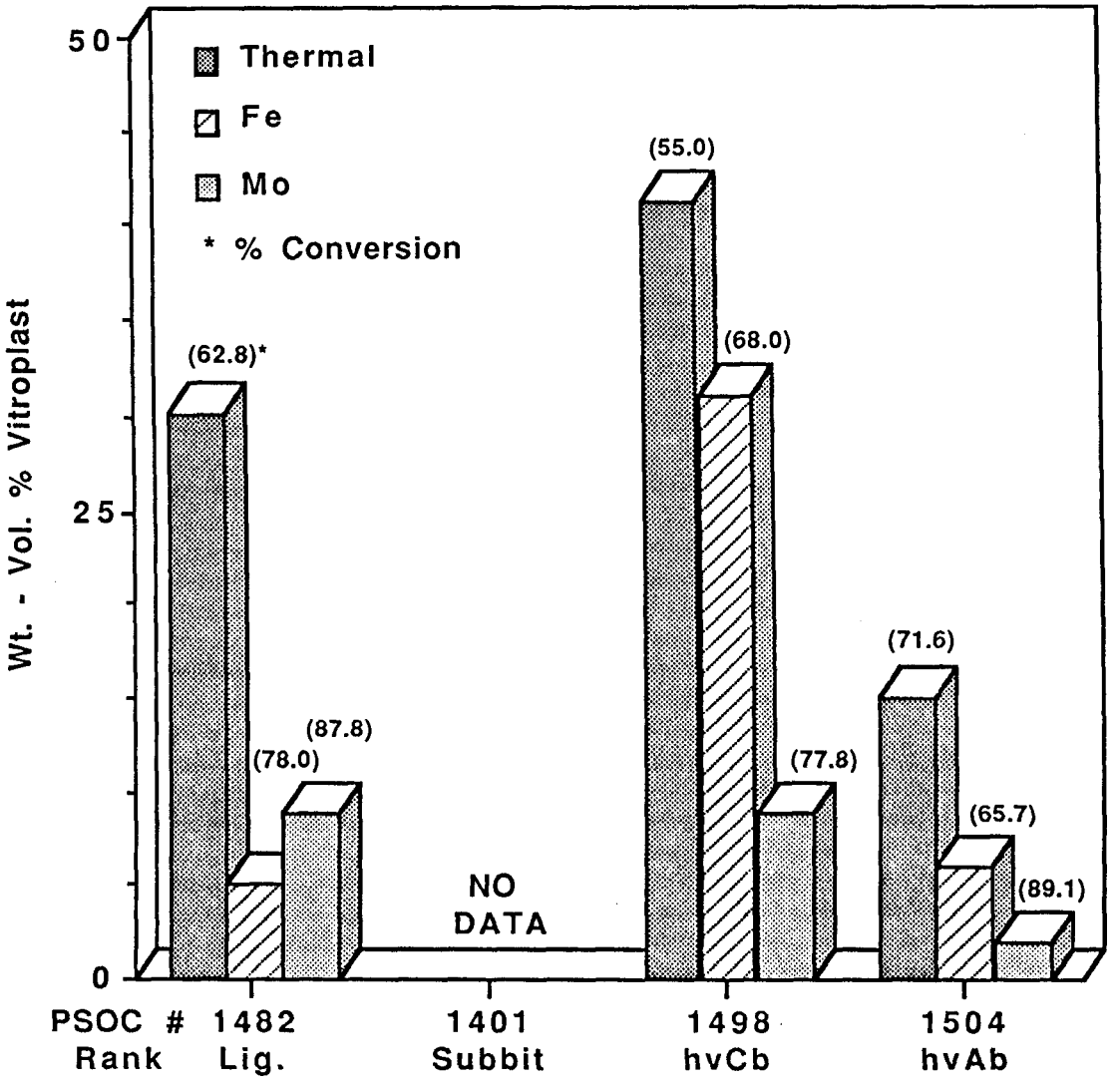

Figure 3.7 Wt. % Vitroplast Measured in Temperature-Staged Hydrogenation Residues Using Distillate Process Solvent as a Function of Coal Rank and Catalyst

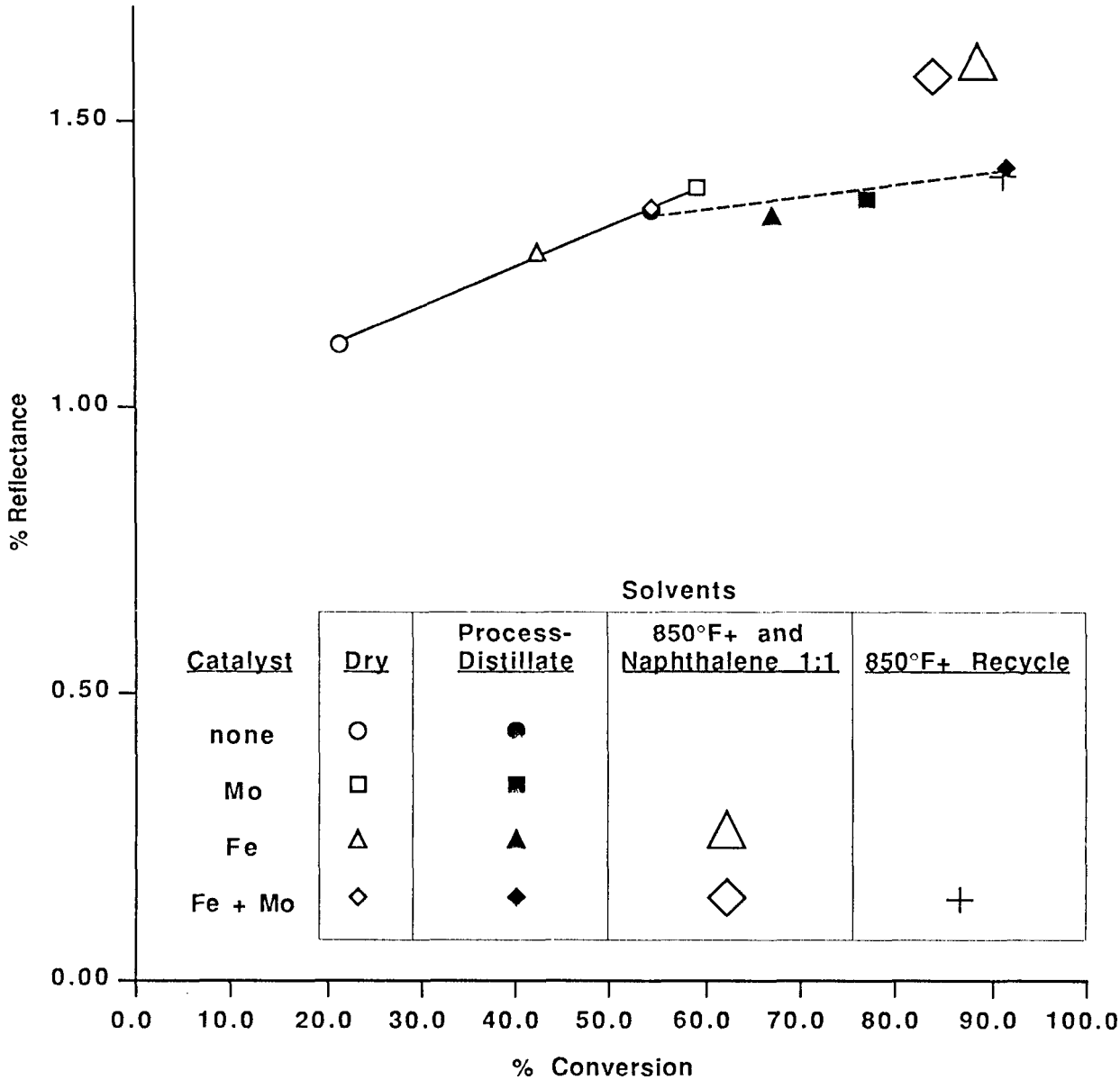

Figure 3.8 Mean Reflectance of Vitroplast and Conversion as a Function of Solvent and Catalyst for Temp.-staged Reaction Using PSOC-1498

However, only two additional data points at much higher conversion continue the linear relationship seen with dry hydrogenation residues. These data points were generated from hydrogenation in a solvent that consisted of a 1:1 blend of the 850+°F recycle and naphthalene. With the 850+°F recycle solvent alone a similar conversion was obtained, but the reflectance of the vitroplast material was significantly lower. Consequently, some of the reaction mechanisms that are active during dry hydrogenation and that produce an insoluble residue of relatively high reflectance (i.e, carbonization reactions) perhaps remain active when the high-boiling recycle solvent is diluted with naphthalene.

For the runs made with the process distillate solvent, a different linear relationship appears. The slope of this line is considerably less than that demonstrated for dry hydrogenation. Because of this relationship we suspect that the process distillate solvent is contributing to both a high total asphaltene content (see Table 2.18, Section 2.3.6) and a much more saturated THF-insoluble residue, which could account for its lower reflectance. The significance of this lower reflectance may be that molecules generated from the solvent are contributing to the insoluble residue, and although a high conversion was obtained, a poor product distribution (negative oil yield) was realized.

Table 3.4 gives a qualitative description of residues from the first and second stages of catalytic (1.0% Mo) and non-catalytic liquefaction runs. In these experiments both naphthalene and tetralin were used in liquefaction of the subbituminous coal (PSOC-1401) under hydrogen and nitrogen atmospheres. Major microscopic changes took place as a result of the second-stage reaction at 425°C. Mass conversion to liquids appear to have been largely controlled by the presence of catalyst (1% Mo) when

Table 3.4. Summary of Microscopic Appearance of Liquefaction Residues from the Reaction of PSOC-1401 in H_2 and N_2 Atmospheres

	First Stage (275°C)		Second Stage (425°C)	
	Naphthalene	Tetralin	Naphthalene	Tetralin
Non-catalytic	Basically the same as the untreated coal.		Massive huminite with dissolution pores in humo-collinite.	Thermally deformed, amorphous huminite with abundant evaporation and dissolution vesicles.
Catalytic	Basically the same as the untreated coal.		Residual skeletons predominant ** No liptinite present in the residues after second-stage reaction ** Inertinite present in the residues after second-stage reaction	

tetralin and naphthalene were used as solvents. In the absence of catalyst, with naphthalene as solvent, the residue was composed predominantly of massive huminite (vitrinite) showing only partial dissolution of the unstructured humocollinite macerals. With tetralin, most of the huminite was thermally altered, with the development of abundant dissolution pores. Where catalyst was employed in the second stage, the residues resulting from the use of either solvent were composed predominantly of residual skeletons. Volumetrically, the skeletons represent less than 10% of the original volume of the vitrinite particles, indicating a very high degree of dissolution.

Reflectance data were obtained from the vitrinite-derived residual materials of the catalytic and non-catalytic runs in naphthalene, and are summarized in Table 3.5. Non-catalytic experiments in naphthalene resulted in considerably less evidence of vitrinite alteration (unreacted vitrinite type) than those runs in which the Mo catalyst was employed. This was also observed for the residues following dry hydrogenation (Table 3.1). Also, when molybdenum was introduced during the high-temperature single-stage reaction, there was a higher volumetric conversion, the vitrinite showed increased signs of thermoplastic behavior and the reflectance of the residue increased significantly.

3.4. CONCLUSIONS

Petrographic analyses were performed on tubing-bomb residues selected to evaluate the advantage of temperature-staging over single-stage liquefaction, and the presence and absence of alternative catalysts, solvents and atmospheres for four different ranks of coal (PSOC-1482, lignite; PSOC-1401, subbituminous; PSOC-1498, hvCb; PSOC-1504, hvAb).

Table 3.5. Maximum Reflectance of Vitrinite-Derived Residue Material from PSOC-1401 in Naphthalene

Reaction Condition	Catalytic (1% Mo)				Non-catalytic			
	Run#	Reflectance, %	Vitrinite Type	Conversion, %	Run#	Reflectance, %	Vitrinite-Type	Conversion, %
Raw	--	0.42	(unreacted)	--	--	0.42	(unreacted)	--
275°C, N_2	34	0.58	(unreacted)	11.0	33	0.54	(unreacted)	12.0
275°C, H_2	37	0.62	(unreacted)	7.0	23	0.59	(unreacted)	10.2
425°C, N_2	26	1.41	(reacted)	34.5	28	1.32	(unreacted)	37.2
425°C, H_2	32	1.47	(reacted)	88.7	20	1.37	(unreacted)	55.4
275°C, N_2 + 425°C, H_2	--	--	--	--	93	1.59	(reacted)	42.5

In general, the use of quantitative petrographic techniques in this study has provided pertinent information on the activity of coals of different ranks, as well as the suitability of reaction conditions. For instance, an important result achieved by comparing petrographic information on residues of different coals suggests that the hvCb coal was not reacted under sufficiently severe conditions to produce high conversions. Unusually low conversions or product yields can be caused by too severe reaction conditions as well as those insufficiently severe; only petrographic study or catastrophic process failure can identify the ultimate cause. The practical application of reflectance analyses has been demonstrated in evaluations of whole-product residues; the work has shown that before solvent extraction, dry hydrogenation residues consist of a low-reflectance population that has relatively high fluorescence and is soluble in THF. The presence of a catalyst increases the production of this low-reflectance population and, in the case of the hvAb coal, results in the development of substantial anisotropic semicoke. Retrogressive reactions suggested by the appearance of anisotropic semicoke following dry hydrogenation are not observed when a vehicle solvent is used during liquefaction.

REFERENCES

1. Mitchell, G.D., Davis, A. and Spackman, W., 1977, in R.T. Ellington, ed., "Liquid Fuels from Coal", Academic Press, pp. 245-270.

2. Wakeley, L.D., Davis, A., Jenkins, R.G., Mitchell, G.D. and Walker, P.L., Jr., 1979, Fuel, 58, 379-385.

3. Walker, P.L., et al., 1978, Characterization of Mineral Matter in Coals and Coal Liquefaction Residues, Annu. Rep. Penna. State Univ. to Electric Power Research Inst. EPRI AF-832, Project 3660-1.

4. Given, P.H., Spackman, W., Davis, A. and Jenkins, R.G., 1980, in D.D. Whitehurst, ed., "Coal Liquefaction Fundamentals", ACS Sympos. Ser. 139, pp. 3-34.

5. Classification of Hydrogenation Residues, International Committee for Coal Petrology, Commission III, Aachen Meeting, 1988.

6. Derbyshire, F., Davis, A. Epstein, M. and Stansberry, P., 1986, Fuel, 65, 1233-1240.

4. THE NATURE OF DISPERSED CATALYST IN COAL LIQUEFACTION

The ultimate objective of this research is to develop a better understanding of the reaction chemistry involved in temperature-staged catalytic liquefaction. It has been demonstrated that catalytic liquefaction is superior to non-catalytic, and that temperature-staging with added catalyst provides an additional increment of conversion and improved product distribution regardless of the solvent or coal used. Consequently, to understand fully the chemical reactions that are occurring as coal converts to lower molecular weight products, more information is needed concerning the chemistry and physical associations of the catalyst as it interacts with the coal-solvent-gas system during liquefaction.

To investigate the function of catalysts during liquefaction, a series of experiments was designed and observations made that address the following questions. 1) During the course of liquefaction, how do reaction conditions affect catalyst composition? 2) Can we identify the active phase(s)? 3) How effectively is the catalyst impregnated into the structure of coals? and 4) How is the catalyst associated with coal organic matter in liquefaction residues?

The techniques used in this phase of the study involve optical and electron microscopy to identify the physical nature as well as the elemental composition of catalyst precursor materials, catalyst residues and remnants found in solvent-insoluble residues following coal liquefaction. We have concentrated our efforts mainly on a sulfided ammonium molybdate (SAM) catalyst precursor, produced in-house, that was introduced to the various coals by impregnation and then freeze-dried to remove water. A limited amount of work was completed on an iron-based catalyst (iron sulfate precursor) as well as a combined molybdenum and iron

catalyst. In the case of SAM, experiments were conducted using the catalyst alone to determine if phase transformations occur as a result of reaction conditions, whereas the other catalysts were studied from coal liquefaction residues. Also, to form a better understanding of the impregnation technique used, individual coal particles were impregnated with the molybdenum catalyst in an attempt to study the extent of penetration of catalyst into the coal structure. In the sections that follow, we will discuss the results of these investigations and what has been learned from our investigation of coal liquefaction catalysts.

4.1. CHARACTERIZATION OF SULFIDED AMMONIUM MOLYBDATE CATALYST AND RESIDUES

4.1.1. Introduction

It has been shown that molybdenum is among the most active metals for coal hydrogenation as long as it can be impregnated in or dispersed on the coal prior to or during liquefaction (1-6). Early workers (2,4), used a water-soluble ammonium molybdate, $(NH_4)_6Mo_7O_{24} \cdot 4H_2O$, that could be dispersed on coal by slurrying. Following the so-called "impregnation" with catalyst, both coal conversion and yield of oil were markedly improved over the addition of the catalyst as a solid, (i.e., 93% vs 34% conversion and 41% vs 14% oil yield, respectively for hydrogenation of Rock Springs coal, no vehicle solvent, for 1 hour, 450°C and 6.9 MPa cold hydrogen pressure (2)).

Weller (3) contended that MoS_2 was most probably the stable molybdenum compound under liquefaction conditions, provided the coal contained enough sulfur for the conversion of the molybdenum oxide catalyst to a disulfide. However, the direct addition of solid MoS_2 as a coal hydrogenation catalyst also results in poor levels of conversion which suggests either that it has low activity or that it must be dispersed to be effective. Anderson and

Bockrath (6), in their study of *in situ* development of iron and molybdenum sulfide catalysts during coal liquefaction, determined that maximum coal conversion was obtained when the S/Mo atomic ratio reached 2.0. They concluded that MoS_2 was the active phase of the molybdenum catalyst and suggested that only enough elemental sulfur need be added above that being released from coal pyrite during the formation of pyrrhotite to complete the formation of MoS_2. Additions of sulfur to bring the S/Mo atomic ratio to three did not further increase coal conversion.

With this in mind, Terrer (7) and Stansberry and Derbyshire (5) developed and evaluated a procedure aimed at impregnating a water-soluble molybdenum sulfide salt into the structure of coal before liquefaction. In this procedure, H_2S is bubbled through an aqueous solution of ammonium heptamolybdate (AHM) to produce a sulfided ammonium molybdate (SAM) which approaches the composition of ammonium tetrathiomolybdate [$(NH_4)_2MoS_4$, ATM)]. According to Naumann (8), ATM readily decomposes under relatively mild heating to form MoS_2. Therefore, in this procedure a sulfided molybdenum compound can be introduced which can decompose in place to form the active phase. In further refinements of the procedure (5), it was found that slurrying the aqueous SAM with coal and then freeze-drying to remove water was more effective, in terms of coal conversion, than drying at 110°C in a vacuum. Also, 0.02 mL of carbon disulfide for each 5 g of coal was added to maintain the SAM in a fully sulfided form during the early phases of temperature-staged coal liquefaction.

As part of the current investigation, a series of experiments was designed to determine the effects of one- and two-stage liquefaction reaction conditions on the sulfided ammonium molybdate catalyst in the absence of coal and solvent. The purpose of this line of experimentation

was to determine what transformations occur in the catalyst during the course of liquefaction; what effects both temperature and gas atmosphere might have on the catalyst precursor; and, to identify more specifically the composition of the active catalyst phase(s). The results of the experiments outlined below provide some basic compositional and X-ray analytical information, and show that we are, in all probability, dealing with a non-crystalline catalyst that is variable in physical and chemical properties.

4.1.2. Experimental

As reported by Stansberry and Derbyshire (5), sulfided ammonium molybdate was prepared by bubbling H_2S gas (at approximately 30 mL/min) through a solution of ammonium heptamolybdate tetrahydrate for about 30 min at room temperature while stirring. The reaction requires about one minute and is accompanied by a color change, i.e., clear to pale orange to dark red. When coal liquefaction experiments are performed, the coal is slurried with the SAM for 30 min before the excess water is removed by freeze-drying.

To better understand catalyst reactions and interactions with coal during liquefaction, the SAM catalyst was subjected to the same series of reaction conditions normally used for the liquefaction of coals. The catalyst was freeze-dried as described above and then about 0.5 g SAM in a Pyrex test tube was placed in a 25 cm^3 stainless-steel tubing-bomb reactor (without coal or solvent). Before sealing the reactor, a calculated amount of CS_2 was added to ensure that sufficient sulfur was present to convert all of the molybdenum to MoS_2. The tubing bomb was purged of air, pressurized to 7 MPa with either nitrogen or hydrogen and then reacted in a fluidized sand bath for the prescribed time and temperature sequence as

described in Section 2.2.2. The only difference between these catalyst reactions and coal liquefaction experiments, is that the tubing bomb was not vented and repressurized with the appropriate gas during temperature-staged reactions.

Table 4.1 identifies the reaction conditions for each sample and provides an elemental analysis for six of the catalyst residues. Over the course of this project, two sets of residues were prepared for each reaction condition owing to the unusual findings obtained from the first sample set (P71-1 through 6). The initial series of catalyst residues was prepared with SAM that had been stored under laboratory conditions for more than six months. Elemental analysis and the subsequent optical characterization demonstrated that each residue was composed of multiple phases that were sulfur-deficient. Accordingly, a second set of catalyst residues (i.e., P71-7 through 12) was generated with freshly prepared SAM.

In order to observe the physical form of the catalyst (SAM) and its precursor material (AHM), evaporated slide mounts of these water-soluble chemicals were prepared and studied using transmitted-light microscopy. Catalyst residues prepared under pretreatment conditions in both nitrogen and hydrogen (P71-1 and 2) also were extracted to determine whether any water-soluble materials remain after reaction. The general procedure employed involved preparing a solution with distilled water, dispersing the mixture by ultrasonic vibration for 30-60 min and then placing a drop of the solution on a clean microscope slide. For the catalyst residues, a syringe and small cotton ball were used to separate the water-soluble materials from the insoluble fraction. The water was allowed to evaporate overnight and the residue was examined under the microscope at 156X magnification in air.

Table 4.1. Analyses of Molybdenum and Sulfur in Selected Catalyst Residues

Sample Id.	Conditions	P71-1 through 6 % Mo	P71-1 through 6 % S
P71-1 and 7	30 min; 275°C; 7MPa H_2	58.81	6.98
P71-2 and 8	30 min; 275°C; 7MPa N_2	56.81	7.30
P71-3 and 9	30 min; 275°C; then 30 min; 425°C; 7MPa H_2	64.41	12.93
P71-4 and 10	30 min; 275°C; then 30 min; 425°C; 7MPa N_2	64.24	8.80
P71-5 and 11	30 min; 425°C; 7MPa H_2	64.63	9.29
P71-6 and 12	30 min; 425°C; 7MPa N_2	62.37	7.68

All of the reacted catalyst residues (P71-1 through 12) were characterized using optical microscopic analyses that included measurement of mean maximum reflectance in oil, and in the case of the first set of residues, point-count analysis to determine the volume percentage of each optically distinct residue phase. Where sufficient sample remained, X-ray diffraction patterns were obtained to determine the presence of MoS_2 and the extent of its crystallinity.

Selected residues were prepared for electron microprobe analysis, including four samples from the first series of residues and all six samples from the second set. An ETEC automated electron microprobe analyzer was employed for both sets of samples. A PET (Pentaerythritol) crystal spectrometer was used for sulfur and molybdenum analyses, while other elements were monitored with an energy-dispersive spectrometer (EDS). For quantitative measurements, pyrite (FeS_2) was used as a standard for sulfur and 99.95% pure molybdenum metal was used for the molybdenum standard. Each set of samples was coated with carbon simultaneously to ensure an identical coating thickness. The accelerating voltage was set at 15 kV and the data were reduced by the ZAF method using an internal software package (MAGIC). Because there is a small interference of the sulfur K_α peak with the K_α peak of molybdenum, a factor of 0.027 times the molybdenum concentration was used to correct the sulfur values for the first sample set, while the sulfur K_β peak was used for the second set of catalyst residues.

4.1.3. The Physical Form of Catalyst Precursor Materials

Ammonium heptamolybdate (AHM) is a white, crystalline powder that is readily soluble in distilled water under ambient conditions. The evaporated deposit prepared as described above is transparent with a slight

greenish tint. In transmitted, plane-polarized white light AHM displays a variety of crystal forms and under crossed nicols all of the material appears anisotropic. Some areas form well-defined six-sided crystals (perhaps hexagonal) as illustrated in Figure 4.1, whereas other crystal forms include fan-shaped dendrites and/or acicular crystals that radiate from a central point of nucleation.

In comparison, freshly prepared sulfided ammonium molybdate appears black to dark red in color, is platy and displays a vitreous luster. The SAM dissolves completely; however, the solution is so dark that it is difficult to distinguish whether it is totally soluble or whether a colloidal material might be present. The evaporated deposit is transparent to opaque under transmitted light depending upon the thickness of the deposit on the slide. In the transparent areas, SAM is deep red and isotropic; crystal growth is conspicuously absent. During evaporation, SAM develops a well-defined fracture system which is illustrated in Figure 4.2. A few of these fractures have become infilled with a granular, anisotropic material that appears to be residual AHM. The fact that the latter fills the fracture areas shows it is the last to solidify during evaporation.

The sulfided molybdate that had been used to generate the first set of liquefaction catalyst residues also was examined under the microscope and found to be completely different from the freshly prepared SAM just described. This material was stored under laboratory conditions for a considerable length of time and, hereafter will be referred to as 'aged SAM'.

The aged SAM appears to be a heterogeneous mixture of an orange to red powder with a white, acicular crystalline material. The orange powder did not dissolve appreciably in distilled water. Therefore, an ultrasonic bath

Figure 4.1 - Crystalline nature of Ammonium Heptamolybdate (AHM) observed in transmitted light in air under crossed nicols from evaporated slide mount.

Figure 4.2 - Platy, fractured and isotropic nature of freshly prepared sulfided ammonium molybdate (SAM) observed in transmitted light in air from evaporated slide mount.

was used to prepare a suspension of the mixture for microscopy. When drops of the suspension were placed on a microscope slide the orange insoluble fraction agglomerated in the center of the droplet. After evaporation, the insoluble fraction was surrounded by a dark green rim. Inspection under transmitted light revealed that the green, water-soluble material is anisotropic and possesses a crystal morphology that was similar to that described for the ammonium heptamolybdate. Accordingly, we believe that the soluble material is probably AHM. The orange, insoluble fraction appears as an aggregate of 5-10 μm sized particles that are mostly opaque. However, in those areas thin enough to transmit light, the insoluble material is isotropic. Based on the color change that occurs when AHM is sulfided, we conclude that this insoluble phase is a molybdenum oxysulfide*.

We can conclude that AHM and SAM are distinctive and separately recognizable under the microscope in transmitted light. The water-soluble molybdate (AHM), is basically white with a greenish tint and upon evaporation from solution develops an anisotropic crystalline form. Freshly prepared SAM, the thiomolybdate, is black to deep red, and upon evaporation from solution forms mostly a platy deposit that is isotropic. The presence of a small portion of an anisotropic and finely crystalline material in the freshly prepared SAM suggests that sulfidization of the

---

*A sample of the aged SAM was provided to Leco Corporation for direct determination of oxygen using their new method of Inert Gas Fusion and spectral analysis. Their results on the as-received aged SAM showed that it contained about 33.7% oxygen. This is slightly less oxygen than a fully hydrated ammonium heptamolybdate would contain (about 36%). Therefore, we conclude that the aged SAM sample had indeed become oxidized during storage and was predominantly a molybdate rather than a thiomolybdate.

molybdate is incomplete. Furthermore, extended storage of SAM in air may result in oxidation of the thiomolybdate, thereby producing a catalyst mixture of sulfides, oxides and oxysulfides of molybdenum.

Identification of two optically distinct materials in the freshly prepared SAM suggests the need for a critical evaluation of the technique used to prepare the SAM catalyst from AHM. Rode and Lebedev (10) used ammonium tetrathiomolybdate in their experiments that was produced by the Kruss method as described in the following equation:

(1) $$(NH_4)_6Mo_7O_{24} \cdot 4H_2O + 28H_2S + 8NH_3 \rightarrow 7(NH_4)_2MoS_4 + 28H_2O$$

As cited, this method involves the saturation of concentrated aqueous ammonium molybdate solution with H_2S in the presence of free ammonia. The presence of excess ammonia will allow for the complete transformation of AHM to ATM and is the principal difference between this technique and the procedure followed in the current study for the production of our liquefaction catalyst. It also means that, without free ammonia, there will be an incomplete conversion of ammonium heptamolybdate to tetrathiomolybdate and that some portion of the catalyst will be either a molybdate or an oxythiomolybdate (e.g. $MoS_2O_2^{-2}$).

4.1.4. Characterization of Catalyst Residues

As stated above, the objective of this work was to form a better understanding of what happens physically and chemically to the SAM catalyst under the range of conditions used in coal liquefaction, but without the possible interference of coal or solvent. With this type of information we may be able to understand better the chemical reactions in which the thiomolybdate catalyst is involved during coal-solvent-gas processing in one- and two-stage liquefaction.

A major part of the work reported below was performed on catalyst residues (from runs without coal or solvent) produced from a precursor that had oxidized to an undetermined extent during storage. Fortunately, all of catalyst materials used in the coal liquefaction experiments were freshly prepared. However, the information gained on how molybdate and, perhaps, oxythiomolybdate respond to different liquefaction conditions is pertinent in view of our demonstration that these substances can be present inadvertently because of the incomplete sulfidization of AHM.

4.1.4.1. Characterization of Aged Sulfided Ammonium Molybdate Residues

4.1.4.1.1. optical microscopy

Material from each aged SAM catalyst residue (P71-1 through 6) was examined by reflected-light microscopy. Preliminary inspection showed that there were at least three distinct phases that could be routinely identified, as well as a number of transitional materials. No attempt was made to name these materials until more was known about their composition and basic stoichiometry. We referred to each by a roman numeral designation, i.e., I, II and III.

Phase I is illustrated in Figure 4.3, and can be described as occurring in broad, massive, angular grains which have a uniform and relatively low reflectance. The particles have a well-developed system of fractures which at higher temperatures allows for disaggregation into smaller particles. The overall three-dimensional shape could be platy, and in some cases, displays a rough, acicular crystal-like structure.

Phase II is typified by the central particle in Figure 4.4 which is composed of a loose aggregate of 1-5 μm, highly reflecting, spherical particles which generally are aggregated into larger, more angular masses. The internal pore space appears to be free of any other material except in the case of pretreatment in nitrogen (P71-2). In this sample, Phase II particles contain a partially water-soluble, low-reflecting and granular matrix material (discussed in Appendix C as transitional material).

Phase III is illustrated in Figures 4.5 and 4.6 and occurs as highly anisotropic, low-reflecting, irregular-shaped particles with a

Figure 4.3 - A dominant component of P71-1 residue, Phase I occurs as a broad, angular particle of relatively low reflectance.

Figure 4.4 - Phase II material observed in P71-1 is a highly reflecting aggregate of 1-5 micron diameter spheres which form in loose, open clusters.

uniformly small internal porosity. In plane-polarized white light, Phase III is orange to red in color, the intensity of which becomes more brilliant in the high-temperature residue from nitrogen runs (P71-6). Figure 4.5 illustrates Phase III material in polarized light, whereas Figure 4.6 is taken under crossed nicols to demonstrate that the particle is anisotropic.

Based on this optical characterization three prominent and distinct phases are identified, as well as two transitional material discussed in Appendix C. To determine the relative importance of each phase, the above classification was employed in a petrographic point-count analysis to determine the volume percentage of each component in the aged catalyst residues from runs without coal. Also, an analysis of mean maximum reflectance was performed on each phase to establish how their properties might change with reaction conditions. Results of these analyses are found in Table 4.2.

Phase I is the dominant component in those residues produced from reaction in a hydrogen atmosphere in the presence of CS_2. As reaction temperature and time increased there was a significant decrease in the concentration of this phase. There was also a slight decrease in the concentration of Phase II in response to reaction severity. The most significant response to change in reaction conditions was the appearance of two additional materials that most likely formed at the expense of or in place of Phase I. A low-reflecting anisotropic material, Phase III, was formed during the single-stage, high-temperature reaction (P71-5), while a material that was transitional in reflectance and appearance between Phases I and II was formed during the two-stage reaction (P71-3). Apparently, pretreatment of the catalyst in a hydrogen atmosphere and in the presence of CS_2 followed by a high-temperature reaction inhibited the formation of Phase III. It is unlikely that this Phase I/II transitional material was a precursor to Phase III, because of its higher reflectance.

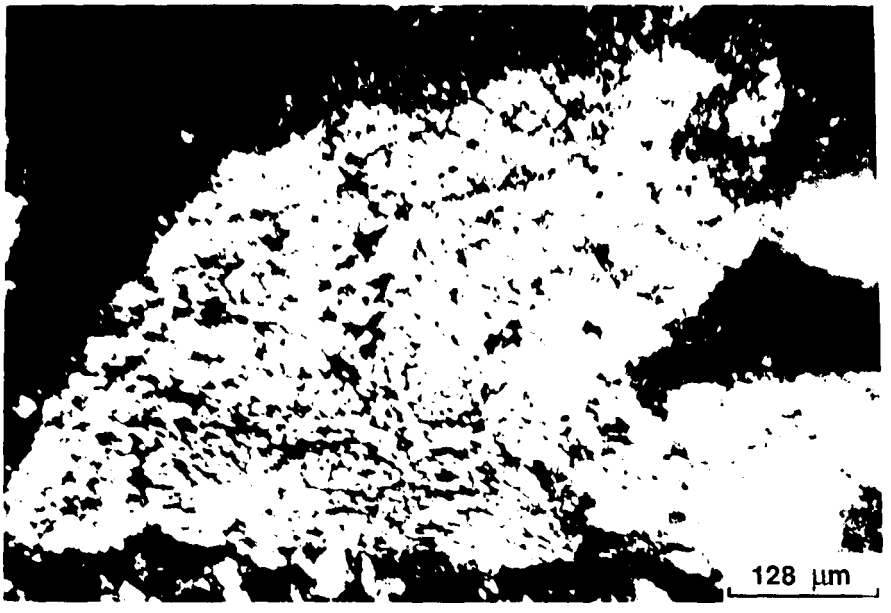

Figure 4.5 - Phase III material (P71-6) as seen here in plane polarized light, is a broad, angular particle with small and uniform porosity.

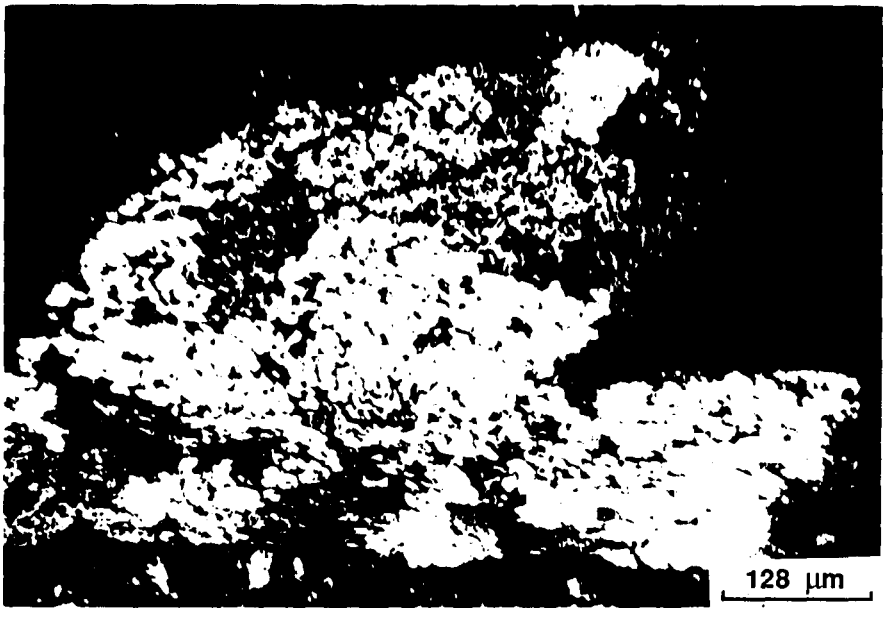

Figure 4.6 - Same Phase III particle as Figure 4.5, but under crossed nicols to demonstrate anisotropy.

Table 4.2. Petrographic Analyses of Catalyst Residues Prepared from Aged SAM

Sample Id.	Reaction Conditions		Point Count, Vol. %					Maximum Reflectance in Oil, %			
	Pretreat.	Liquef.	Phase I	Phase II	Phase III	Phase I/II Transition	Matrix	Phase I	Phase II	Phase III	Phase I/II Transition
P71-1	275°C, ½h, H_2	--	70	30	--	--	--	2.6	5.7	--	--
P71-2	275°C, ½h, N_2	--	--	22	--	--	78	--	∿ 6.5	--	--
P71-3	275°C, ½h, H_2	425°C, ½h, H_2	43	27	--	30	--	4.5	>10.5	--	7.8
P71-4	275°C, ½h, N_2	425°C, ½h, N_2	20	25	55	--	--	4.4	8.8	1.7	--
P71-5	--	425°C, ½h, H_2	50	20	30	--	--	5.2	>10.5	3.3	--
P71-6	--	425°C, ½h, N_2	11	35	54	--	--	4.9	10.1	2.7	--

Much less Phase I material was observed in residues that were produced during reaction of the aged SAM in a nitrogen atmosphere and with CS_2. In fact under pretreatment conditions (P71-2), no Phase I material was produced. Following both high-temperature reactions (single- and two-stage) in nitrogen, Phase III accounted for more than half the residue by volume. Phase II material was at its highest concentration in the single-stage, high-temperature experiment (35%, P71-6), but decreased significantly in the two-stage reaction (25%, P71-4).

In general, the reflectance (in oil) of Phases I, II and III increased as experimental conditions changed from pretreatment to two-stage to single-stage, high-temperature reactions in both atmospheres (Table 4.2). Reaction of the aged SAM at 425°C resulted in a two-fold increase in percentage reflectance for each Phase. Residue components produced in nitrogen are slightly lower in reflectance than those produced in hydrogen for any given reaction condition. Based on the known reflectance of molybdenite (MoS_2) in oil (11.6%), the increase in reflectance probably indicates that the composition of Phase II may be approaching that of molybdenum disulfide.

4.1.4.1.2. electron microprobe studies

Four of the catalyst residues were prepared for electron microprobe analysis, namely all of the residues produced under a hydrogen atmosphere (P71-1, 3 and 5) and that of the temperature-staged reaction in nitrogen (P71-4). The objective of this investigation was to determine the distribution of molybdenum and sulfur in each of the residue components which had been identified by optical microscopy (Phases I, II, III and the Phase I/II transition).

The procedure used to analyze each component in the catalyst residues was to identify positively a particular phase using the microprobe white-light optics, and then to collect x-ray counts for 20 sec each for sulfur and molybdenum. Between 7 and 20 different particles of each phase in each sample were analyzed in this manner. Further, the EDS system was used at times throughout these analyses to determine the elemental composition of the mass not accounted for by measurement of sulfur and molybdenum. At no time was any other element detected greater in atomic number than sodium (Z = 11), which means that the mass unaccounted for is either oxygen, nitrogen or carbon from the CS_2 added to each experiment.

Table 4.3 gives the results of the microprobe analysis along with the standard deviation and total mass accounted for by molybdenum and sulfur. In general, these data show that each component of the residues contains slightly more than 50% molybdenum and has a variable amount of sulfur. Phase I material showed a clear increase in sulfur content with reaction severity for those residues produced under hydrogen, whereas sulfur concentration remained very low for Phase I produced under a nitrogen atmosphere; Phase III material has a very low sulfur concentration regardless of atmosphere; and, Phase II has the highest sulfur concentrations and total mass accounted for by the elements analyzed. Sulfur and molybdenum determinations for the Phase I/II transition material suggested that it was indeed transitional between the two phases, but closer to Phase II.

The standard deviations for all of these analyses are high and suggest that the composition of each phase was not only variable as a result of reaction conditions, but that the variations must be significant among different particles of the same phase. A test was performed to determine

Table 4.3. Average Weight Concentrations of Mo and S as Determined by Electron Microprobe Analysis in Distinct Phases of Aged Catalyst Residue

	Phase I			Phase II			Phase III			Phase I/II Transition		
Sample ID	%Mo	%S	Total	%Mo	%S	Total	%Mo	%S	Total	%Mo	%S	Total
P71-1; 275°C, ½h, H_2	55.3	11.1	56.4	47.2	23.9	71.1	-	-	-	-	-	-
std*	2.1	1.0	-	5.4	8.6	-	-	-	-	-	-	-
P71-3; 275°C, ½h, H_2; 425°C, ½h, H_2	56.1	3.3	59.4	50.7	21.0	71.6	-	-	-	55.5	15.3	70.8
std	4.1	0.8	-	4.0	6.0	-	-	-	-	3.2	5.2	-
P71-5; 425°C, ½h, H_2	58.4	8.0	66.4	50.9	25.4	76.2	54.6	0.3	54.9	-	-	-
std	2.0	2.5	-	6.5	8.7	-	6.5	0.6	-	-	-	-
Average	56.6	4.1	60.7	49.6	23.4	73.0	54.6	0.3	54.9	-	-	-
P71-4; 275°C, ½h, N_2; 425°C, ½h, N_2	52.8	0.3	53.1	56.2	31.6	77.8	51.5	0.4	52.0	-	-	-
std	5.9	0.4	-	6.0	5.5	-	3.0	0.4	-	-	-	-

*std = Standard Deviation

sulfur and molybdenum variability within the same particle. This was only possible with Phase I, because of its broad particle outline and minimal porosity. Repeat analyses within the same particle of Phase I showed that only about 1% of the molybdenum variation could be accounted for by particle heterogeneity, whereas the values of sulfur varied more than 50% (i.e., Mo = 57.06 ± 0.91 and S = 0.28 ± 0.16). Because of the high standard deviation, these microprobe data should be considered semi-quantitative at best. However, even with some uncertainty it is clear that Phase II is the main molybdenum sulfide phase, and that Phases I and III are distinct molybdate compounds.

4.1.4.2. *Characterization of Freshly Sulfided Ammonium Molybdate Residues*

In contrast to the aged SAM, residues produced from the freshly prepared catalyst (P71-7 through 12) behaved more predictably. Figures 4.7 and 4.8 illustrate the cross-sectional area of the platy catalyst, showing that it is of fairly uniform reflectance and possesses a slight granular anisotropy with individual isochromatic units of less than 1 μm. Major differences between residues produced under the varying reaction conditions are not readily apparent from visual inspection.

In comparison to the aged SAM, the gross physical properties of the fresh catalyst residues appear similar to the Phase I material. However, the reflectance of the new residues is higher and on a par with that reported for Phase II material, even in the lower temperature residues (compare Tables 4.4 with Table 4.2). Reflectance values for the residues of fresh catalyst show some variation with reaction conditions. The range of reflectances is lower for the catalyst pretreated in hydrogen and nitrogen in comparison to the fairly uniform reflectance of the temperature-staged or high-temperature residues. Reflectance distributions for the

Figure 4.7 - A dominant component of all residues prepared from fresh SAM are these broad, high-reflecting elongated particles (P71-9) as seen in plane polarized light.

Figure 4.8 - Same particle as in Figure 4.7, but under crossed nicols to illustrate the pin-point anisotropy.

Table 4.4. Mean Maximum Reflectance (oil) of Catalyst Residues Prepared from Fresh SAM

ID	Conditions	% Mean Max. Ro	Range	Comments	% Mean Ro
P71-7	PT-H_2	10.9	5.8 - 12.7	1. 94% of Counts = 11.1 2. 6% of Counts = 7.9	
P71-8	PT-N_2	6.6	5.8 - 8.7	1. 80% of Counts = 6.1 2. 20% of Counts = 8.1	
P71-9	TS-H_2	13.6	11.8 - 15.5		
P71-10	TS-N_2	12.4	10.8 - 14.1		
P71-11	HT-H_2	11.8	10.6 - 14.1		
P71-12	HT-N_2	12.6	11.4 - 14.1		

PT = Pretreatment, 275°C; 30 min
TS = Temperature-staged, 275°C, 30 min; 425°C, 30 min
HT = High temperature, 425°C, 30 min

pretreated catalyst show that there are two populations of reflectance, one higher and one lower. The lower reflecting material represents about 80% of the nitrogen pretreatment residue, but only about 6% of the hydrogen residue. Although there are some variations in the mean reflectance values for the temperature-staged and high-temperature residues, they are not significant when the standard error of the mean for each determination is considered.

As with the first series of residues from the aged catalyst, each of the residues from the fresh catalyst was analyzed on the electron microprobe for their concentrations of Mo and S. Our analytical procedure was much the same as described for the first set of residues, in that 10 to 20 individual particles were analyzed per phase per sample at the same x-ray count rate. The EDS system was again employed at times during these analyses to identify the presence of other elements greater in atomic weight than sodium. To determine whether the x-ray sampling volume had exceeded the depth of a particle, this series of samples were mounted in an iodine-substituted epoxy resin. Thus, if iodine was detected with the EDS, then that particular analysis point could be rejected. For the pretreatment samples, both high- and low-reflecting materials were evaluated. Also, a representative particle in each of the temperature-staged and high-temperature residues was selected to determine the variation in Mo and S that could be expected as a result of sample heterogeneity.

Table 4.5 provides the average weight percentages of Mo and S for each sample along with the total mass accounted for by these elements and their S/Mo atomic ratios. On average, those samples reacted under a hydrogen atmosphere are composed of 53% Mo and 44% S, accounting for 97% of the

Table 4.5. Electron Microprobe Results: Average Weight Concentrations of Mo and S in Catalyst Residues Produced from Fresh SAM

Sample Id.	Reaction* Condition	High-Ro Particles % Mo	% S	Total	S/Mo Ratio	Low-Ro Particles % Mo	% S	Total	S/Mo Ratio
P71-7	PT-H_2	53.67	43.84	97.51	2.44	53.98	42.72	96.70	2.37
Std. Dev.		1.29	1.66			1.26	0.90		
P71-9	TS-H_2	54.98	44.30	99.28	2.41	-	-	-	-
Std. Dev.		0.95	1.33						
P71-11	HT-H_2	51.17	44.05	95.22	2.58	-	-	-	-
Std. Dev.		1.63	2.11						
$\bar{x}$	H_2	53	44	97	2.48				
P71-8	PT-N_2	47.92	41.74	89.66	2.61	49.12	42.34	91.46	2.58
Std. Dev.		1.00	1.86			2.08	1.73		
P71-10	TS-N_2	51.31	46.57	97.88	2.72	-	-	-	-
Std. Dev.		0.86	1.64						
P71-12	HT-N_2	50.50	47.06	97.56	2.79	-	-	-	-
Std. Dev.		1.18	2.34						
$\bar{x}$	N_2	50	45	95	2.71				

*See Table 4.4 for description of reaction condition

mass. In comparison, those residues reacted in a nitrogen atmosphere have slightly lower Mo (50%) and slightly higher S (45%), with about 95% of the total mass accounted for. Consequently, the S/Mo atomic ratios are lower for the residues produced in hydrogen than those reacted in nitrogen, which supports the idea that hydrogen will help reduce $(NH_4)_2MoS_4$ to $MoS_2 + H_2S$. Standard deviations for each element are provided in Table 4.5 and although there appear to be variations in the distribution of Mo and S as a function of reaction conditions, for the most part these variations are not significant. From single-particle repeatability analyses, it was determined that <1.5% of the variation in Mo and <2.0% of the variation in S values can be attributed to the heterogeneous distribution of those elements within any given particle.

No significant difference can be observed between the Mo and S compositions of the high- and low-reflecting components of the pretreatment residues. However, one additional microscopic observation might help to explain the observed reflectance differences. During initial inspection of the Pyrex tubes in which the reactions were conducted, a black film was observed coating the walls of the high-temperature and temperature-staged reactions in nitrogen. This material could be an amorphous carbon black resulting from reactions involving CS_2. It is thought that CS_2 is involved in a sulfiding reaction (as yet undetermined) with the thiomolybdate when a nitrogen atmosphere is used and, perhaps, is one reason that these residues have higher S/Mo atomic ratios. In hydrogen, the CS_2 can react with the available hydrogen to form CH_4 and H_2S at the higher temperatures, thereby eliminating the carbon and increasing the H_2S partial pressure. About 80% of the pretreatment residue produced in nitrogen has a lower reflectance, compared to about 6% in hydrogen. We suggest, therefore, that most of the

CS_2 sulfur has been incorporated into the thiomolybdate under pretreatment conditions in nitrogen, whereas in hydrogen a much smaller proportion becomes incorporated as a result of the incomplete hydrogenation of CS_2 at 275°C.

To form a better understanding of the composition and crystallinity of the catalyst after reaction, four of the samples were evaluated by x-ray diffraction using Cu Kα radiation. Figure 4.9 compares the diffraction patterns obtained for P71-7, 8, 10 and 11 with one obtained from crystalline MoS_2. As expected, the diffraction patterns for the two pretreatment residues (P71-7 and 8) are quite diffuse; only very broad peaks are observed for the 002 and 101 at 2θ = 14 and 34, respectively. The 101 peak is missing for the pretreatment sample in nitrogen, which may be the result of incorporation of carbon into the catalyst material. At higher temperatures, in both nitrogen (P71-10) and hydrogen (P71-11), the 002 and 101 peaks are more well defined and a 110 peak is developed at 2θ = 58.5. Also, a suggestion of a 103 peak at 2θ = 39.5 has appeared, but is very broad at this stage of development. Consequently, the higher temperature residues show some indication of a poorly crystalline or amorphous MoS_2 structure. This is also confirmed by our optical evaluation of these samples, which showed that a submicron granular anisotropy exists in all of the samples and that the mean reflectance is lower than would be expected for the mineral molybdenite (natural MoS_2).

4.1.4.3. Discussion

Ample evidence has been presented to show that the aged SAM catalyst is principally composed of molybdate with a relatively small amount of thio- or oxythio-molybdate. The catalyst was found to be composed originally of soluble and insoluble materials which undoubtedly contributes

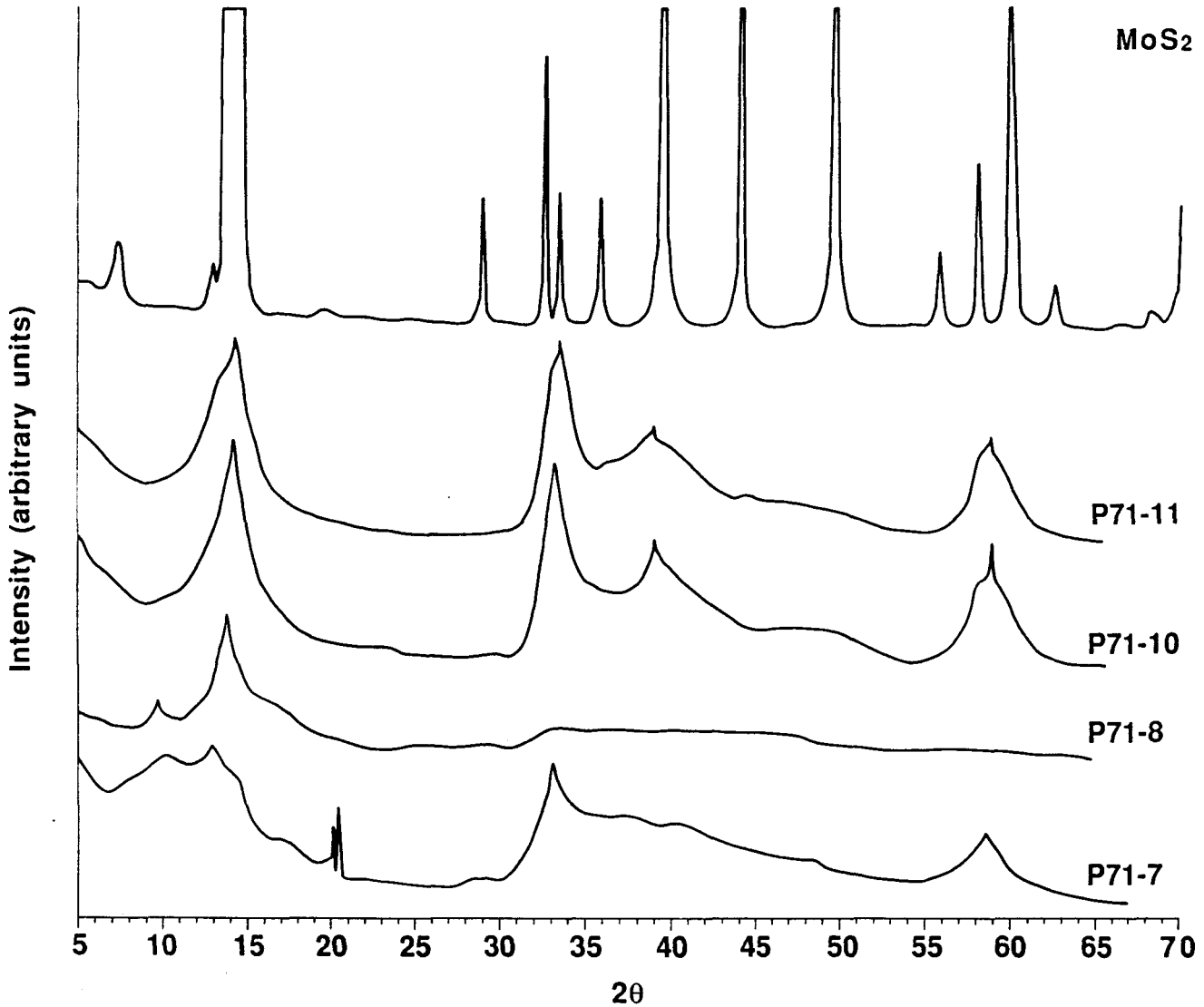

Figure 4.9 - Comparison of x-ray diffractograms of freshly prepared catalyst residues with crystalline MoS_2.

to the heterogeneity of the reacted catalyst samples. Our circumstantial evidence suggests that at least part of the Phase II material found in the aged SAM catalyst residues corresponds to the initial insoluble fraction, whereas the soluble material is mainly molybdate. When the aged SAM catalyst is subjected to liquefaction conditions, two distinct molybdate Phases (I and III) are formed in the residues.

The presence of a very low reflecting, partially soluble matrix material in P71-2, shows that treatment at 275°C for 30 min in a nitrogen atmosphere in the presence of CS_2 does not result in further sulfidization of the precursor or conversion to an insoluble molybdate. However, during reaction in a hydrogen atmosphere an insoluble molybdate is produced from the aged precursor in the form of the Phase I material that may have been partially sulfided by CS_2.

In the high-temperature, single-stage residues, a low-reflecting, anisotropic insoluble molybdate is formed (Phase III). The Phase III material is formed principally in a nitrogen atmosphere, and is associated with the production of a relatively minor amount of the Phase I material. Because the Phase I reflectance is greater than Phase III, it is likely that Phase III is produced instead of Phase I under these conditions. Following reactions in hydrogen (P71-5), Phase I material is dominant and has a relatively high sulfur content (8.0%), which implies that some of the molybdate may have been sulfided in the presence of CS_2 and hydrogen.

For the temperature-staged residues (P71-3 and 4), both of the molybdate Phases (I and III) formed under a nitrogen atmosphere, each having a very low sulfur content ($<0.5\%$). In a hydrogen atmosphere, however, there appears to have been significant sulfidization of the Phase I material; not only is the sulfur concentration in Phase I relatively high

(3.3%), but a Phase I/II transition material develops that is comparable in reflectance and sulfur content to Phase II, the main thiomolybdate component found in these residues.

From our characterization of the aged SAM catalyst residues, we have found some evidence for the *in situ* sulfidization of molybdate in the presence of CS_2 and H_2. However, apparently there is also a competing reaction when hydrogen is present that results in a loss of sulfur from the thiomolybdate. This effect is demonstrated by comparing the S/Mo atomic ratios of products from nitrogen and hydrogen runs in which the fresh catalyst was used (Table 4.5). In all cases, the S/Mo atomic ratios are higher for runs made under a nitrogen atmosphere than when hydrogen was employed. This same effect may be observed to a lesser degree in the electron microprobe results from the aged SAM catalyst residues (Table 4.3). The sulfur content of Phase II material was higher following the temperature-staged reaction in nitrogen than for all of the residues produced under a hydrogen atmosphere.

Residue from the freshly prepared and more fully sulfided catalyst are quite homogeneous when compared to those produced from the aged SAM material. Only in those residues produced under pretreatment conditions have we observed multiple phases as shown by reflectance differences. As explained, differences in reflectance may result directly from the incorporation of carbon derived from CS_2 into the molybdenum sulfide when using a nitrogen atmosphere. At higher temperatures, carbon is expelled, perhaps as a gaseous hydrocarbon (in hydrogen reactions) or as amorphous carbon black (in nitrogen reactions).

The S/Mo atomic ratios obtained from the fresh SAM residues (Table 4.5) show that under temperature-staged conditions, the molybdenum sulfide

formed is not strictly MoS_2, but may be a mixture of MoS_2 and perhaps elemental sulfur. X-ray diffraction and the optical anisotropy of the residue material suggests that an amorphous, submicron-sized MoS_2 may be present, but overall there is excess sulfur. Hei et al. (8) demonstrated that the presence of elemental sulfur and excess H_2S promotes bond cleavage of model compounds by the formation of active sulfur radicals ($S_x(H)$, where $x > 1$). Evidence from the current study shows that hydrogen reacts with the thiomolybdate catalyst, resulting in a loss of some sulfur and perhaps the formation of both hydrogen and hydrogen sulfide radicals. Catalyst in close proximity to coal during liquefaction could provide a source of these radicals to react with thermally disrupted bonds formed in the coal.

The thermal decomposition of ammonium tetrathiomolybdate (ATM) has been addressed in the literature. Both Naumann et al. (9) and Rode and Lebedev (10) state that decomposition takes place along the following path to produce a subcrystalline MoS_2:

(2) $$(NH_4)_2MoS_4 \rightarrow 'MoS_3' + 2NH_3 + H_2S$$

(3) $$'MoS_3' \rightarrow MoS_2 + S$$

Although it depends on the mode of preparation of the thio salt as well as the conditions under which decomposition occurs, Rode and Lebedev (10) found that ATM decomposes to form MoS_3 between 190-200°C in the absence of oxygen. The decomposition products were composed of 50.5% molybdenum and 47.8% sulfur with an S/Mo atomic ratio of 3.16. They determined that the composition of the product was $MoS_{3+x} \cdot yH_2O$, where $0 < x < 1$ and $y > 0$, and suggested that there may be excess sulfur in the free state associated with MoS_3. Thermographic analysis of ATM produced by the Kruss method, showed an endothermic reaction occurring between 200-254°C, corresponding

to the decomposition described in equation 2. Naumann et al. (9) also found an endotherm between 170-256°C while heating ATM in a stream of 10% H_2 in argon. Above 360°C an exothermic reaction occurs that signals a further decomposition of MoS_3 and the development of amorphous molybdenum disulfide as indicated by equation 3. The temperature at which this exothermic reaction occurs is apparently sensitive to heating rate and ATM preparation technique (9-12), because the peak temperature has been measured between 290-398°C and double peaks have been observed. Between 550-730°C additional sulfur is expelled from the structure and crystalline MoS_2 is formed (11 and 12).

In the current study of the catalyst reaction residues, it has been demonstrated that even the freshly prepared catalyst was not pure ATM, but may contain both sulfides and oxides of molybdenum. Further, reaction times were from 30 min to one hour and heating rates higher than used in previous studies. In the present study it is apparent that even though temperatures are sufficiently high to produce MoS_3 under pretreatment conditions (275°C) and MoS_2 under two-stage and high-temperature treatment conditions (425°C), there is insufficient sulfur to account for MoS_3 at lower temperatures and excess sulfur present at higher temperatures. The reasons for our observations differing from those reported in the literature undoubtedly results from a combination of different reaction conditions (heating rate, time, and atmosphere), use of an impure catalyst precursor and the presence of CS_2.

4.1.5. Conclusions

From the results presented in this portion of our study, we have demonstrated that the technique used to prepare the catalyst results in an incomplete sulfidization of ammonium heptamolybdate to ammonium

tetrathiomolybdate. It also has been demonstrated that care should be taken to preserve the catalyst during storage, and that re-oxidation of the catalyst is possible. From reactions of both aged and fresh SAM catalyst under the conditions of coal liquefaction and in the presence of CS_2, it has been shown that there are two separate reactions that involve sulfidization of molybdate and the loss of excess sulfur from the thiomolybdate when reactions are carried out in a hydrogen atmosphere. Reactions conducted in a nitrogen atmosphere show that there is less sulfur loss from the thiomolybdate when CS_2 is present and practically no reaction with the molybdate. The S/Mo atomic ratio of the thiomolybdate catalyst is lower following reaction in a hydrogen atmosphere than in nitrogen. Under all reaction conditions, the resulting catalytic material has a higher S/Mo atomic ratio than MoS_2 and is non-crystalline. We suggest that the loss of excess sulfur from the thiomolybdate is capable of producing radicals of hydrogen and of hydrogen sulfide under liquefaction conditions that can promote coal hydrogenation.

4.2. A STUDY OF COAL IMPREGNATION BY CATALYST

4.2.1. Introduction

Another major area of investigation has been to determine how effectively the catalyst material penetrates into the coal structure during impregnation. It has been claimed that impregnation of the molybdenum catalyst is important in order to achieve good conversion and product distribution during coal liquefaction (3,5 and 7). Therefore, this portion of our investigation was designed to study the relationships between catalyst and coal surfaces and to determine whether the catalyst may be absorbed into the pore and fracture structure of a coal during impregnation and after mild thermal treatment in hydrogen.

4.2.2. Experimental

Observations using electron and optical microscopy have been made of individual particles of both a subbituminous (Fort Union, PSOC-1488) and a high volatile A bituminous (Upper Sunnyside, PSOC-1504) coal. A number of 2-5 cm particles of each coal were imbedded in an epoxy resin and polished so as to expose the bedding plane structure of the coals. Two sets of particles were impregnated by placing a drop of the sulfided ammonium molybdate solution (SAM) onto the polished surface of each particle and then freeze-drying to remove the water. One set of samples was examined after impregnation, while the other set was examined after treatment at 250°C for 30 min in hydrogen at 7 MPa.

After the samples were treated, remnants of the catalyst were readily observed on the surface of each coal particle. Those particles which had been impregnated were reasonably competent; only the subbituminous coal showed signs of fracturing as a result of the dehydration process. Samples that had been heat treated in hydrogen were considerably fractured, but the area of catalyst deposition was clearly visible. Initially, the coating of catalyst appeared fairly uniform, but as time in storage increased the coating on the impregnated samples began to peel and fall from the coal surface in small flakes.

At this point, the samples were prepared for observation under the Scanning Electron Microscope (SEM) by coating each with a thin layer of carbon. A coating is necessary to reduce heat damage by the electron beam and to eliminate the buildup of surface charges which can interfere with imaging and analysis. An ISI-SX-40 SEM was used for imaging and was complemented with a Kevex 5100 X-ray energy spectrometer for qualitative analysis of elements greater in atomic weight than sodium. The energy

dispersive spectrometer (EDS) was used to detect the presence of molybdenum in the catalyst coating as well as on the surface of the coal. After characterization by the SEM, each sample was re-embedded in an iodine-substituted epoxy resin and the cross-sectional area exposed and polished. These cross-sectional areas were then observed under the electron microscope to observe the potential depth of catalyst penetration into the coal structure and whether there might be preferential absorption of the catalyst by different coal macerals.

4.2.3. Results and Discussion

Figures 4.10 and 4.11 are SEM micrographs showing the relationship between the coal surface and the impregnated catalyst. Figure 4.10 is a secondary electron image of the high volatile bituminous coal and Figure 4.11 shows the subbituminous coal sample. In these micrographs, the catalyst appears in higher contrast (whiter) with respect to the coal surface owing to the difference in their atomic numbers, i.e., molybdenum in the catalyst versus mainly carbon in coal. Figure 4.10 shows a typical fracture pattern which has developed in the catalyst, exposing the darker coal surface below. Most of the coal surface remains covered with the catalyst. However, it is apparent that the catalyst is curling at its edges and spalling away from the coal surface. Within the catalyst there is a higher contrast, spherical phase that is about 1 micron in diameter. Using the EDS it was possible to resolve a Mo and S peak from the catalyst coating, but not possible to determine any relative difference in Mo concentration in the spherical phase. Furthermore, when the EDS was used to characterize the coal surface no Mo peaks were observed, suggesting that once the catalyst coating peeled away, no Mo remains.

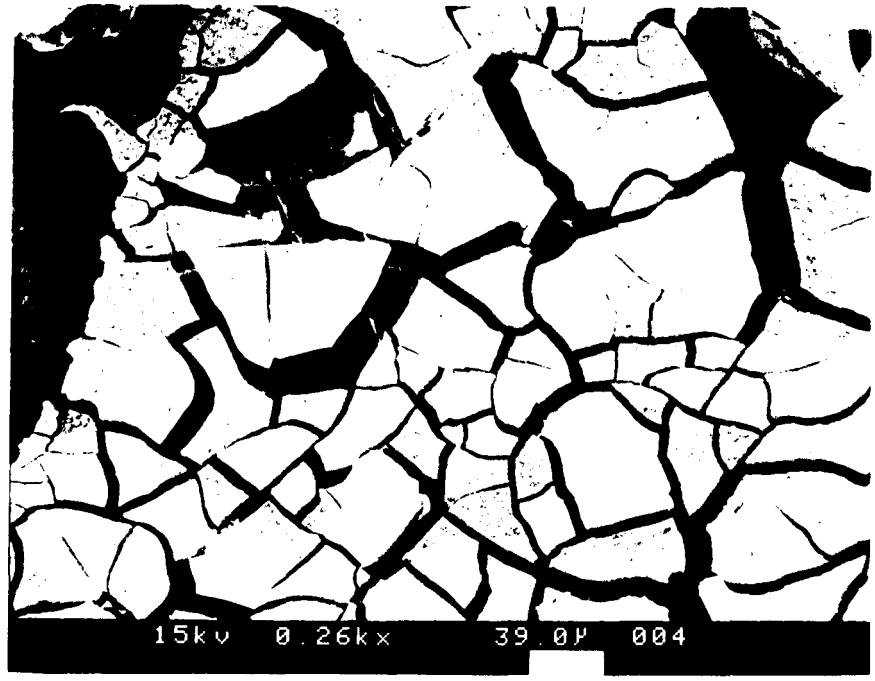

Figure 4.10 - SEM photomicrograph of SAM catalyst coating on surface of Upper Sunnyside seam coal particle (PSOC-1504).

Figure 4.11 - SEM photomicrograph of catalyst peeling away from fractured surface of subbituminous Fort Union seam coal particle (PSOC-1488).

Figure 4.11 shows a small area from which the catalyst coating has peeled away from the polished surface of the subbituminous coal. Although there were fewer of these areas found than with the bituminous coal, the results are similar. The catalyst coating is fractured in the same manner and has peeled from the surface. Fractures that developed in the subbituminous coal during the course of freeze-drying are clearly visible as white lines because of surface charging in the SEM. At higher magnification (Figure 4.12), acicular and rod-like crystal structures are observed adhering to the coal surface. These crystals have characteristic x-ray energies of Ca and S. No molybdenum peak was observed, either associated with these crystals or on the coal surface. The coal surface upon which catalyst had failed to deposit also gave a fairly strong calcium peak, although no crystalline materials were found. This is consistent with an analysis of the high-temperature ash of this coal which shows a relatively high concentration of CaO (16.1%). The needle-like crystals observed in Figure 4.12 are suggestive of gypsum ($CaSO_4 \cdot 2H_2O$). From these observations we tentatively conclude that some of the free sulfur associated with the sulfided catalyst reacts with organically bound calcium salts originally present on or near the coal surface to form calcium sulfate. However, the mechanism for this reaction is not known. Another possible mechanism for the formation of gypsum at the catalyst-coal interface is that the calcium sulfate may have leached from the coal into the catalyst solution and then crystallized during freeze-drying.

Samples of each coal that were heat treated in hydrogen were characterized by a fairly uniform coating of catalyst material. Although there was less tendency for the catalyst to peel from the coal surface after hydrotreatment, the coating appeared to curl at its edges and to be

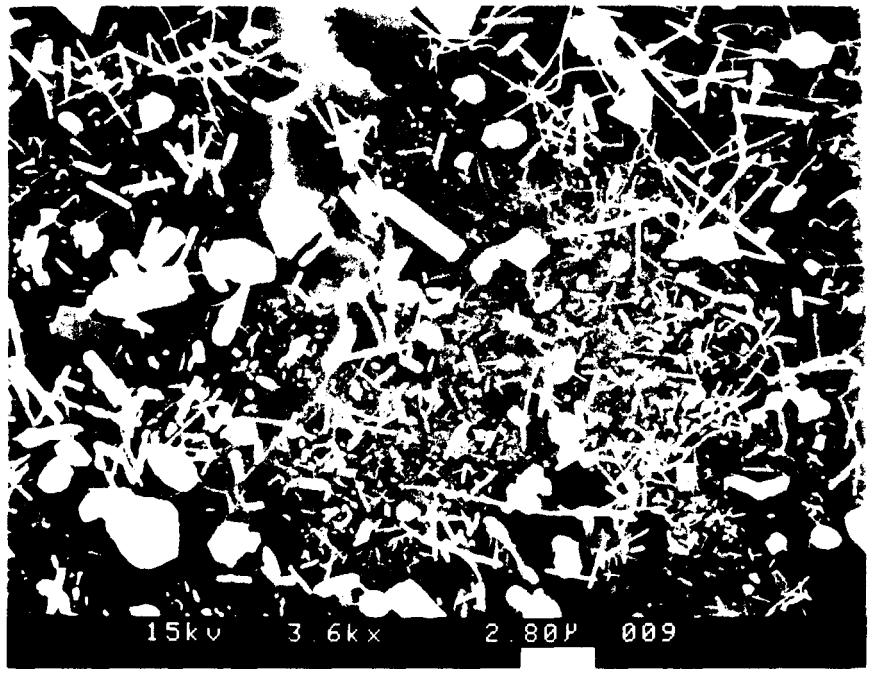

Figure 4.12 - Acicular calcium sulfate crystals on coal surface from center area of Figure 4.11.

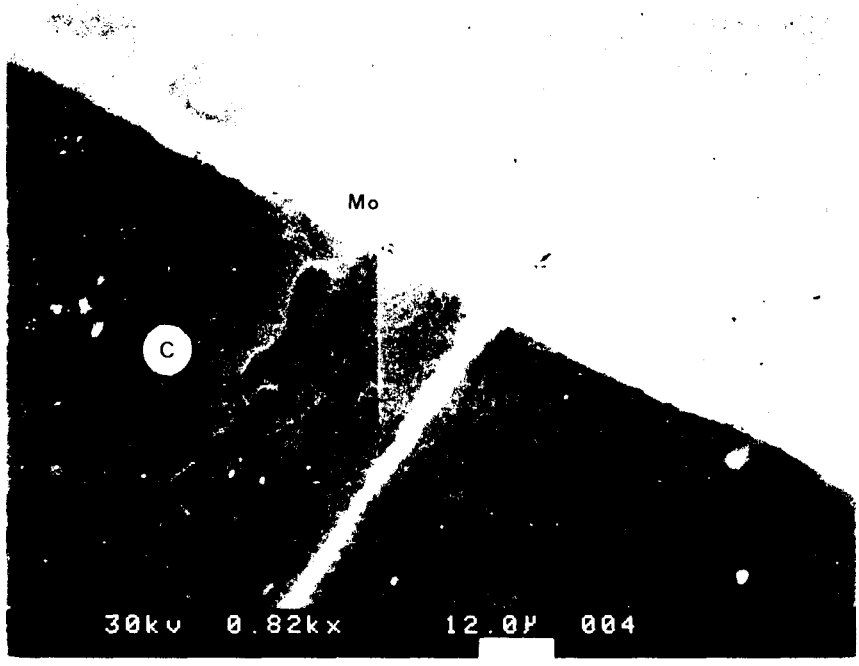

Figure 4.13 - Cross sectional view on SEM of catalyst coating (Mo) on coal particle (PSOC-1488) surface (C) after hydrotreatment at 250°C.

resting on the coal surface, so that again there was no apparent evidence of impregnation. Observation of cross-sectional areas of each of the heat-treated particles also demonstrated that there was no apparent reaction front of the molybdenum catalyst into the coal structure. Figure 4.13 illustrates the high contrast coating as it rests on the coal surface after hydrotreatment, and demonstrates that there is no penetration of the catalyst into the coal surface, at least at the micron scale. The figure clearly shows that the catalyst may penetrate into pre-existing fractures in the coal during impregnation.

4.2.4. Conclusions

With the qualitative evidence described here we have determined that the water-soluble molybdenum catalyst probably does not penetrate the coal surface, but forms a coating that, with time, will peel from the surface leaving little or no molybdenum associated with the coal. Because of this, no preference of the catalyst for any specific coal maceral was observed. For the subbituminous coal, freeze-drying the catalyst during impregnation results in the formation of a calcium sulfate mineral at the catalyst-coal interface. The mode of formation of this mineral is not understood. With hydrotreatment at 250°C, the catalyst coating apparently becomes attached to the coal surface, but does not significantly penetrate. Our study has shown that the impregnation technique employed during the course of our liquefaction experiments only provides a reasonably good surface dispersion of SAM catalyst on coal surfaces, but does not give the level of penetration which had been anticipated.

4.3. CHARACTERIZATION OF CATALYST REMNANTS FOLLOWING COAL HYDROGENATION

4.3.1. Introduction

Another area of study in this project has been the investigation of catalyst interactions with coal during liquefaction. The approach here has been first to locate catalyst remnants in the insoluble residues, and then to characterize any association with the organic remnants of the coal. The objective has been to obtain some insight into the effectiveness of the catalyst over the course of the experiments. For instance, if the catalyst does not remain in intimate contact with coal during thermal depolymerization, then one could assume that it would be less effective in catalyzing hydrogenation of free radicals as they form in the coal. Also, from a practical viewpoint, it would be important to determine whether the catalyst is being removed in the solvent-soluble product stream. Finally, we need to locate and characterize the catalyst remnants in order to understand the chemical changes that occur to the catalyst under the conditions of liquefaction in the presence of coal (and possible coal minerals).

In the current study, a series of THF-insoluble residues produced from the liquefaction of a high volatile C bituminous coal (PSOC-1498) using an iron sulfate, a sulfided ammonium molybdate and a mixture of these catalysts were prepared using a special sample preparation technique. Samples were characterized using both optical and electron microscopy.

4.3.2. Experimental

A procedure for improving the contrast between an organic epoxy resin and carbonaceous residue under the Scanning Electron Microscope has been employed (13), with some modifications, in our current investigations. Basically, the technique involves chemical substitution of iodine into the

structure of the epoxy resin. Iodine improves the chemical and atomic number contract from both secondary and backscatter electron images in the SEM. The procedure uses Epolite 5313 A and B epoxy resin and hardener, manufactured by the Hexcel Corporation and 99% Iodoform (CHI_3). Iodoform was mixed at 15% by weight with the 5313-A resin and dissolved by immersing the mixture in hot water bath held at a constant 75°C for approximately 30 min. The reaction is temperature sensitive and can violently devolatilize above about 100°C. Consequently, the resin was cooled slightly before the hardener was mixed in a 1:9 ratio. Also, because the resin/hardener reaction is exothermic, addition of too much hardener can cause devolatilization. There is a slight increase in the curing time for the iodine-substituted epoxy. Samples were cured at least 24 h before polishing.

Polished sections were prepared from a series of THF-insoluble residues produced following the liquefaction of a high volatile C bituminous coal (PSOC-1498) with a mixed iron sulfate (1.0% Fe) - SAM (0.1% Mo) catalyst, the iron sulfate (1.0% Fe) and the SAM (1.0% Mo) catalysts alone. A list of the residues is given in Table 4.6. Conversion and product yields information can be found in Appendix B.

4.3.3. Location and Nature of Catalyst Remnants

Examination of the residues using reflected-light microscopy revealed little difference in the characteristics of remnant catalyst material when comparing those runs with the mixed Fe/Mo catalyst and the Fe catalyst. As expected, there were major differences in catalyst materials among the residues produced under different reaction conditions, i.e., pretreatment vs temperature-staged and high-temperature experiments.

Table 4.6. THF-insoluble Residues Characterized for Catalyst Remnants (PSOC-1498)

Sample ID	Catalyst	Reaction Conditions
P73-G1-R2	1.0% Fe, 0.1% Mo	275°C, 30 min, 7 MPa H_2; 1:1 naphthalene and 850°F+ recycle solvent
P73-G2-R2	1.0% Fe, 0.1% Mo	275°C, 30 min, 7 MPa H_2; 425°C, 30 min, 7 MPa H_2; 1:1 naphthalene and 850°F+ recycle solvent
P73-G3-R2	1.0% Fe, 0.1% Mo	425°C, 30 min, 7 MPa H_2; 1:1 naphthalene and 850°F+ recycle solvent
P73-G4-R2	1.0% Fe	275°C, 30 min, 7 MPa H_2; 1:1 naphthalene and 850°F+ recycle solvent
P73-G5-R2	1.0% Fe	275°C, 30 min, 7 MPa H_2; 425°C, 30 min, 7 MPa H_2; 1:1 naphthalene and 850°F+ recycle solvent
P73-G6-R2	1.0% Fe	425°C, 30 min, 7 MPa H_2; 1:1 naphthalene and 850°F+ recycle solvent
P73-4-R7	1.0% Mo	275°C, 30 min, 7 MPa H_2; 425°C, 30 min, 7 MPa H_2; process distillate solvent
P73-4-R6	1.0% Mo	275°C, 30 min, 7 MPa H_2; 425°C, 30 min, 7 MPa H_2; dry

Residues produced under pretreatment conditions (P73-G1-R2 and P73-G4-R2) show only nominal signs of reaction; most of the coal particles were intact with some minor abrasion of particle edges. Because of the limited reaction, we expected to find the catalyst still coating the particles; however, under these relatively mild reaction conditions catalyst material could not be readily identified under an optical microscope. Using the SEM, some catalyst material was located, but not in the concentrations expected. Figure 4.14 shows a more-or-less 'typical' coal particle in the pretreatment residue (P73-G1-R2). Using the energy dispersive spectrometer (EDS) for elemental identification, it was determined that most of the high-contrast material observed within the particle boundary is either aluminosilicate (clays) or calcium-rich material (presumable calcium carbonate). However, one area observed along a particle boundary in Figure 4.14 gave Fe and S peaks, while another gave an Mo peak; we believe that these isolated grains are remnant catalyst materials still adhering to the coal surface.

Under the optical microscope there is little qualitative difference between the catalyst remnants in the temperature-staged (P73-G2-R2 and P73-G5-R2) and high-temperature (P73-G3-R2 and P73-G6-R2) residues. However, there is one common inorganic component in all of the residues where the iron sulfate catalyst was used. This mineral is pyrrhotite ($Fe_{1-x}S$), recognizable as an anisotropic mineral of relatively lower reflectance than pyrite, which is isotropic. It is well known that pyrrhotite is formed from coal-derived pyrite during hydrogenation. Analysis of PSOC-1498 reports only 0.03% pyritic sulfur and 3.6% Fe_2O_3 in the high-temperature ash, values which would seem to be insufficient to account for all of the iron sulfide present in the residues. Accordingly,

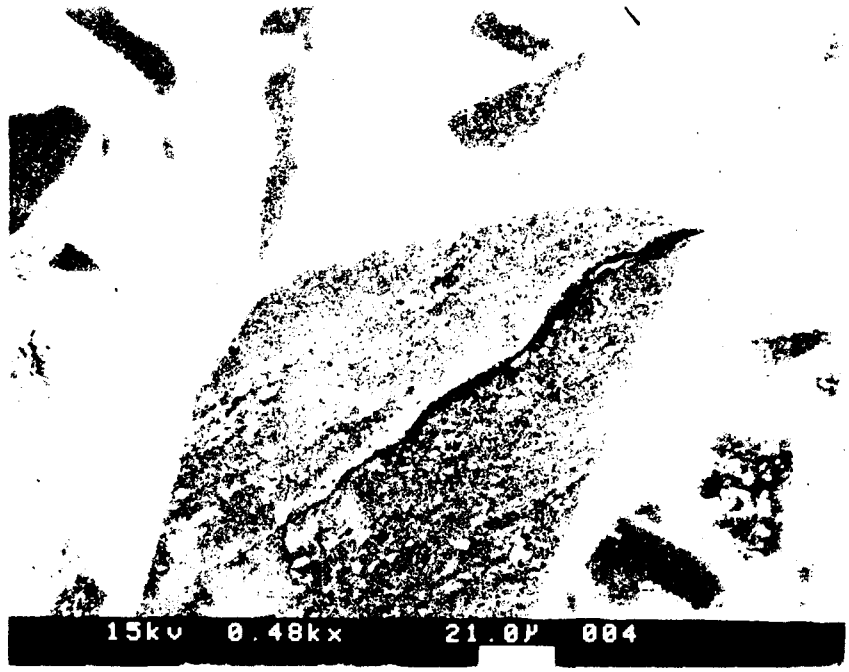

Figure 4.14 - Coal particle (A) showing internal high-contrast grains that are mostly Al & Si (aluminosilicate, clays) or Ca (calcium carbonate). Two areas on particle-epoxy interface give Fe & S and Mo peaks in P73-G1-R2.

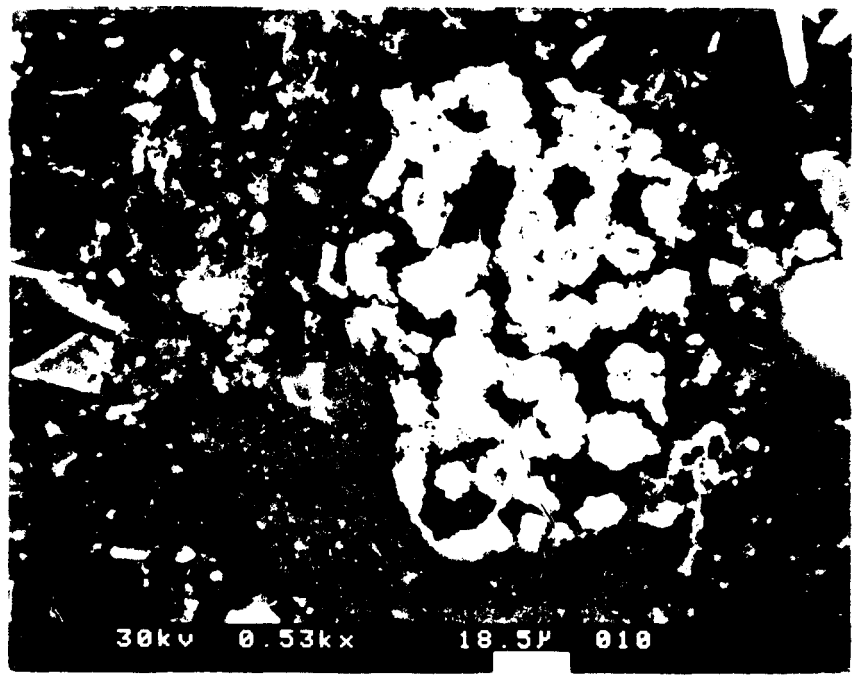

Figure 4.15 - SEM photomicrograph of reactor-solid, pyrrhotite agglomerate of framboids seen in P73-G2-R2.

we suspect that the iron sulfate catalyst is involved in the formation of pyrrhotite.

Anderson and Bockrath (6) have also reported the formation of pyrrhotite during coal hydrogenation experiments in which an organometallic salt of iron was used as a catalyst precursor. In their experiments, elemental sulfur was added to the reaction vessel to produce an *in situ* iron sulfide catalyst. The current investigation appears to show that pyrrhotite also may form during liquefaction of coal from an iron sulfate precursor. Figures 4.15 and 4.16 show two different forms of the iron sulfide in an SEM micrograph and in reflected light, respectively. The EDS system on the SEM confirms the presence of strong Fe and S peaks from these different components.

The first type of catalyst remnant is referred to as a reactor solid and its general form is shown in Figure 4.15. This form of the sulfide appears as a close aggregate of micron-sized crystallites. Groups of these crystallites form roughly spherical framboids that are often aggregated into massive areas like that seen in Figure 4.15. The second particle type, illustrated in Figure 4.16, is an aggregate of much larger size individual anisotropic units compared to those seen in Figure 4.15; in this case, they are on the order of 10-20 μm. Many of these particle types are associated with an anisotropic semicoke produced from the deposition and coalescence of mesophase as seen in Figure 4.16.

One significant observation here is that there was little or no development of the iron sulfide under pretreatment conditions; in the higher temperature residues the iron catalyst occurs as reactor solids which are not physically associated with the coal as it undergoes reaction. Where the iron sulfide occurs in large aggregate sizes, it apparently

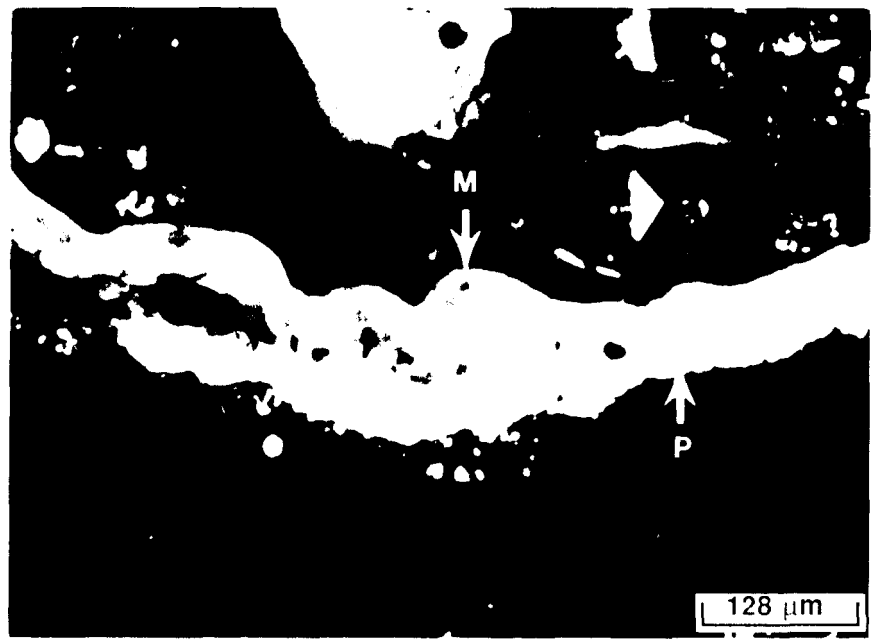

Figure 4.16 - Reflected-light photomicrograph of mesophase-derived carbon (M) on coarse pyrrhotite (P) in P73-G2-R2.

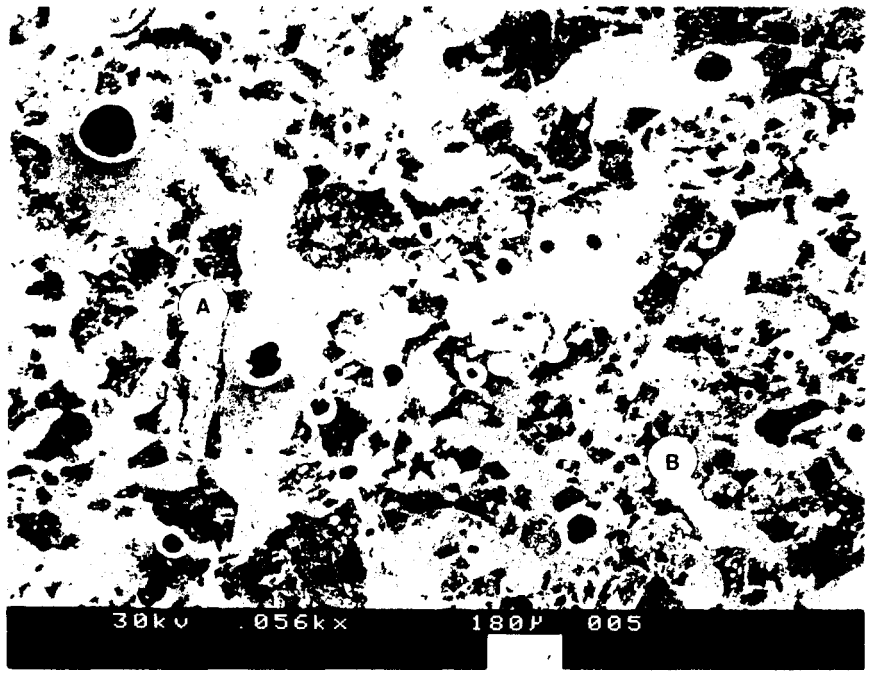

Figure 4.17 - SEM photomicrograph of liquefaction residue showing molybdenum catalyst reactor-solids (particles A & B) as seen in P73-4-R6.

becomes a suitable substrate for the deposition of mesophase. This association is particularly interesting, because any loss of sulfur from the catalyst precursor would tend to interfere with the growth and coalescence of mesophase. Therefore, its transformation to pyrrhotite probably occurred before the deposition of mesophase.

In those residues produced with the mixed Fe/Mo catalyst (P73- G1, G2 and G3 -R2), only one occurrence of molybdenum was observed, that being in a pretreatment sample. The low loading (0.1% Mo) is most likely responsible for the difficulty in locating molybdenum in these residues.

Two temperature-staged liquefaction residues of PSOC-1498 in which a 1.0% Mo catalyst loading was employed were characterized under the SEM. For one of these samples (P73-4-R6) no solvent was used during hydrogenation; in the other (P73-4-R7) a process distillate was used. Molybdenum sulfide occurs in various forms in these residues and, as with the iron sulfate catalyst, there is a reactor-solid type as well as a dispersed form of the catalyst. In Figures 4.17 and 4.18, the reactor solid material appears as an elongated, rod-like or perhaps platy structure that is similar to the coating caused by impregnation seen in Figure 4.13. In Figure 4.17, one of the two reactor-solid particles present (identified as A), is associated with organic material (dark coating). The other particle in Figure 4.17 appears more like those seen in Figure 4.18, for the temperature-staged reaction conducted with the process distillate solvent. The particle types illustrated in Figure 4.18 show that they are zoned structures, in which one side of the particle is very dense and of high contrast, and the other is more porous and of lower contrast. Using the EDS system, all of these particle types gave very strong S and Mo peaks as well as relatively strong peaks for Ca, Si and Al. It was not possible

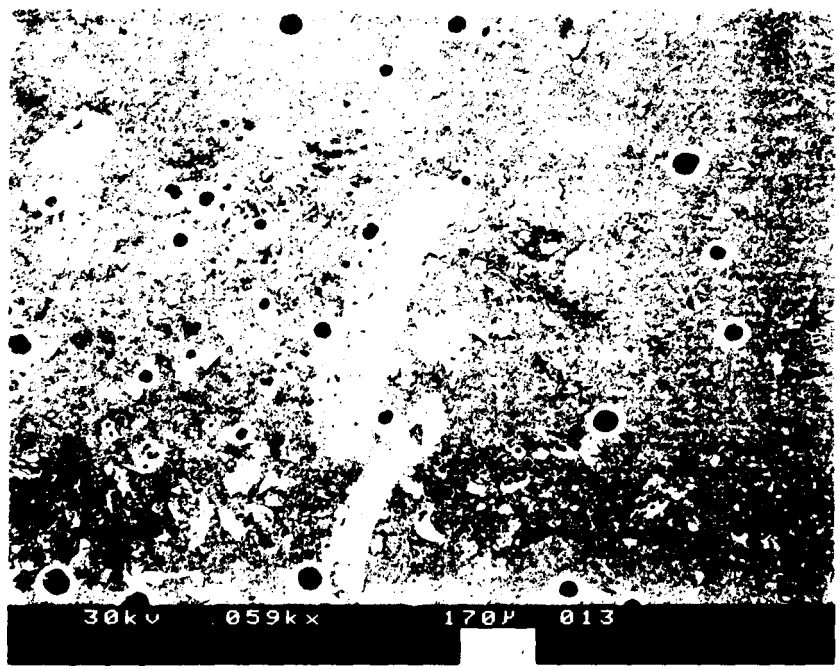

Figure 4.18 - SEM photomicrograph showing the zoned nature of molybdenum catalyst reactor-solids in P73-4-R7.

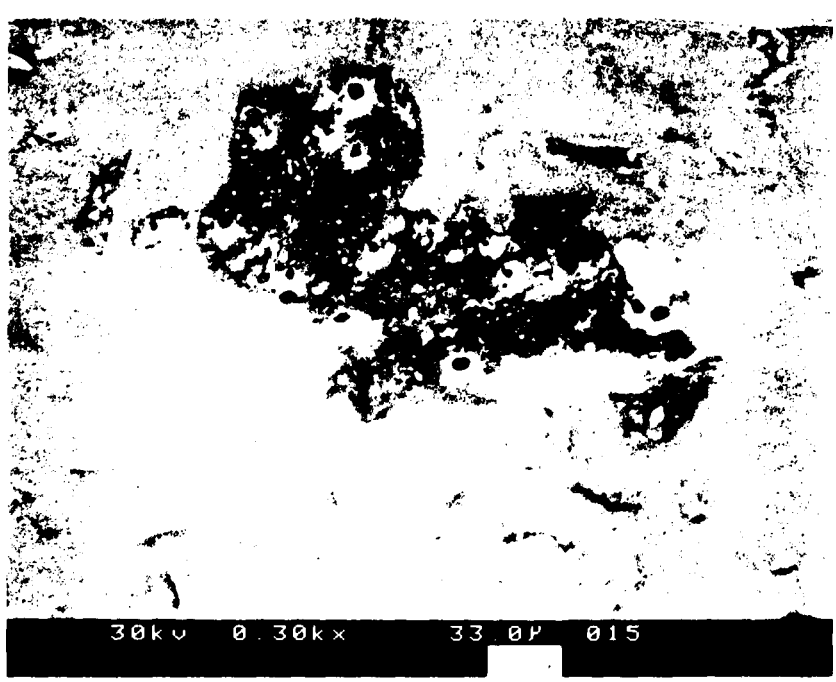

Figure 4.19 - SEM photomicrograph of low-contrast organic particle in P73-4-R7 that contains high contrast dispersed molybdenum catalyst particles.

to determine any relative differences in Mo intensity in the two zones, but the Ca, Si, Al and S peaks were qualitatively more intense on the low contrast side of the particle. Nevertheless, the physical association of these elements suggest that some of the coal inorganic matter (clays, calcium sulfate or perhaps calcium associated with carboxylate groups) may be agglomerating or reacting with the thiomolybdate catalyst. It is also the second independent observation of the association of Ca with the SAM catalyst (see section 4.2).

An observation should be made regarding the overall dimensions of these molybdenum reactor-solid particles. Those particles seen in Figure 4.18 exceed 200 μm and range up to about 700 μm in length. It is unlikely that these particles are coatings that have separated from coal surfaces because they exceed the dimensions of -60 mesh (250 μm) coal particles. We suggest that these particles are formed during the impregnation process. Coal and catalyst are slurried together in a container in which they are then freeze-dried. It is likely that some of the catalyst forms a coating on the side of the slurry vessel during dehydration. This physical evidence suggests that not all of the molybdenum sulfide catalyst is associated with coal surfaces, but may be present as discrete particles during liquefaction. The concentration of these discrete particles relative to the amount of catalyst actually dispersed on coal surfaces may vary from sample to sample and could be a source of small fluctuations in conversion and product yield during coal hydrogenation.

The second thiomolybdate particle type typically is disseminated throughout an organic matrix as is shown in Figure 4.19. Not all of the high-contrast particles seen in the central dark area are catalyst, because some gave Ca, Si, Fe and Al peaks as well; however, the particle did give

significantly strong Mo and S peaks. Perhaps this second particle type results from that part of the molybdenum catalyst that was in direct contact with the coal surface before liquefaction. Qualitatively, the finely divided catalyst is the least commonly identified form in the residues. However, because it is finely dispersed, it may escape detection during examination.

4.3.4. Conclusions

By locating and identifying catalyst materials in tubing-bomb coal liquefaction residues, we have determined that much of it exists in a reactor-solid form that is separate from the coal organic material. This is particularly true in the case of the iron sulfate catalyst, and somewhat less pronounced with the molybdenum catalyst. Apparently, during coal impregnation some of the catalyst material is deposited onto the walls of the slurry vessel. Therefore, a portion of the catalyst may not be physically associated with coal surfaces, but is present as discrete particles. This helps to explain the large size of the pyrrhotite aggregates observed in the high-temperature residues, the difficulty in locating catalyst materials in contact with coal in the pretreatment residues, and the exceptionally elongated thiomolybdate particles found in the temperature-staged residues using the molybdenum catalyst. Finally, there is some qualitative evidence to suggest that the molybdenum catalyst may be involved in reactions with coal inorganic materials.

REFERENCES

1. Hawk, C.O. and Hiteshue, 1965, U.S. Dept. of the Interior, Bureau of Mines, Bulletin 622.

2. Weller, S. and Pelipetz, 1951, Ind. Eng. Chem. 43, 1243-1246.

3. Weller, S.W., 1982, 4th International Conference on Chemistry and Uses of Molybdenum, (Ed. H.F. Barry and P.C. Mitchell), Climax Molybdenum Co., Ann Harbor, Michigan.

4. Warren, T.E., Bowles, K.W. and Gilmore, R.E., 1939, Ind. Eng. Chem. Anal. Ed. 11, 415.

5. Stansberry, P.G. and Derbyshire, F.J., 1988, 'The Mobile Phase in Coals: Its Nature and Modes of Release', Final Report Part 3 to U.S. DOE, Rep. No. DOE-PC-60811-F3, Grant No. DE-FE22-83PC60811, July.

6. Anderson, R.R. and Bockrath, B.C., 1984, Fuel 63, 329-333.

7. Terrer, M.-T. and Derbyshire, F.J., 1986, 'The Mobile Phase in Coals: Its Nature and Modes of Release', Final Report Part 1 to U.S. DOE, Rep. No. DOE-PC-68011-F1, Grant No. DE-FE22-83PC60811, December.

8. Hei, R.D., Sweeny, P.G. and Stenberg, V.I., 1986, Fuel, 65, 577-585.

9. Naumann, A.W., Behan, A.S. and Thorsteinson, E.M., 1982, 4th International Conference on Chemistry and Uses of Molybdenum, (Ed. H.F. Barry and P.C. Mitchell), Climax Molybdenum Co., Ann Harbor, Michigan, 313-318.

10. Rode, E.Ya. and Lebedev, B.A., 1961, Russian Jour. Inorg. Chem., 6, (5), 608-613.

11. Ratnasamy, P. and Leonard, A.J. 1972, Jour. Catalysis, 28, 352-358.

12. Ratnasamy, P., Rodrique, L. and Leonard, A.J. 1973, Jour. Phys. Chem., 77, (18), 2242-2245.

13. Mosa, A., Strickler, D.W. and Austin, L.G., Scanning Electron Microscopy, 1978, vol. 1, pp. 289-292.

APPENDIX A

PETROGRAPHIC DATA FROM LIQUEFACTION RESIDUES

APPENDIX A

Residue Petrography, Weight -- Volume % of dmmf Coal

Run#	Reaction Condition	Atmosphere	Solvent Vehicle	Catalyst	Extraction Solvent	Vitroplast	Anisotropic Semicoke	Granular Residue	Skeletons	Partially Reacted Coal Macerals: Vitrinite	Partially Reacted Coal Macerals: Inertinite	Partially Reacted Coal Macerals: Liptinite	Residue Yield wt %
PSOC-1482													
EX-3-6	TS	H_2:H_2	Dry	Mo	THF	9	15	3	--	--	2	--	28.5
EX-3-5	TS	H_2:H_2	Dry	Mo	None	75	17	2	--	--	2	--	96.6
P74-18-R1	TS	H_2:H_2	Dry	None	THF	53	9	1	--	--	2	--	64.9
P74-13-R1	TS	H_2:H_2	Dry	Fe	THF	15	33	--	--	--	1	--	48.1
P74-15-R2	TS	H_2:H_2	Dry	Fe + Mo	THF	18	12	3	--	--	1	--	33.5
P74-19-R2	TS	H_2:H_2	Process distillate	None	THF	30	--	1	TR	1	3	1	37.6
P74-12-R2	TS	H_2:H_2	Process distillate	Mo	THF	9	--	--	1	1	1	--	12.2
P74-15-R1	TS	H_2:H_2	Process distillate	Fe	THF	5	2	10	TR	TR	3	1	22.0
P74-17-R1	TS	H_2:H_2	Process distillate	Fe + Mo	THF	21	--	--	--	3	3	TR	26.5
PSOC-1401													
58	TS	H_2:H_2	Dry	None	THF	57	TR	--	--	--	2	--	59.6
87	TS	H_2:H_2	Dry	Mo	THF	27	2	--	--	--	4	--	32.6
40	TS	H_2:H_2	Tetralin	Mo	THF	1	TR	2	5	--	1	--	9.0
809-54-B-1	TS	H_2:H_2	Naphthalene	Mo	THF	8	--	TR	--	--	2	--	9.3

PT = pretreatment, 275°C
TS = temperature-staged, 275°C + 425°C
HT = high-temperature single-stage, 425°C
TR = trace, ≤ 0.5%

APPENDIX A (cont.)

Residue Petrography, Weight -- Volume % of dmmf Coal

Run#	Reaction Condition	Atmosphere	Solvent Vehicle	Catalyst	Extraction Solvent	Vitroplast	Anisotropic Semicoke	Granular Residue	Skeletons	Partially Reacted Coal Macerals: Vitrinite	Inertinite	Liptinite	Residue Yield wt %
PSOC-1498													
P73-F1A-R2	TS	H_2:H_2	850+°F recycle	Fe + Mo	THF	2	1	4	1	--	1	--	8.5
P73-F24-R4	HT	H_2	850+°F recycle	Fe + Mo	THF	4	TR	3	1	--	1	--	9.5
P73-G1-R2	PT	H_2	850+°F w/naphthalene	Fe + Mo	THF	--	--	--	--	73	10	1	84.6
P73-G2-R2	TS	H_2:H_2	850+°F w/naphthalene	Fe + Mo	THF	1	6	4	1	--	1	--	12.9
P73-G3-R2	HT	H_2	850+°F w/naphthalene	Fe + Mo	THF	1	10	4	1	--	1	--	17.0
P73-G4-R2	PT	H_2	850+°F w/naphthalene	Fe	THF	--	--	--	--	73	10	1	85.3
P73-G5-R2	TS	H_2:H_2	850+°F w/naphthalene	Fe	THF	1	4	4	1	--	1	--	11.1
P73-G6-R2	HT	H_2	850+°F w/naphthalene	Fe	THF	1	4	4	1	--	1	--	11.1
P73-4-R1	TS	H_2:H_2	Dry	None	THF	74	--	--	3	--	2	--	78.7
P73-4-R6	TS	H_2:H_2	Dry	Mo	THF	39	--	TR	--	--	2	--	40.9
P73-4-R8	TS	H_2:H_2	Dry	Fe	THF	56	--	TR	--	--	1	--	57.5
P73-4-R10	TS	H_2:H_2	Dry	Fe + Mo	THF	44	--	--	--	--	1	--	45.4
P73-4-R5	TS	H_2:H_2	Process distillate	None	THF	41	--	2	1	--	1	--	45.0
P73-4-R7	TS	H_2:H_2	Process distillate	Mo	THF	9	--	5	8	--	1	--	22.2
P73-4-R9	TS	H_2:H_2	Process distillate	Fe	THF	31	--	TR	TR	--	1	--	32.0
P73-4-R11	TS	H_2:H_2	Process distillate	Fe + Mo	THF	6	1	TR	TR	--	TR	--	8.2

PT = pretreatment, 275°C
TS = temperature-staged, 275°C + 425°C
HT = high-temperature single-stage, 425°C
TR = trace ≤ 0.5%

APPENDIX A (cont.)

Residue Petrography, Weight -- Volume % of dmmf Coal

Run#	Reaction Condition	Atmosphere	Solvent Vehicle	Catalyst	Extraction Solvent	Vitroplast	Anisotropic Semicoke	Granular Residue	Skeletons	Partially Reacted Coal Macerals: Vitrinite	Partially Reacted Coal Macerals: Inertinite	Partially Reacted Coal Macerals: Liptinite	Residue Yield wt %
PSOC-1504													
EX-1-1	TS	H_2:H_2	Dry	None	None	90	--	--	--	--	9	--	98.5
P-1-1	TS	H_2:H_2	Dry	None	THF	64	--	4	--	--	4	--	71.7
P-2-3	TS	H_2:H_2	Dry	Mo	None	45	47	--	--	--	7	--	99.0
EX-2-4	TS	H_2:H_2	Dry	Mo	THF	18	19	2	--	--	1	--	40.8
EX-15-14	TS	H_2:H_2	850+°F recycle	Mo	THF	4	TR	6	TR	--	1	--	11.6
EX-12-13	TS	N_2:N_2	850+°F recycle	Mo	THF	10	1	8	2	--	2	--	22.7
P75-5-R1	TS	H_2:H_2	Dry	None	THF	14	52	--	--	--	5	--	70.7
P75-8-R2	TS	H_2:H_2	Dry	Fe	THF	35	22	--	--	--	4	--	61.1
P75-10-R1	TS	H_2:H_2	Dry	Fe + Mo	THF	13	20	7	--	--	3	--	42.7
P75-6-R2	TS	H_2:H_2	Process distillate	None	THF	15	8	2	--	--	3	TR	28.4
P75-8-R1	TS	H_2:H_2	Process distillate	Mo	THF	2	--	7	TR	--	2	--	10.9
P75-9-R3	TS	H_2:H_2	Process distillate	Fe	THF	6	21	4	--	--	4	--	34.3
P75-11-R2	TS	H_2:H_2	Process distillate	Fe + Mo	THF	2	TR	15	--	1	1	--	18.5

PT = pretreatment, 275°C
TS = temperature-staged, 275°C + 425°C
HT = high-temperature single-stage, 425°C
TR = trace ≤ 0.5%

APPENDIX B

LIST OF PETROGRAPHIC ANALYSES PERFORMED ON RESIDUAL MATERIALS AND CONVERSION AND PRODUCT YIELD INFORMATION FOR EACH RUN

APPENDIX B

List of Petrographic Analyses Performed on Residual Materials from Tubing Bomb Liquefaction

Run#	Reaction Condition	Atmosphere	Solvent Vehicle	Catalyst	Extraction Solvent	Analyses Performed: Point-Count	Analyses Performed: Reflectance	Analyses Performed: Fluorescence	Conversion, %	Asphaltene, %	Oil & Gas, %
PSOC-1482 (Lig) Hagle Seam											
P74-18-R1	TS	H_2:H_2	Dry	None	THF	X	X		35.1	11.2	23.9
EX-3-6	TS	H_2:H_2	Dry	Mo	THF	X	X		61.8	22.8	39.0
EX-3-5	TS	H_2:H_2	Dry	Mo	None	X	X		NA	NA	NA
#51	PT	H_2	Dry	None	THF		X		2.8	2.0	0.8
#63	PT	N_2	Dry	None	THF		X		1.1	0.5	0.6
#55	HT	H_2	Dry	None	THF		X		35.1	4.0	31.1
#67	HT	N_2	Dry	None	THF		X		29.0	1.8	27.2
#59	TS	H_2:H_2	Dry	None	THF		X		34.0	5.3	28.7
#71	TS	N_2:N_2	Dry	None	THF		X		31.1	1.4	29.8
P74-13-R1	TS	H_2:H_2	Dry	Fe	THF	X			51.9	19.1	32.8
P74-15-R2	TS	H_2:H_2	Dry	Fe + Mo	THF	X			66.5	25.4	41.1
P74-19-R2	TS	H_2:H_2	Process distillate	None	THF	X			62.4	37.0	25.8
P74-12-R2	TS	H_2:H_2	Process distillate	Mo	THF	X			87.8	47.0	40.8
P74-15-R1	TS	H_2:H_2	Process distillate	Fe	THF	X			78.0	50.6	27.4
P74-17-R1	TS	H_2:H_2	Process distillate	Fe + Mo	THF	X			73.5	49.7	23.8

PT = pretreatment, 275°C, 30 min
TS = temperature-staged, 275°C, 30 min; 425°C, 30 min
HT = high-temperature, single-stage; 425°C, 30 min

APPENDIX B (cont.)

List of Petrographic Analyses Performed on Residual Materials from Tubing Bomb Liquefaction

Run#	Reaction Condition	Atmosphere	Solvent Vehicle	Catalyst	Extraction Solvent	Analyses Performed: Point-Count	Analyses Performed: Reflectance	Analyses Performed: Fluorescence	Conversion, %	Asphaltene, %	Oil & Gas, %
PSOC-1401 (Sub-bit) L. Wyodak											
62	PT	N_2	None	None	THF		X		7.7	1.6	6.1
50	PT	H_2	None	None	THF		X		9.0	0.6	8.4
66	HT	N_2	None	None	THF		X		32.0	1.8	30.2
54	HT	H_2	None	None	THF		X		33.7	2.6	31.1
78	TS	N_2:H_2	None	None	THF		X		41.0	3.3	37.7
74	TS	H_2:N_2	None	None	THF		X		32.0	1.3	30.7
70	TS	N_2:N_2	None	None	THF		X		32.2	0.5	31.7
58	TS	H_2:H_2	None	None	THF	X	X		40.4	4.1	36.3
82	PT	N_2	None	Mo	THF		X		4.5	1.3	3.2
83	PT	H_2	None	Mo	THF		X		4.1	1.7	2.4
84	HT	N_2	None	Mo	THF		X		25.9	1.9	24.0
85	HT	H_2	None	Mo	THF		X		60.3	20.9	39.4
88	TS	N_2:H_2	None	Mo	THF		X		58.7	19.1	39.6
89	TS	H_2:N_2	None	Mo	THF		X		25.7	1.6	24.1
86	TS	N_2:N_2	None	Mo	THF		X		24.8	1.2	23.6
87	TS	H_2:H_2	None	Mo	THF	X	X		67.4	24.1	43.3

PT = pretreatment; 275°C, 30 min
TS = temperature-staged, 275°C, 30 min; 425°C, 30 min
HT = high-temperature, single-stage; 425°C, 30 min

APPENDIX B (cont.)

List of Petrographic Analyses Performed on Residual Materials from Tubing Bomb Liquefaction

Run#	Reaction Condition	Atmosphere	Solvent Vehicle	Catalyst	Extraction Solvent	Analyses Performed: Point-Count	Reflectance	Fluorescence	Conversion, %	Asphaltene, %	Oil & Gas, %
PSOC-1401 (cont.)											
33	PT	N_2	Naphthalene	None	THF		X	X	12.0	3.8	8.2
23	PT	H_2	Naphthalene	None	THF		X	X	10.2	3.7	6.5
28	HT	N_2	Naphthalene	None	THF		X		37.2	3.4	33.8
20	HT	H_2	Naphthalene	None	THF		X		55.4	7.8	47.6
93	TS	N_2:H_2	Naphthalene	None	THF		X		42.5	11.8	30.7
34	PT	N_2	Naphthalene	Mo	THF		X	X	11.0	3.5	7.5
37	PT	H_2	Naphthalene	Mo	THF		X	X	7.0	3.1	3.9
26	HT	N_2	Naphthalene	Mo	THF		X		34.5	3.0	31.5
32	HT	H_2	Naphthalene	Mo	THF		X		88.7	38.1	50.6
40	TS	H_2:H_2	Tetralin	Mo	THF	X			91.0	28.2	62.8
809-54-B-1	TS	H_2:H_2	Naphthalene	Mo	THF	X			90.7	36.9	46.7
PSOC-1498 (hvCb) Wadge Seam											
P73-F1A-R2	TS	H_2:H_2	850+°F	Fe + Mo	THF	X	X		91.5	52.8	38.7
P73-F24-R4	HT	H_2	850+°F	Fe + Mo	THF	X	X		90.5	63.7	26.8
P73-G1-R2	PT	H_2	Naphthalene + 850+°F	Fe + Mo	THF	X	X		15.4	33.6	-18.2
P73-G2-R2	TS	H_2:H_2	Naphthalene + 850+°F	Fe + Mo	THF	X	X		87.1	47.9	39.2

PT = pretreatment; 275°C, 30 min
TS = temperature-staged, 275°C, 30 min; 425°C, 30 min
HT = high-temperature, single-stage; 425°C, 30 min

APPENDIX B (cont.)

List of Petrographic Analyses Performed on Residual Materials from Tubing Bomb Liquefaction

Run#	Reaction Condition	Atmosphere	Solvent Vehicle	Catalyst	Extraction Solvent	Analyses Performed: Point-Count	Analyses Performed: Reflectance	Analyses Performed: Fluorescence	Conversion, %	Asphaltene, %	Oil & Gas, %
PSOC-1498 (cont.)											
P73-G3-R2	HT	H_2	Naphthalene + 850+	Fe + Mo	THF	X	X		83.0	52.2	30.80
P73-G4-R2	PT	H_2	Naphthalene + 850+	Fe	THF	X	X		14.7	16.6	- 1.90
P73-G5-R2	TS	H_2:H_2	Naphthalene + 850+	Fe	THF	X	X		88.9	49.3	39.60
P73-G6-R2	HT	H_2	Naphthalene + 850+	Fe	THF	X	X		88.9	57.5	31.40
P73-4-R1	TS	H_2:H_2	None	None	THF	X	X		21.3	10.6	10.70
P73-4-R6	TS	H_2:H_2	None	Mo	THF	X	X		59.1	37.2	21.90
P73-4-R8	TS	H_2:H_2	None	Fe	THF	X	X		42.5	24.2	18.00
P73-4-R10	TS	H_2:H_2	None	Fe + Mo	THF	X	X		54.6	33.2	21.40
P73-4-R5	TS	H_2:H_2	Process distillate	None	THF	X	X		55.0	71.9	-17.00
P73-4-R7	TS	H_2:H_2	Process distillate	Mo	THF	X	X		77.8	77.8	- 0.03
P73-4-R9	TS	H_2:H_2	Process distillate	Fe	THF	X	X		68.0	76.0	- 8.00
P73-4-R11	TS	H_2:H_2	Process distillate	Fe + Mo	THF	X	X		91.8	94.0	- 2.90
P73-4-R1	TS	H_2:H_2	None	None	None		X		NA	NA	NA
P73-4-R6	TS	H_2:H_2	None	Mo	None		X		NA	NA	NA
P73-4-R3	HT	H_2	None	None	THF	X	X		NA	NA	NA
P73-4-R4	Reverse TS	H_2:H_2	None	None	THF	X	X		NA	NA	NA
P73-4-R2	PT	H_2	None	None	THF	X	X		NA	NA	NA
P73-4-R1	TS	H_2:H_2	None	None	THF	X	X		NA	NA	NA

PT = pretreatment; 275°C, 30 min
TS = temperature-staged, 275°C, 30 min; 425°C, 30 min
HT = high-temperature, single-stage; 425°C, 30 min

APPENDIX B (cont.)

List of Petrographic Analyses Performed on Residual Materials from Tubing Bomb Liquefaction

Run#	Reaction Condition	Atmosphere	Solvent Vehicle	Catalyst	Extraction Solvent	Analyses Performed: Point-Count	Analyses Performed: Reflectance	Analyses Performed: Fluorescence	Conversion, %	Asphaltene, %	Oil & Gas, %
PSOC-1504 (hvAb) Upper Sunnyside											
53	PT	H_2	Dry	None	THF		X	X	11.5	9.6	1.9
65	PT	N_2	Dry	None	THF		X	X	10.4	10.0	0.4
57	HT	H_2	Dry	None	THF		X		31.0	14.1	16.9
69	HT	N_2	Dry	None	THF		X		27.0	10.7	16.3
61	TS	H_2:H_2	Dry	None	THF		X		35.0	18.1	16.9
73	TS	N_2:N_2	Dry	None	THF		X		26.8	10.0	16.8
#1, P-1-2	TS	H_2:H_2	Dry	None	THF	X	X		28.3	23.9	4.4
#1, EX-1-1	TS	H_2:H_2	Dry	None	None	X	X		1.5	NA	NA
#2, P-2-3	TS	H_2:H_2	Dry	Mo	None	X	X		1.0	NA	NA
#2, EX-2-4	TS	H_2:H_2	Dry	Mo	THF	X	X		59.2	42.7	16.5
#15, EX-15-14	TS	H_2:H_2	850+°F	Mo	THF	X	X		88.4	59.3	29.1
#12, EX-12-13	TS	N_2:N_2	850+°F	Mo	THF	X	X		77.3	67.7	9.6
P75-5-R1	TS	H_2:H_2	Dry	None	THF	X			29.3	15.1	14.2
P75-8-R2	TS	H_2:H_2	Dry	Fe	THF	X			38.9	25.6	13.3
P75-10-R1	TS	H_2:H_2	Dry	Fe + Mo	THF	X			57.3	30.8	26.5
P75-6-R2	TS	H_2:H_2	Process distillate	None	THF	X			71.6	62.4	9.2
P75-8-R1	TS	H_2:H_2	Process distillate	Mo	THF	X			89.1	76.2	12.9
P75-9-R3	TS	H_2:H_2	Process distillate	Fe	THF	X			65.7	54.8	10.9
P75-11-R2	TS	H_2:H_2	Process distillate	Fe + Mo	THF	X			81.5	51.1	30.4

PT = pretreatment; 275°C, 30 min
TS = temperature-staged, 275°C, 30 min; 425°C, 30 min
HT = high-temperature, single-stage; 425°C, 30 min

APPENDIX C

TRANSITIONAL MATERIALS FOUND IN RESIDUES PRODUCED FROM THE AGED SAM CATALYST

APPENDIX C

Two transitional materials were characterized in the residues produced from the aged SAM catalyst, the first of which was observed only in the P71-2 residue (275°C, 30 min, N_2). Figure C.1 shows a particle with relatively high reflectance components scattered throughout a matrix that has negative relief with respect to the polished surface. The matrix is composed of a weak agglomerate of low-reflecting particles that are easily pulled out of the surface during polishing. Based on its reflectance, the higher reflecting material dispersed throughout this matrix appears to be Phase II. An occasional transparent, crystalline material was observed on the polished surface in close proximity to particles like that illustrated in Figure C.1. This substance, which disappeared completely after repolishing, could be a water-soluble remnant of the catalyst. This suggests that pretreatment in nitrogen is not sufficient to cause the same type of phase transformations that occur when hydrogen is used. It also suggests that the presence of hydrogen and carbon disulfide may be important in the development of the Phase I material.

To further investigate the water-soluble remnant associated with the catalyst residues produced under pretreatment conditions (P71-1 in hydrogen and P71-2 in nitrogen), a series of evaporated slide mounts were prepared as described in Section 4.1.2. Upon evaporation, a dark green rim formed from both samples that was thicker and darker for the residue produced under a nitrogen atmosphere (P71-2). In transmitted light, the green material from P71-2 exhibited anisotropy and considerable crystal growth, similar to that of the pure ammonium heptamolybdate. From this we concluded that at least part of the 'matrix' material observed in this residue may be a molybdate compound. A lesser amount of soluble, green

Figure C.1 - Matrix material found in the P71-2 residue is observed in negative relief in contrast to the high-reflecting Phase II material.

Figure C.2 - Central particle represents the Phase I/II transitional material observed in the P71-3 residue. A Phase I particle is on the left.

material was extracted from the pretreatment residue produced in hydrogen (P71-1). Only a small portion of the rim material was transparent and a smaller portion was anisotropic. This correlates well with the observation that no matrix material was observed in the P71-1 residue.

A second transitional material occurred only in the residue produced from two-stage hydrogenation (P71-3) and appeared to be an intimate mixture of Phases I and II. Figure C.2 provides a comparison of this higher reflectance transitional material with a Phase I particle. In some particles the high-reflecting Phase II material was nearly uniformly dispersed as micron-sized spheres throughout a matrix of Phase I. In other particles it appeared as though the Phase I material had attained higher reflectance. Nevertheless both particle types display an intermediate reflectance between Phases I and II, and both are isotropic.